ISSN 1732-9353 (suspended)
eISSN 2543-7496

Scientific Review

Engineering and Environmental Sciences

Przegląd Naukowy
Inżynieria i Kształtowanie Środowiska

Vol. 35 (2) 2026 Issue 112
Quarterly

SCIENTIFIC REVIEW
ENGINEERING AND ENVIRONMENTAL SCIENCES
Quarterly

EDITORIAL OFFICE ADDRESS
Wydział Budownictwa i Inżynierii Środowiska SGGW, ul. Nowoursynowska 159, 02-776 Warsaw, Poland
tel. (+48 22) 59 35 363, 59 35 210, 59 35 302
e-mail: srees@sggw.edu.pl
https://srees.sggw.edu.pl

Electronic version of the Scientific Review Engineering and Environmental Sciences is primary version

All papers are indexed in the data bases as follows: AGRO(Poznań), BazTech, Biblioteka Nauki, **CrossRef**, **DOAJ**, **Google Scholar**, **Index Copernicus**, INFONA, POL-Index, **SCOPUS**, SIGŻ(CBR)

Scientific Review

Engineering and Environmental Sciences

Przegląd Naukowy

Inżynieria i Kształtowanie Środowiska

Vol. 35 (2) 2026 Issue 112

Contents

Wydawnictwo SGGW, Warsaw 2026

 Wydawnictwo SGGW  wydawnictwosggw

Editorial work – Anna Dołomisiewicz, Tomasz Ruchniewicz

ISSN 1732-9353 (suspended) eISSN 2543-7496

Scientific Review Engineering and Environmental Sciences (2026), 35 (2), 117–138

Sci. Rev. Eng. Env. Sci. (2026), 35 (2) https://srees.sggw.edu.pl

ISSN 1732-9353 (suspended) eISSN 2543-7496 DOI 10.22630/srees.10910

Received: 30.10.2025
Accepted: 11.03.2026

Somboon CHAIPRAKARN[1]
Paphaon KHEAWSEEMA[2]
Chanakarn SAKULTHAEW[3]
Panudet SAENGSEEDAM[1]✉

[1] Rajamangala University of Technology Krungthep, Faculty of Engineering, Thailand

[2] University of Phayao, School of Dentistry, Thailand

[3] Nakhon Sawan Rajabhat University, Faculty of Science and Technology, Thailand

✉panudech.s@mail.rmutk.ac.th

The association between ambient fine particulate matter ($PM_{2.5}$) concentrations and air pollution-related respiratory disease at the pollution control zone of Rayong Province, Thailand

Keywords: $PM_{2.5}$, respiratory disease, air pollution, pollution control zone, time-lag analysis

Introduction

Airborne particles smaller than 2.5 μm in diameter ($PM_{2.5}$), known as fine particles, are among the most harmful air pollutants globally with substantial effects on human health. These small particles can penetrate extremely deep into pulmonary alveoli and result in extensive respiratory disease and premature death.

Traffic is heavy in industrial zones, such as the pollution control zone of Rayong Province in Thailand and biomass burning is common; therefore, $PM_{2.5}$ pollution is an important and long-term public health issue. Exposure to $PM_{2.5}$ causes millions of deaths annually and disproportionately affects the populations of low- and middle-income countries (World Health Organization [WHO], 2021). Thailand's industrial provinces also contain high concentrations of $PM_{2.5}$ that exceed surpass the WHO guideline annual average of 15 $\mu g \cdot m^{-3}$, highlighting the need for further research to better understand associated health effec ts and provide a basis for policy action (Kanchanasuta et al., 2020). This research focuses on the pollution control zone of Rayong Province, a major industrial cluster, to study how exposure to $PM_{2.5}$ relates to respiratory outcomes of health.

There has been considerable epidemiological research on the impact of $PM_{2.5}$ and lung health in recent years. Various studies have repeatedly shown that exposure to $PM_{2.5}$ is associated with an elevated risk of asthma, bronchitis, and other respiratory complications, especially in urban-industrial settings (Choo et al., 2023; Zhu et al., 2023). In Southeast Asia, industrial pollution and seasonal biomass burning have been identified as the predominant sources of elevated levels of $PM_{2.5}$, and short-term exposure has been linked with higher rates of hospital admissions due to respiratory illnesses (Phosri et al., 2019; Amnuaylojaroen et al., 2020). Time-lag analyses have revealed that $PM_{2.5}$ exposure can have immediate or delayed adverse health effects, with vulnerable subgroups such as the elderly and children being especially affected (Kim et al., 2012; Chantaraprachoom et al., 2024). These findings underscore the importance of regional analysis in order to better characterize local patterns of pollution and their associated health effects.

The literature suggests that the health impacts of $PM_{2.5}$ differ based on exposure duration, concentration levels, and population vulnerability. Research in Thailand suggests that industrial estates, such as Rayong, have higher levels of $PM_{2.5}$ than areas such as Bangkok, but data on the short-term adverse effects of $PM_{2.5}$ exposure in industrial environment remain limited (Vichit-Vadakan et al., 2008; Cheanklin et al., 2012). The "harvesting effect," whereby $PM_{2.5}$ exposure can cause morbidity in susceptible persons, has been observed in many studies illustrating the complex temporal patterns of exposure–response relationships (Anggraeni & Lestari, 2023; Suwanprapha et al., 2024). These gaps highlight the importance of local research that combines air quality and health information to assess the short-term impact of $PM_{2.5}$ exposure on respiratory morbidity in industrial environments (Pothirat et al., 2016; Muenmee & Bootdee, 2021). Despite the growing body of international

and national evidence regarding the health effects of $PM_{2.5}$ exposure, limited empirical research has specifically examined short-term temporal associations in designated industrial pollution control zones in Thailand. In particular, there remains insufficient integration of multi-station air quality monitoring data with hospital-based morbidity records at the provincial level. Therefore, this study aims to address this gap by systematically analyzing daily $PM_{2.5}$ concentrations and respiratory disease outcomes within the pollution control zone of Rayong Province using time-lag correlation analysis.

The objective of this research is to evaluate trends in $PM_{2.5}$ levels and respiratory disease morbidity in the pollution control zone of Rayong Province between 2020 and 2023. The study will investigate short-term associations between daily concentrations of $PM_{2.5}$ and respiratory diseases using time-lag analysis to explore immediate and delayed health outcomes. By integrating air pollution data from monitoring stations with hospital admission data, this article provides empirical evidence to support strategic air quality management and public health interventions in industrial areas.

Material and methods

Study design

This study employed a retrospective analytical design based on secondary data obtained from air quality monitoring stations and hospital patient record systems.

Study area and air quality monitoring stations

A geographical map illustrating the spatial distribution of air quality monitoring stations within the pollution control zone of Rayong Province is presented in Figure 1. The map provides context for understanding station locations in relation to industrial estates, residential zones, and transportation corridors.

A descriptive summary of each monitoring station, including land-use classification and proximity to major emission sources, is provided in Table 1. These additional details facilitate the interpretation of inter-station variability in $PM_{2.5}$ concentrations and allow for the assessment of potential location-specific influences.

Chaiprakarn, S., Kheawseema, P., Sakulthaew, C., Saengseedam, P. (2026). The association between ambient fine particulate matter ($PM_{2.5}$) concentrations and air pollution-related respiratory disease at the pollution control zone of Rayong Province, Thailand. *Sci. Rev. Eng. Env. Sci.*, *35* (2), 117–138. DOI 10.22630/srees.10910

FIGURE 1. Geographic distribution of $PM_{2.5}$ monitoring stations and the hospital catchment area within the pollution control zone of Rayong Province

Source: own work.

TABLE 1. Characteristics of $PM_{2.5}$ monitoring stations included in the study

Station code	Monitoring site	Nearby sources
28T	Pluakdaeng District Health Office, Rayong, Thailand	industrial estate, port activities
29T	Health Promotion Hospital Maptaphut, Rayong, Thailand	petrochemical complex, traffic
30T	Rayong Provincial Agricultural Office, Rayong, Thailand	traffic, mixed land use
31T	Field Crop Research Center, Rayong, Thailand	agricultural activities, open areas
74T	Government Center, Rayong, Thailand	residential traffic, commercial area

Source: own work.

$PM_{2.5}$ concentrations from fixed-site monitoring stations were used as proxies for ambient population-level exposure within the pollution control zone. These stations were assumed to reflect general air quality conditions across the hospital catchment area; however, spatial variability in pollutant distribution may result in exposure misclassification at the individual level.

The study did not include geocoded residential data; therefore, precise distances between individual patient residences and monitoring stations could not be calculated. Exposure was assigned at the ecological level rather than the individual level. Daily $PM_{2.5}$ concentrations were analyzed separately for each monitoring station to explore spatial heterogeneity. In addition, an area-level average

concentration across all five stations was calculated to represent general ambient exposure within the pollution control zone of Rayong Province. The monitoring stations are located approximately 3–18 km from the hospital catchment area.

Health data collection

Health data were obtained from Her Royal Highness Princess Maha Chakri Sirindhorn Memorial Hospital, which functions as a major tertiary care facility serving the Pollution Control Zone of Rayong Province. The hospital receives referrals for moderate to severe respiratory conditions from surrounding districts within the study area.

Although additional primary healthcare units operate in the region, inpatient respiratory admissions are predominantly managed at this center. Therefore, the hospitalization data are considered broadly representative of respiratory morbidity patterns within the study population.

The study utilized both daily-level and monthly aggregated datasets. Daily $PM_{2.5}$ concentrations and daily respiratory case counts were used for the short-term time-lag assessment. In parallel, monthly averages and monthly aggregated case counts were constructed for ecological correlation analysis across the study period.

Data collection

The study utilized both daily-level and monthly aggregated datasets. Daily $PM_{2.5}$ concentrations and daily respiratory case counts were used to evaluate short-term exposure–response relationships and time-lag associations. Monthly averages and aggregated case counts were additionally constructed to examine broader ecological temporal patterns across the study period.

Lag analysis was performed to explore temporal displacement patterns between $PM_{2.5}$ concentrations and respiratory morbidity within the aggregated monthly framework. These lag estimates do not represent true daily distributed lag effects but rather relative shifts in temporal association.

Daily 24-hour $PM_{2.5}$ concentrations were collected from five air pollution monitoring stations within the Rayong pollution control area, including Stations 28T, 29T, 30T, 31T, and 74T. The data were collected from January 1, 2017, to December 31, 2023, and were expressed as concentrations in micrograms per cubic meter [$\mu g \cdot m^{-3}$].

Chaiprakarn, S., Kheawseema, P., Sakulthaew, C., Saengseedam, P. (2026). The association between ambient fine particulate matter ($PM_{2.5}$) concentrations and air pollution-related respiratory disease at the pollution control zone of Rayong Province, Thailand. *Sci. Rev. Eng. Env. Sci.*, *35* (2), 117–138. DOI 10.22630/srees.10910

Health information on outpatients and inpatients was collected from Her Royal Highness Princess Maha Chakri Sirindhorn Memorial Hospital Siam Grand Palace, Rayong. It covered only patients with respiratory and air pollution diseases, as classified by the International Statistical Classification of Diseases and Related Health Problems 10th revision (ICD-10) codes J00–J99. Seven respiratory disease categories were selected based on their clinical relevance and prior epidemiological evidence indicating sensitivity to air pollution exposure. These conditions represent a combination of acute inflammatory diseases (e.g., pneumonia, bronchitis) and chronic respiratory disorders (e.g., asthma, COPD) that are commonly reported in regional health surveillance data. Other ICD-10 codes within J00–J99 were not included due to low case frequency or limited evidence of short-term air pollution sensitivity. The examination focused on seven general categories of diseases: (1) COPD, (2) asthma, (3) pneumonia, (4) influenza, (5) acute pharyngitis, (6) chronic rhinitis, and (7) bronchitis.

Monthly average $PM_{2.5}$ concentrations and monthly aggregated counts of respiratory disease cases were used in the analysis. This ecological design, based on monthly temporal resolution, limits the ability to evaluate short-term daily lag effects and should be interpreted accordingly.

Study period

Although air quality monitoring data were available from 2017 onward, complete and standardized hospital admission records were consistently accessible only from 2020. To ensure data completeness and comparability, the analytical period was therefore restricted to 2020–2023.

Data analysis

Descriptive statistics were calculated to summarize air pollution levels and respiratory morbidity.

Daily-level time-series assessment. Daily 24-hour $PM_{2.5}$ concentrations and daily counts of respiratory disease cases were analyzed to examine short-term exposure–response relationships. The Spearman rank correlation coefficient was applied due to the non-normal distribution of the data.

Time-lag analyses were conducted for lag days 0–7 to explore delayed associations following exposure. These analyses represent unadjusted exploratory correlations and do not constitute causal time-series modeling. The daily-level

dataset included approximately 1,461 observations (January 2020–December 2023). Days with incomplete $PM_{2.5}$ or hospital records were excluded from the daily-level correlation analyses. No imputation was performed. All statistical tests were two-tailed, and statistical significance was defined as $p < 0.05$.

Daily $PM_{2.5}$ concentrations were calculated as the average of the five fixed monitoring stations to represent population-level exposure within the study area. Both daily-level and monthly-level analyses were conducted to examine short-term exposure–response relationships as well as broader ecological temporal patterns.

Monthly-level ecological correlation. Monthly average $PM_{2.5}$ concentrations and monthly aggregated respiratory case counts were analyzed to assess broader ecological co-variation patterns. Spearman rank correlation coefficient was used to evaluate associations between each monitoring station and each respiratory disease category at the monthly level ($N \approx 48$ months). All analyses were performed using IBM SPSS Statistics, version 26.0.

Ethical approval

This research received ethical approval from the Research Ethics Review Committee, Rajamangala University of Technology Tawan-ok (RMUTTO REC Reference No. 033/2024) on July 15, 2024, based on the ethical guidelines described in the Declaration of Helsinki and Guidelines on Good Clinical Practice (ICH-GCP). No individual data was collected, and patient identifiers were anonymized to the extent possible. The analysis used aggregated data.

Results and discussion

$PM_{2.5}$ concentrations at pollution control zone of Rayong Province in Thailand

The trend analysis revealed an overall increase in $PM_{2.5}$ levels across Rayong's pollution control areas during the study period, as shown in Table 2, Figures 2 and 3. The mean overall concentration from all monitoring points rose from 18.19 $\mu g \cdot m^{-3}$ in 2020 to 20.55 $\mu g \cdot m^{-3}$ in 2023, representing a 13% increase. Station 29T recorded the highest mean $PM_{2.5}$ concentration at 19.42 $\mu g \cdot m^{-3}$ while Station 74T recorded the lowest concentration at 18.33 $\mu g \cdot m^{-3}$. The highest value was 21.93 $\mu g \cdot m^{-3}$, recorded at Station 29T in 2023. Although these values were

Chaiprakarn, S., Kheawseema, P., Sakulthaew, C., Saengseedam, P. (2026). The association between ambient fine particulate matter ($PM_{2.5}$) concentrations and air pollution-related respiratory disease at the pollution control zone of Rayong Province, Thailand. *Sci. Rev. Eng. Env. Sci.*, *35* (2), 117–138. DOI 10.22630/srees.10910

still within Thailand's national air quality standard of 50 $\mu g \cdot m^{-3}$, they were above WHO guideline value of 15 $\mu g \cdot m^{-3}$ by about 37%. The ongoing rise in $PM_{2.5}$ concentrations, especially at Station 29T and Station 31T, emphasizes the necessity of ongoing monitoring and action towards safeguarding public health in Rayong's industrial estates.

TABLE 2. Average concentrations of $PM_{2.5}$ by monitoring station and year at the pollution control zone of Rayong Province in Thailand during 2020–2023 [$\mu g \cdot m^{-3}$]

Year	Station					Mean (all stations)	Max	Min
	28T	29T	30T	31T	74T			
2020	20.94	16.43	17.75	16.75	19.07	18.19	20.94	16.43
2021	20.02	19.42	16.49	17.51	17.41	18.17	20.02	16.49
2022	16.74	19.91	19.16	18.63	16.83	18.25	19.91	16.74
2023	18.79	21.93	20.30	21.72	19.99	20.55	21.93	18.79
Average	19.12	19.92	18.43	18.65	18.33	18.89	21.93	16.43

Source: own work.

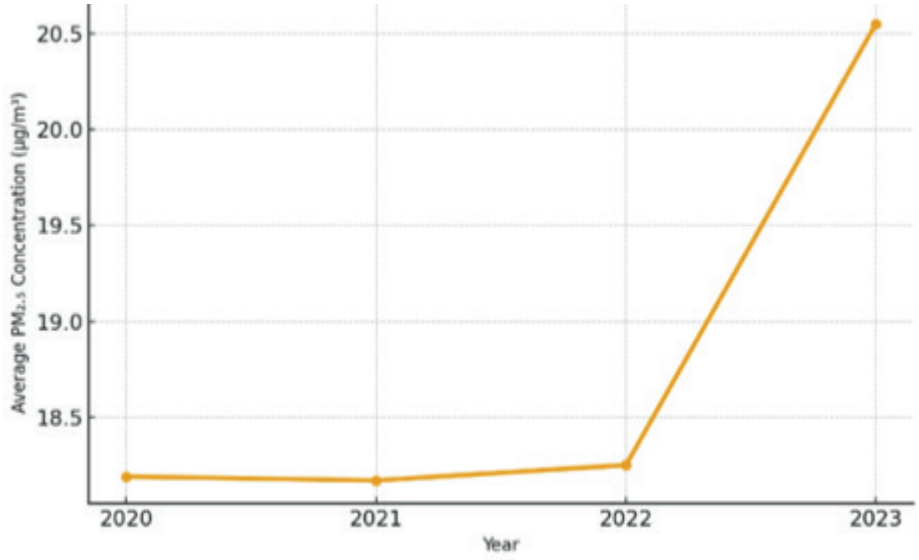

FIGURE 2. Annual trend of average $PM_{2.5}$ concentrations from all monitoring stations at the pollution control zone of Rayong Province in Thailand during 2020–2023

Source: own work.

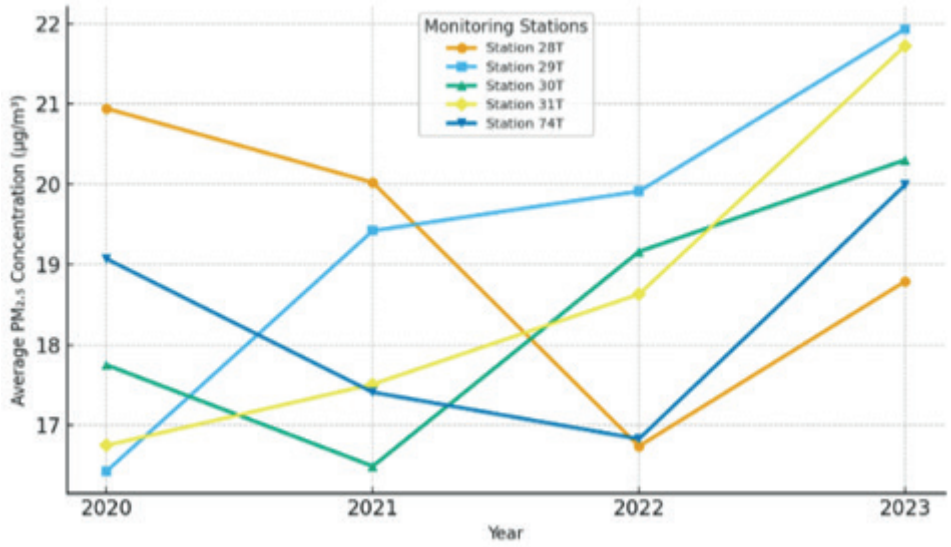

FIGURE 3. Temporal variation in $PM_{2.5}$ concentrations by station during 2020–2023
Source: own work.

Trends in the number of patients with respiratory diseases

As shown in Table 3, respiratory disease trends are summarized numerically through annual case counts across disease categories.

TABLE 3. Number of patients with respiratory diseases by category and year at the pollution control zone of Rayong Province in Thailand during 2020–2023

Disease	2020	2021	2022	2023	Total (4 years)	Mean (1 year)	Max	Min
Chronic obstructive pulmonary disease (COPD)	722	566	704	688	2,680	670.0	722	566
Asthma	1,384	1,222	1,360	1,784	5,750	1,437.5	1,784	1,222
Pneumonia	707	413	571	1,127	2,818	704.5	1,127	413
Influenza	274	6	194	2,530	3,004	751.0	2,530	6
Acute pharyngitis	1,255	578	1,554	2,235	5,622	1,405.5	2,235	578
Chronic rhinitis	31	27	21	22	101	25.3	31	21
Bronchitis	1,141	367	706	1,090	3,304	826.0	1,141	367
All diseases combined	5,514	3,179	5,110	9,476	23,279	5,819.8	–	–

Source: own work.

Chaiprakarn, S., Kheawseema, P., Sakulthaew, C., Saengseedam, P. (2026). The association between ambient fine particulate matter ($PM_{2.5}$) concentrations and air pollution-related respiratory disease at the pollution control zone of Rayong Province, Thailand. *Sci. Rev. Eng. Env. Sci.*, *35* (2), 117–138. DOI 10.22630/srees.10910

Association between $PM_{2.5}$ concentrations and respiratory diseases over time

As presented in Table 4 and Figure 4, the correlation analysis revealed significant positive correlations between $PM_{2.5}$ concentrations and three respiratory diseases. Pneumonia incidence showed a strong positive correlation with $PM_{2.5}$ at Station 31T ($r = 0.276$, $p < 0.05$). (2) Bronchitis was also highly correlated with same-day $PM_{2.5}$ levels at Station 74T ($r = 0.276$, $p < 0.05$), whereas significant positive correlations were observed at Station 28T (lag 4: $r = -0.419$, $p < 0.01$) and Station 29T (lag 4: $r = -0.331$, $p < 0.05$). (3) Asthma also showed a positive correlation with $PM_{2.5}$ concentration at Station 31T at a lag of 1 day (lag 1: $r = 0.283$, $p < 0.05$).

Negative correlations were observed at lags 3–5 at certain stations, suggesting that acute exposure to elevated levels of $PM_{2.5}$ may result in increased respiratory morbidity among susceptible populations initially, followed by a subsequent reduction in morbidity as the susceptible population is diminished. There were no statistically significant correlations for the remaining categories of respiratory illness investigated in this research.

Correlation analysis revealed varying degrees of association between $PM_{2.5}$ concentrations and respiratory disease incidence across monitoring stations. Significant positive correlations were identified at Stations 31T and 74T ($r = 0.276$, $p = 0.012$), while weaker or non-significant associations were observed at other stations. However, the magnitude of the correlation was modest ($r < 0.30$), explaining less than 10% of the variance.

TABLE 4. Spearman correlation coefficients (r) between $PM_{2.5}$ concentrations and respiratory diseases by monitoring station at the pollution control zone of Rayong Province in Thailand during 2020–2023

Disease	Station					Mean (r)
	28T	29T	30T	31T	74T	
Chronic obstructive pulmonary disease (COPD)	0.072	−0.006	0.057	0.042	0.075	0.062
Asthma	0.052	0.208	0.153	0.255	0.259	0.206
Pneumonia	0.062	0.260	0.159	0.276*	0.242	0.223
Influenza	−0.023	0.203	0.129	0.256	0.204	0.170
Acute pharyngitis	−0.110	0.104	0.031	0.134	0.069	0.051
Chronic rhinitis	−0.041	−0.175	−0.099	−0.189	−0.151	−0.153
Bronchitis	0.153	0.199	0.166	0.258	0.276*	0.232
All diseases combined	0.024	0.186	0.110	0.239	0.212	0.169

Spearman rank correlation coefficients were calculated based on monthly aggregated data (N = 45–52 months depending on data completeness; *$p < 0.05$). Values represent contemporaneous monthly associations. No lag structure was applied at the monthly level.

Source: own work.

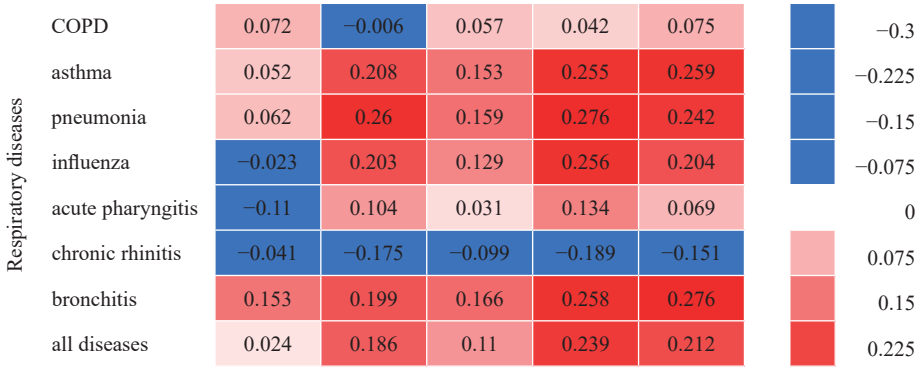

FIGURE 4. Correlation matrix illustrating relationships between $PM_{2.5}$ concentrations and respiratory disease categories across monitoring stations. All correlation coefficients are numerically presented in Table 4

Source: own work.

Lag analysis of $PM_{2.5}$ exposure and respiratory diseases (0–7 days) – evidence of an acute effect

As shown in Table 5 and Figure 5, a weak but statistically significant positive correlation was observed between $PM_{2.5}$ concentration and bronchitis cases at Station 74T on the same day ($r = 0.276$, $p = 0.048$).

TABLE 5. Statistically significant Spearman correlations (r) between daily $PM_{2.5}$ concentrations and respiratory diseases across lag periods (0–7 days) at pollution control zone of Rayong Province in Thailand during 2020–2023 (approximately 1,461 daily observations)

Disease	Station	lag	r	Significance
Chronic obstructive pulmonary disease (COPD)	28T	lag 7	−0.296	*
Asthma	28T	lag 4	−0.304	*
Asthma	31T	lag 1	0.283	*
Acute pharyngitis	28T	lag 2	−0.295	*
Acute pharyngitis	28T	lag 3	−0.337	*
Acute pharyngitis	28T	lag 4	−0.310	*
Bronchitis	28T	lag 3	−0.354	*
Bronchitis	28T	lag 5	−0.317	*
Bronchitis	28T	lag 4	−0.419	**
Bronchitis	29T	lag 4	−0.331	*
Bronchitis	29T	lag 5	−0.296	*
Bronchitis	74T	lag 0	0.276	*

Chaiprakarn, S., Kheawseema, P., Sakulthaew, C., Saengseedam, P. (2026). The association between ambient fine particulate matter ($PM_{2.5}$) concentrations and air pollution-related respiratory disease at the pollution control zone of Rayong Province, Thailand. *Sci. Rev. Eng. Env. Sci.*, *35* (2), 117–138. DOI 10.22630/srees.10910

TABLE 5 (cont.)

Disease	Station	lag	*r*	Significance
Bronchitis	74T	lag 4	−0.303	*
All diseases combined	28T	lag 3	−0.333	*
All diseases combined	28T	lag 4	−0.349	*

*$p < 0.05$; **$p < 0.01$.

Source: own work.

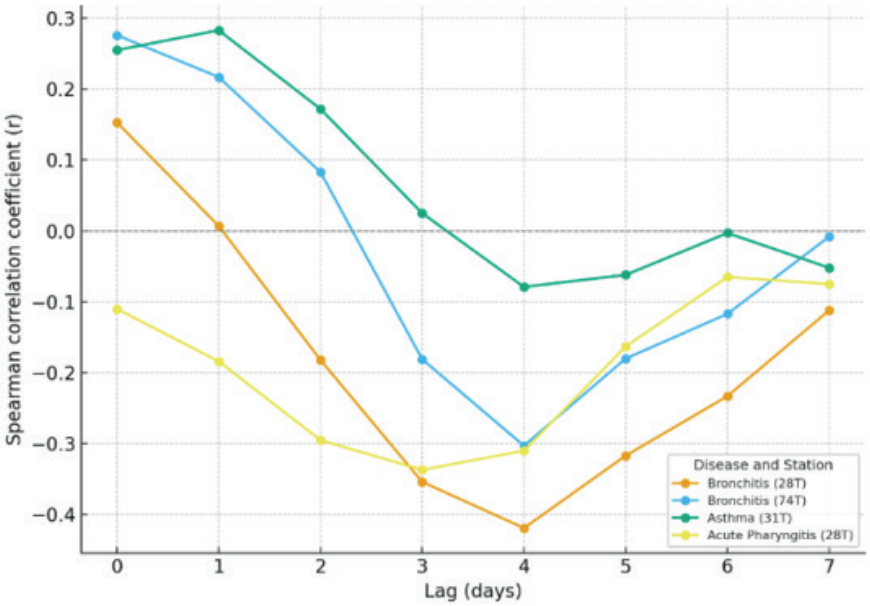

FIGURE 5. The Spearman correlation analysis between $PM_{2.5}$ exposure and selected respiratory diseases
Source: own work.

This finding suggests a modest temporal association between elevated ambient $PM_{2.5}$ levels and increased bronchitis visits. In contrast, negative correlations were observed at lag days 3–5 at Stations 28T and 29T, indicating possible short-term displacement patterns. Although the magnitude of the association was small, the same-day pattern is consistent with the hypothesis that short-term increases in $PM_{2.5}$ may contribute to acute bronchial irritation, particularly among susceptible populations such as children, older adults, and individuals with pre-existing respiratory conditions.

The "harvesting effect" phenomenon

As Table 5 and Figure 5 illustrate, various respiratory illnesses were negatively correlated with $PM_{2.5}$ concentrations at lag times ranging from 3 to 5 days, which may suggest a possible harvesting effect. Of particular note, bronchitis at Station 28T (lag 4: $r = -0.419$, $p < 0.01$) and pharyngitis at Station 28T (lag 3: $r = -0.337$, $p < 0.05$) exhibited strong negative correlations. In contrast, pollution may trigger acute illness among susceptible individuals shortly after safe pollution levels peak. This may subsequently reduce the number of susceptible individuals in the short term, contributing to the decline in case numbers after the initial increase. This temporal pattern is consistent with the air pollution-morbidity research using time series analyses. Past investigations have confirmed that such patterns of pollution-related health effects are plausible.

Interstation variability suggesting different pollution sources

As shown in Table 5 and Figure 5, the correlations varied significantly across monitoring stations. Station 74T showed the strongest immediate effect ($r = 0.276$, $p < 0.05$) while Stations 28T and 29T displayed distinct negative lagged correlations, suggesting a possible harvesting effect. However, no statistically significant correlations were observed for data collected at Station 30T and Station 31T. These spatial variations may reflect differences in the structure and origin of $PM_{2.5}$. Some of these differences may be attributable to combustion sources, motor vehicle exhaust, and local site characteristics.

No observable association for certain disease groups

As shown in Table 5, no significant correlations were identified for chronic rhinitis or influenza across all stations. This finding is consistent with the understanding that these diseases are primarily caused by viral or bacterial infections rather than direct particulate exposure. Nonetheless, $PM_{2.5}$ may act as a co-factor that exacerbates symptoms or increases susceptibility in individuals with underlying conditions, warranting further investigation in future epidemiological studies.

Conclusion and discussion

Short-term elevations in $PM_{2.5}$ in the pollution control zone of Rayong Province in Thailand were associated with increased respiratory morbidity, with the strongest signals observed for bronchitis (lag 0) and asthma (lag 1), and indications of harvesting at lags of 3–5 days. Significant positive correlations were observed for bronchitis ($r = 0.276$, $p < 0.05$) and asthma ($r = 0.283$, $p < 0.05$), with lag effects detected up to three days following exposure. Even where concentrations remained below the Thai standard, exceedance of the WHO guideline suggests that "moderate" pollution can still trigger clinically relevant events. Public health actions should include continuous monitoring, rapid risk communication, and targeted protection of susceptible groups, alongside emission controls tailored to industrial source profiles. Methodologically, future studies should adopt distributed lag (non-linear) and small-area designs and incorporate co-pollutants, meteorology, and chemical speciation to refine exposure–response estimates and causal interpretation.

This study provides exploratory evidence of a short-term temporal association between fine particulate matter ($PM_{2.5}$) and respiratory diseases in Rayong Province, an industrialized area of Thailand designated as a pollution control zone. The results indicated that elevated $PM_{2.5}$ concentrations were weak but significantly correlated with increased bronchitis and asthma cases on the same day and the following day. Negative correlations observed at lags of three to five days may reflect short-term temporal displacement, sometimes described as a harvesting effect. However, given the aggregated monthly design and the absence of distributed lag time-series modeling, this interpretation remains speculative. These findings are broadly consistent with previous time-series and multi-city studies reporting associations between short-term $PM_{2.5}$ exposure and respiratory hospital admissions, although differences in methodology limit direct comparability (Han et al., 2022; Wang et al., 2025).

The observed acute effects correspond to biological mechanisms reported in experimental and epidemiological literature, where $PM_{2.5}$ has been associated with oxidative stress and airway inflammation in experimental and epidemiological studies, airway inflammation, and reduced lung function (Atkinson et al., 2014; Mueller et al., 2021). Moreover, the pattern of negative correlations at lags of 3–5-day, also known as the "harvesting effect," has been widely documented in short-term mortality and morbidity studies across Asia and Europe (Gasparrini, 2022; Quijal-Zamorano et al., 2024). This phenomenon occurs when pollution events precipitate illness in vulnerable individuals, temporarily reducing the population at risk in subsequent days (Burnett et al., 2018). Spatial heterogeneity among

monitoring stations in Rayong suggests differences in emission sources and pollutant composition. Stations near petrochemical complexes (e.g., Station 74T) showed stronger acute effects, whereas those near mixed residential areas exhibited delayed responses consistent with findings from industrial regions where particle composition influences toxicity (Bootdee et al., 2023). A previous Thai study also reported significant associations between $PM_{2.5}$ and respiratory admissions in industrial areas of Eastern Thailand (Chatphuti & Jayathavaj, 2025), reinforcing the localized relevance of these findings. While the average $PM_{2.5}$ concentrations (18–21 $\mu g \cdot m^{-3}$) in this study remained below the Thai 24-hour standard (50 $\mu g \cdot m^{-3}$), they consistently exceeded the WHO, 2021 guideline of 15 $\mu g \cdot m^{-3}$. Global evidence indicates that adverse health effects can occur even at low-to-moderate concentrations of $PM_{2.5}$, suggesting that there is effectively no safe threshold for exposure (Health Effects Institute & Institute for Health Metrics and Evaluation [HEI & IHME], 2024; Parasin & Amnuaylojaroen, 2024). The stronger associations observed for pneumonia and bronchitis compared to COPD may reflect the acute inflammatory response triggered by short-term $PM_{2.5}$ exposure, which has been shown to increase airway inflammation and susceptibility to respiratory infections (Kyung & Jeong, 2020; Han et al., 2022; Teeranoraseth et al., 2024). Acute respiratory conditions are generally more sensitive to short-term environmental fluctuations, whereas chronic diseases such as COPD may demonstrate more heterogeneous or delayed responses across monitoring stations (Atkinson et al., 2014; Zhu et al., 2023). The magnitude of the associations observed in this study was relatively small. Such modest correlations are consistent with the multifactorial nature of respiratory diseases, in which air pollution represents one of several contributing environmental factors rather than a sole determinant.

This observation is consistent with international evidence demonstrating that both chronic and acute exposure to $PM_{2.5}$ are associated with increased mortality and morbidity, particularly from respiratory and cardiovascular diseases (Burnett et al., 2018). From a methodological perspective, this study employed a retrospective design utilizing Spearman correlation and lag analyses to identify short-term temporal associations. This approach is consistent with recent Thai studies that have successfully applied time-series and correlation methods to forecast pollution-related health outcomes (Li et al., 2023; Choocheep et al., 2024; Chumnicherngka et al., 2024). While this approach offers an accessible means of interpreting lagged effects, future investigations should incorporate distributed lag non-linear models (DLNMs) and Bayesian spatial frameworks to more comprehensively capture complex exposure–response relationships and spatial dependencies (Gasparrini, 2022; Quijal-Zamorano et al., 2024).

Integrating meteorological variables, co-pollutants, and source-specific emission data will further enhance the precision of exposure assessments and strengthen causal inference in future research. In the context of Thailand's environmental health management, the results indicate a need to strengthen local air quality surveillance, integrate environmental monitoring data with hospital admission and health surveillance systems, and enforce industrial emission regulations within designated pollution control zones (Chumnicherngka et al., 2024; Tanasirirak et al., 2024). These measures align with national strategies outlined in the Ministry of Natural Resources and Environment's Air Quality Action Plan and are reinforced by recent evidence linking $PM_{2.5}$ exposure to increased mortality from non-communicable diseases across Thailand (Yan, 2023; Parasin & Amnuaylojaroen, 2024).

This study provides additional evidence supporting a short-term association between $PM_{2.5}$ exposure and respiratory morbidity in an industrialized region of Thailand.

Finally, this study reinforces that short-term elevations in $PM_{2.5}$ concentrations, even at moderate levels, may contribute to increased respiratory health risk, particularly among vulnerable populations. These findings emphasize the necessity of continuous air quality monitoring, stricter emission control measures, and targeted preventive health policies to mitigate the growing burden of air pollution-related diseases in industrialized regions.

Continuous air quality monitoring, early warning systems, and the integration of environmental data into public health planning are recommended to reduce respiratory health risks in industrial regions.

Future studies incorporating meteorological variables and multivariate statistical models are warranted to better clarify potential causal pathways.

In conclusion, the present study demonstrated statistically significant but modest short-term associations between ambient $PM_{2.5}$ concentrations and respiratory morbidity in the pollution control zone of Rayong Province during 2020–2023. The strongest associations were observed for bronchitis on the same day of exposure and for asthma with a one-day lag, with evidence suggestive of short-term temporal displacement at lags of three to five days. Although effect sizes were small, $PM_{2.5}$ concentrations consistently exceeded WHO guideline levels, indicating that even moderate pollution may contribute to measurable respiratory health impacts in industrialized settings. These findings represent exploratory ecological evidence derived directly from the study analysis and underscore the public health relevance of continued air quality monitoring and targeted prevention strategies in pollution-affected regions.

Limitations

This study utilized hospitalization data from a single tertiary care hospital. While this institution serves as a major referral center in the region, the absence of data from smaller healthcare facilities may limit the complete capture of mild respiratory cases.

The absence of pre-pandemic morbidity data limits long-term comparisons of respiratory disease trends and constrains the interpretation of COVID-19-related behavioral effects within a broader historical context.

The absence of adjustment for potential confounders, including meteorological factors and co-pollutants, represents an important limitation. Seasonal patterns shared by air pollution and respiratory diseases may partially explain the observed correlations. Future research should apply time-series regression models or DLNMs to better isolate the independent short-term effects of $PM_{2.5}$ exposure.

The use of monthly aggregated data substantially reduces temporal resolution and limits the ability to evaluate true short-term daily exposure–response relationships. Daily-level time-series analyses would provide greater statistical power and conceptual consistency for distributed lag assessment. Therefore, the current findings should be interpreted as exploratory ecological associations rather than definitive short-term causal effects.

The use of fixed monitoring stations as exposure proxies and the absence of residential-level linkage may introduce exposure misclassification, potentially attenuating observed associations.

The analysis combined outpatient and inpatient visits within each diagnostic category. Differences in disease severity and healthcare utilization patterns may influence sensitivity to air pollution exposure. This aggregation could potentially dilute effect estimates, and future studies should consider stratified analyses by care setting.

Acknowledgments

This research could not have been completed without the support of the Faculty of Engineering, Rajamangala University of Technology Krungthep, which provided essential information and facilities for conducting the study. Furthermore, the researcher wishes to express sincere gratitude to the research team for their unwavering support and encouragement throughout the research process.

References

Amnuaylojaroen, T., Parasin, N., & Limsakul, A. (2022). Health risk assessment of exposure near-future $PM_{2.5}$ in Northern Thailand. *Air Quality, Atmosphere & Health*, *15*(11), 1963–1979. https://doi.org/10.1007/s11869-022-01231-x

Atkinson, R. W., Kang, S., Anderson, H. R., Mills, I. C., & Walton, H. A. (2014). Epidemiological time-series studies of $PM_{2.5}$ and daily mortality and hospital admissions: A systematic review and meta-analysis. *Thorax*, *69*(7), 660–665. https://doi.org/10.1136/thoraxjnl-2013-204492

Anggraeni, R. A. Y., & Lestari, K. S. (2023). The impact of $PM_{2.5}$ air pollutant exposure on human respiratory health: A literature review. *World Journal of Advanced Research and Reviews*, *19*(2), 1057–1064. https://doi.org/10.30574/wjarr.2023.19.2.1680

Bootdee, S., Tipayangkul, S., Timyoo, S., & Kawichai, S. (2023). Health risk assessment of $PM_{2.5}$ exposure in the initiative of the Eastern Economic Corridor Area Project during dry season in 2022: Case study of Rayong City. *The Journal of Industrial Technology*, *19*(1), 36–37. http://ojs.kmutnb.ac.th/index.php/joindtech/article/view/6306

Burnett, R., Chen, H., Szyszkowicz, M., Fann, N., Hubbell, B., Pope III, C. A., Apte, J. S., Brauer, M., Cohen, A., Weichenthal, S., Coggins, J., Di, Q., Brunekreef, B., Frostad, J., Lim, S. S., Kan, H., Walker, K. D., Thurston, G. D., Hayes, R. B., & … Spadaro, J. V. (2018). Global estimates of mortality associated with long-term exposure to outdoor fine particulate matter. *Proceedings of the National Academy of Sciences*, *115*(38), 9592–9597. https://doi.org/10.1073/pnas.1803222115

Chatphuti, C., & Jayathavaj, V. (2025). The association between $PM_{2.5}$ and the disease under surveillance from air pollution in Mueang Chiang Mai District, Chiang Mai Province. *Journal of Science and Technology to Community*, *3*(3), 31–43. https://doi.org/10.57260/stc.2025.1081

Chantaraprachoom, N., Shimadera, H., Uranishi, K., Mui, L. V., Matsuo, T., & Kondo, A. (2024). A nation-by-nation assessment of the contribution of southeast Asian open biomass burning to $PM_{2.5}$ in Thailand using the community multiscale air quality-integrated source apportionment method model. *Atmosphere*, *15*(11), 1358. https://doi.org/10.3390/atmos15111358

Cheanklin, N., Parniangtong, S., Manimnakorn, S., & Charoensuntisuk, N. (2017). Health Impacts in Pollution Control Area: Rayong Province. *Journal of Health Science of Thailand*, *21*(6), 1105–1118. https://thaidj.org/index.php/JHS/article/view/1196

Choocheep, P., Jayathavaj, V., & Swangsoonthonwes, P. (2024). Association between the Number of Cases of Air Pollution-Related Diseases and Air Quality in Mueang Nakhon Ratchasima District. *Journal of Health Promotion and Environmental Health, Health Center*, *18*(2), 473–484. https://he02.tci-thaijo.org/index.php/RHPC9Journal/article/view/266406

Choo, E. L. W., Janhavi, A., Koo, J. R., Yim, S. H., Dickens, B. L., & Lim, J. T. (2023). Association between ambient air pollutants and upper respiratory tract infection and pneumonia disease burden in Thailand from 2000 to 2022: a high frequency ecological analysis. *BMC Infectious Diseases*, *23*(1), 1–13. https://doi.org/10.1186/s12879-023-08185-0

Chumnicherngka, N., Jayathavaj, V., & Prommala, W. (2024). Forecasting the number of patients with air pollution-related diseases Health Region 9, Nakhon Ratchasima province. *Nakhon Ratchasima Rajabhat University Journal of Research in Science and Technology*, *9*(1), 20–26. https://ph02.tci-thaijo.org/index.php/sciencenrrujournal/article/view/250921

Gasparrini, A. (2022). A tutorial on the case time series design for small-area analysis. *BMC Medical Research Methodology*, *22*(1), 129, 1–8. https://doi.org/10.1186/s12874-022-01612-x

Han, C. H., Pak, H., Lee, J. M., & Chung, J. H. (2022). Short-term effects of exposure to particulate matter on hospital admissions for asthma and chronic obstructive pulmonary disease. *Medicine*, *101*(35), e30165. https://doi.org/10.1097/MD.0000000000030165

Health Effects Institute, & Institute for Health Metrics and Evaluation [HEI, & IHME]. (2024). *State of Global Air 2024 report*. https://www.stateofglobalair.org/resources/archived/state-global-air-report-2024

Kanchanasuta, S., Sooktawee, S., Patpai, A., & Vatanasomboon, P. (2020). Temporal variations and potential source areas of fine particulate matter in Bangkok, Thailand. *Air, Soil and Water Research*, *13*, 1178622120978203. https://doi.org/10.1177/1178622120978203

Kim, S. Y., Peel, J. L., Hannigan, M. P., Dutton, S. J., Sheppard, L., Clark, M. L., & Vedal, S. (2012). The temporal lag structure of short-term associations of fine particulate matter chemical constituents and cardiovascular and respiratory hospitalizations. *Environmental Health Perspectives*, *120*(8), 1094–1099. https://doi.org/10.1289/ehp.1104721

Kyung, S. Y., & Jeong, S. H. (2020). Particulate-matter related respiratory diseases. *Tuberculosis and Respiratory Diseases*, *83*(2), 116–121. https://doi.org/10.4046/trd.2019.0025

Li, J., Liang, L., Lyu, B., Cai, Y. S., Zuo, Y., Su, J., & Tong, Z. (2023). Double trouble: Interaction of $PM_{2.5}$ and O_3 on respiratory hospital admissions. *Environmental Pollution*, *33*8, 1–8. https://doi.org/10.1016/j.envpol.2023.122665

Mueller, W., Vardoulakis, S., Steinle, S., Loh, M., Johnston, H. J., Precha, N., Kliengchuay, W., Sahanavin, N., Nakhapakorn, K., Sillaparassamee, R., Tantrakarnapa, K., & Cherrie, J. W. (2021). A health impact assessment of long-term exposure to particulate air pollution in Thailand. *Environmental Research Letters*, *16*(5), 055018. https://doi.org/10.1088/1748-9326/abe3ba

Muenmee, S. & Bootdee, S. (2021). Health risk assessment of exposure $PM_{2.5}$ from industrial area in Pluak Daeng district, Rayong province. *Health Science, Science and Technology Reviews*, *14*(3), 95–110. https://li01.tci-thaijo.org/index.php/journalup/article/view/248513

Parasin, N., & Amnuaylojaroen, T. (2024). Effect of $PM_{2.5}$ on burden of mortality from non-communicable diseases in northern Thailand. *PeerJ*, *12*, e18055. https://doi.org/10.7717/peerj.18055

Phosri, A., Ueda, K., Phung, V. L. H., Tawatsupa, B., Honda, A., & Takano, H. (2019). Effects of ambient air pollution on daily hospital admissions for respiratory and cardiovascular diseases in Bangkok, Thailand. *The Science of the Total Environment*, *651*(Pt 1), 1144–1153. https://doi.org/10.1016/j.scitotenv.2018.09.183

Pothirat, C., Tosukhowong, A., Chaiwong, W., Liwsrisakun, C., & Inchai, J. (2016). Effects of seasonal smog on asthma and COPD exacerbations requiring emergency visits in Chiang Mai, Thailand. *Asian Pacific Journal of Allergy and Immunology*, *34*(4), 284–289. https://doi.org/10.12932/AP0668

Quijal-Zamorano, M., Martinez-Beneito, M. A., Ballester, J., & Marí-Dell'Olmo, M. (2024). Spatial Bayesian distributed lag non-linear models (SB-DLNM) for small-area exposure-lag-response epidemiological modelling. *International Journal of Epidemiology*, *53*(3), dyae061. https://doi.org/10.1093/ije/dyae061

Suwanprapha, M., Srisaard, T., Pongtong, P., Sukcharoen, J., Mueankan, S., Udomwiset, N., & Numpa, S. (2024). Quantity of fine particulate matter ($PM_{2.5}$) and assessment of respiratory health risks among individuals at a university in inner Bangkok. *Disease Control Journal*, *50*(4), 703–715. https://doi.org/10.14456/dcj.2024.57

Tanasirirak, N., Chamnichongkha, N., Jayathavaj, V., & Sunan, R. (2024). Forecasting the number of patients with the disease due to the effects of air pollution and its relationship with air pollution levels, Chiang Rai province. *Chiang Rai Medical Journal (CRMJ)*, *16*(3), 35–46. https://he01.tci-thaijo.org/index.php/crmjournal/article/view/271153

Teeranoraseth, T., Chaiyasate, S., & Roongrotwattanasiri, K. (2024). Acute effect of particulate matter 2.5 ($PM_{2.5}$) on acute upper respiratory tract infection in Chiang Mai, Thailand. *Journal of the Medical Association of Thailand*, *107*(2), 114–119. https://doi.org/10.35755/jmedassocthai.2024.2.13948

Vichit-Vadakan, N., Vajanapoom, N., & Ostro, B. (2008). The Public Health and Air Pollution in Asia (PAPA) Project: Estimating the mortality effects of particulate matter in Bangkok, Thailand. *Environmental Health Perspectives*, *116*(9), 1179–1182. https://doi.org/10.1289/ehp.10849

Wang, Y., Chen, J., Zhou, Q., Kang, S., Jiang, Y., Xiang, J., Wu, J., Li, J., Chen, Z., & Wu, C. (2025). Time series analysis of low-concentration air pollution and hospital respiratory disease outpatient visits. *Frontiers in Public Health*, *13*, 1–14. https://doi.org/10.3389/fpubh.2025.1585086

World Health Organization [WHO]. (2021). *WHO global air quality guidelines: Particulate matter ($PM_{2.5}$ and PM_{10}), ozone, nitrogen dioxide, sulfur dioxide and carbon monoxide.* https://www.who.int/publications/i/item/9789240034228

Yan, W. (2023). Effect of $PM_{2.5}$ air pollution on the incidence of respiratory diseases: A Python-based data analysis. *Theoretical and Natural Science*, *8*(1), 70–75. https://doi.org/10.54254/2753-8818/8/20240361

Zhu, R. X., Nie, X. H., Liu, X. F., Zhang, Y. X., Chen, J., Liu, X. J., & Hui, X. J. (2023). Short-term effect of particulate matter on lung function and impulse oscillometry system (IOS) parameters of chronic obstructive pulmonary disease (COPD) in Beijing, China. *BMC Public Health*, *23*(1), 1417. https://doi.org/10.1186/s12889-023-16308-0

Appendix

TABLE S1. Full Spearman correlation matrix across all lag periods (N = 45–52)

Disease	Station	lag 0	lag 1	lag 2	lag 3	lag 4	lag 5	lag 6	lag 7	Strongest correlation
Chronic obstructive pulmonary disease (COPD)	28T	0.072	0.098	−0.009	−0.107	−0.142	−0.130	−0.268	−0.296*	−0.296* (lag 7)
	29T	−0.006	0.194	0.067	−0.029	−0.039	0.017	−0.227	−0.241	NS
	30T	0.057	0.240	0.080	−0.102	−0.019	−0.004	−0.209	−0.209	NS
	31T	0.042	0.195	0.125	0.013	−0.006	0.050	−0.172	−0.233	NS
	74T	0.075	0.206	0.095	−0.020	−0.068	−0.001	−0.210	−0.245	NS
Asthma	28T	0.052	−0.016	−0.145	−0.240	−0.304*	−0.278	−0.252	−0.230	−0.304* (lag 4)
	29T	0.208	0.252	0.153	−0.024	−0.125	−0.140	−0.027	−0.087	NS
	30T	0.153	0.160	0.072	−0.019	−0.047	0.002	0.050	0.056	NS
	31T	0.255	0.283*	0.172	0.025	−0.079	−0.062	−0.003	−0.052	0.283* (lag 1)
	74T	0.259	0.230	0.101	−0.042	−0.151	−0.078	−0.050	−0.073	NS
Influenza	28T	−0.023	−0.080	−0.215	−0.268	−0.259	−0.189	−0.164	−0.101	NS
	29T	0.203	0.225	0.116	−0.019	−0.033	0.030	0.062	0.102	NS
	30T	0.129	0.141	0.012	−0.043	−0.055	0.043	0.100	0.157	NS
	31T	0.256	0.262	0.155	0.025	0.007	0.094	0.092	0.086	NS
	74T	0.204	0.172	0.083	−0.060	−0.074	0.024	0.019	0.027	NS
Acute pharyngitis	28T	−0.110	−0.184	−0.295*	−0.337*	−0.310*	−0.163	−0.065	−0.075	−0.337* (lag 3)
	29T	0.104	0.146	0.077	−0.044	−0.078	0.048	0.186	0.172	NS
	30T	0.031	0.069	−0.003	−0.077	−0.100	0.039	0.159	0.156	NS
	31T	0.134	0.168	0.087	−0.041	−0.062	0.101	0.210	0.140	NS
	74T	0.069	0.085	0.007	−0.158	−0.184	−0.005	0.099	0.060	NS
Chronic rhinitis	28T	−0.041	0.121	0.127	0.149	0.097	0.055	0.011	−0.118	NS
	29T	−0.175	0.059	0.152	0.060	0.016	0.090	0.043	−0.059	NS
	30T	−0.099	0.137	0.167	0.082	0.119	0.075	0.066	−0.091	NS
	31T	−0.189	0.048	0.106	0.038	0.017	0.113	0.057	−0.089	NS
	74T	−0.151	0.110	0.107	0.043	−0.010	0.122	0.078	−0.071	NS
Bronchitis	28T	0.153	0.007	−0.182	−0.354*	−0.419	−0.317*	−0.233	−0.112	−0.419** (lag 4)
	29T	0.199	0.160	0.066	−0.211	−0.331*	−0.296*	−0.194	−0.077	−0.331* (lag 4)
	30T	0.166	0.135	−0.020	−0.206	−0.229	−0.099	−0.005	0.063	NS
	31T	0.258	0.240	0.122	−0.152	−0.273	−0.193	−0.117	−0.038	NS
	74T	0.276*	0.217	0.083	−0.181	−0.303*	−0.180	−0.117	−0.008	0.276* (lag 0)
All diseases combine	28T	0.024	−0.067	−0.224	−0.333*	−0.349*	−0.242	−0.164	−0.117	−0.349* (lag 4)
	29T	0.186	0.207	0.094	−0.110	−0.183	−0.096	0.016	0.061	NS
	30T	0.110	0.140	0.023	−0.098	−0.121	−0.007	0.109	0.158	NS
	31T	0.239	0.260	0.142	−0.061	−0.128	−0.010	0.071	0.070	NS
	74T	0.212	0.203	0.074	−0.126	−0.200	−0.057	0.011	0.029	NS

*$p < 0.05$; **$p < 0.01$; NS – not statistically significant; lag 0 – same-day exposure.

Chaiprakarn, S., Kheawseema, P., Sakulthaew, C., Saengseedam, P. (2026). The association between ambient fine particulate matter ($PM_{2.5}$) concentrations and air pollution-related respiratory disease at the pollution control zone of Rayong Province, Thailand. *Sci. Rev. Eng. Env. Sci.*, *35* (2), 117–138. DOI 10.22630/srees.10910

Summary

The association between ambient fine particulate matter ($PM_{2.5}$) concentrations and air pollution-related respiratory disease at the pollution control zone of Rayong Province, Thailand. This study investigated the association between ambient $PM_{2.5}$ concentrations and respiratory diseases at the pollution control zone of Rayong Province in Thailand during 2020–2023. Daily $PM_{2.5}$ data were obtained from air quality monitoring stations, and hospital records of pneumonia, bronchitis, asthma, and chronic obstructive pulmonary disease (COPD) were analyzed. Spearman rank correlation and time-lag analyses (lags 0–7 days) were performed using IBM SPSS Statistics version 26.0. Significant positive correlations were observed between $PM_{2.5}$ concentrations and bronchitis ($r = 0.276$, $p < 0.05$) and asthma ($r = 0.283$, $p < 0.05$), with lag effects detected up to three days following exposure. Weaker or non-significant associations were found for COPD. These findings suggest that short-term exposure to elevated $PM_{2.5}$ levels may increase the risk of acute respiratory conditions. Continuous air quality monitoring and early warning systems are therefore essential to mitigate health impacts in industrial regions.

Scientific Review Engineering and Environmental Sciences (2026), 35 (2), 139–157

Sci. Rev. Eng. Env. Sci. (2026), 35 (2) https://srees.sggw.edu.pl

ISSN 1732-9353 (suspended) eISSN 2543-7496 DOI 10.22630/srees.10965

Received: 23.11.2025
Accepted: 11.03.2026

Michał TRZECIAK[1]✉

Daria SIKORSKA[2]

[1] Warsaw University of Life Sciences – SGGW, Faculty of Civil and Environmental Engineering, Poland

[2] Warsaw University of Life Science – SGGW, Centre for Climate Research, Poland

✉m.trzeciak99@gmail.com

The role of roadside vegetation near school in mitigating air pollution: an exploratory case study in Zielonka

Keywords: urban air pollution, particulate matter, PM, urban vegetation, leaf area index, LAI, seasonal variation, children's exposure

Introduction

Air pollution is a major environmental and public health issue, with an estimated contribution to 7.9 million deaths in 2023. It currently ranks as the leading environmental risk factor for mortality worldwide, particularly impacting urban areas (Health Effects Institute & Institute for Health Metrics and Evaluation [HEI & IHME], 2025). Vehicle emissions and the use of fossil fuels for heating are significant sources of harmful pollutants (Karagulian et al., 2015; Liu et al., 2025). Children are particularly vulnerable to high pollutant concentrations due to their frequent outdoor activities, which can negatively impact their respiratory, cardiovascular, and cognitive health (Roche et al.,

Trzeciak, M., Sikorska, D. (2026). The role of roadside vegetation near school in mitigating air pollution: an exploratory case study in Zielonka. *Sci. Rev. Eng. Env. Sci.*, *35* (2), 139–157. DOI 10.22630/srees.10965

2024). Fine particulate matter (PM_1, $PM_{2.5}$, PM_{10}) poses significant health risks as it penetrates deep into the respiratory system (Kim et al., 2015). This exposure often occurs near roads and schools, highlighting the need for strategies to reduce pollution during children's daily commutes. One promising approach is the introduction and enhancement of urban greenery, which utilizes plants' ability to trap pollutants on the leaf surface. Urban vegetation, especially trees, can effectively capture airborne particles on leaf surfaces, thereby lowering concentrations of particulate matter (PM) and ultimately providing measurable health benefits (Escobedo et al., 2011; Nowak et al., 2014). These particles are primarily captured through interception, where they adhere to the leaf surface or become embedded in the wax layer (Przybysz et al., 2019). Research indicates that home-to-school walking routes with higher visible greenery are associated with better exposure metrics and increased potential for well-being benefits (Khanian et al., 2024). While most particles remain loosely attached and can be washed away by rain, those trapped in waxes are immobilized for extended periods (Beckett et al., 2000; Przybysz et al., 2014). Strategic planting of trees and shrubs can reduce ambient $PM_{2.5}$ levels by up to 10% in densely built environments (McDonald et al., 2007), resulting in significant health benefits that extend beyond improved respiratory health (Lee et al., 2015). However, seasonal, structural, and spatial factors limit the ability of urban trees to mitigate air pollution. Although vegetation can intercept airborne particles, its effectiveness depends on factors such as canopy density, species characteristics, and air circulation patterns (Barwise & Kumar, 2020). Seasonal variations further constrain performance; during winter dormancy, reduced leaf area leads to decreased pollutant interception. Trees along children's school routes provide limited PM reduction in winter, and dense vegetation can sometimes increase local pollutant concentrations (Hoppa et al., 2022).

In this study, we will evaluate how the density of roadside vegetation, measured by LAI, affects children's exposure to particulate matter (PM_1, $PM_{2.5}$, PM_{10}). We will collect data along the most frequented school routes in a suburban setting using a mobile PM monitoring device during typical morning commute hours. We aim to explore the relationship between LAI and PM levels based on two measurement campaigns representing leaf-off (March) and leaf-on (September) conditions. Our findings will provide valuable insight which may be useful to design vegetation interventions that effectively reduce children's exposure to pollutants.

Material and methods

Study area

The study was conducted in the city of Zielonka, a suburban municipality on the eastern edge of the Warsaw metropolitan area, characterized by a mix of forested areas, low-density housing, small parks and several transport corridors. This heterogeneity creates neighborhood-scale contrasts in vegetation structure and traffic emissions relevant for analyzing particulate matter concentrations.

The town has four public primary schools, each situated in a distinct neighborhood (Fig. 1). We included all four schools to obtain geographically replicated sampling sites that capture variation in local vegetation and emission conditions within a single municipality. Primary schools provide an informative proxy for children's daily exposure because: (i) young children are more vulnerable to air pollution, (ii) Polish primary pupils typically attend the nearest school due to regionalization policies, meaning that the school environment reflects their immediate residential area, and (iii) this age group is the most likely to walk or use public transport, making the school surroundings representative of exposure conditions along their everyday commuting routes.

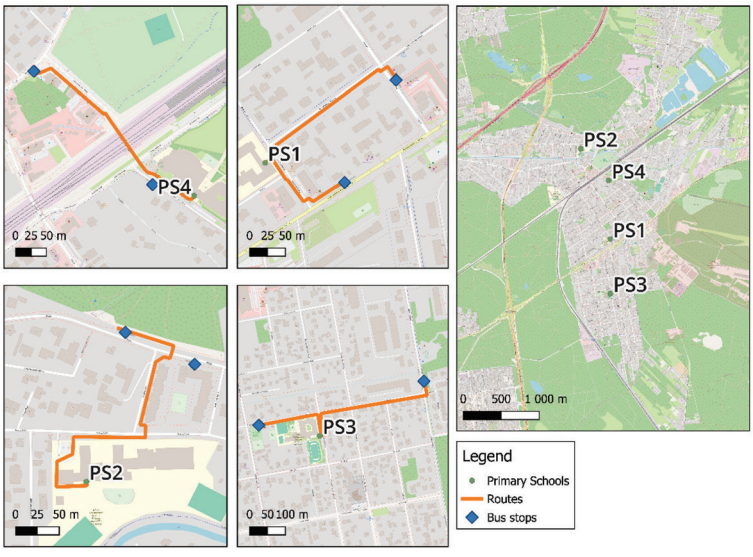

FIGURE 1. Study area within Zielonka, lines represent analyzed school routes
Source: own work on the basis of a background generated in portalmap OpenStreetMap (2025).

Traffic context

Detailed traffic count data were not available for all streets in Zielonka at the time of the study. However, the town is crossed by two major regional roads (No. 631 and No. 634), which can be classified as high-traffic routes based on the general traffic measurement conducted by the General Directorate for National Roads and Motorways (GDDKiA, 2020). These roads can be considered major sources of vehicular emissions in the study area. Primary School 1 (PS1) is located directly adjacent to one of these high-traffic roads, whereas Primary Schools 2 and 3 (PS2 and PS3) are situated approximately 500 m away. Primary School 4 (PS4) is located at a greater distance, approximately 1,000 m from the nearest major traffic corridor. Local residential streets along the school routes were assumed to carry substantially lower traffic volumes, typically on the order of 1,000–5,000 vehicles per day and were therefore expected to have a considerably smaller influence on ambient particulate matter dispersion compared to the main roads.

Sampling design and data collection

To identify the most relevant pedestrian routes for sampling, we combined pilot observations and local knowledge with GIS analysis (QGIS Development Team, 2023). Routes we chose were based on: (i) frequency of use by pupils commuting to school, (ii) presence of roadside vegetation with potential for air-quality mitigation, and (iii) accessibility from public transport stops and safe pedestrian pathways. For each school we mapped segments connecting the nearest bus stops to the school entrance (Fig. 1) and later verified them in the field. Segment lengths ranged from 230 m to 500 m, capturing areas where the majority of pupils are likely exposed to vegetation and traffic-related pollutants. Importantly, these routes were not treated as homogeneous units. They were selected to represent strong spatial gradients in vegetation structure, which are characteristic of school surroundings in Zielonka. Contrasts between sparsely vegetated street sections and highly vegetated areas near school grounds, parks, or forest edges allowed us to examine how particulate matter concentrations varied along short distances with changing canopy density.

Air pollution assessment

We measured PM_1, $PM_{2.5}$, PM_{10} concentrations along the selected routes using a Sniffer4D mobile air-quality monitor. The sensor was carried at a height of approximately 1.3 m to reflect the breathing zone of children. We conducted measurements on two weekday mornings, starting around 8:00 AM, corresponding to peak pupil commuting times and traffic intensity, ensuring representative exposure levels. We conducted field campaigns on March 19 (minimal vegetation cover) and September 4 (peak vegetation activity). Regional meteorological conditions were verified using archival data from the nearest available synoptic station (Institute of Meteorology and Water Management [IMGW-BIP], 2025). Both measurement days were dry, with no recorded precipitation. Mean daily wind speed was moderate in March (4.2 $m \cdot s^{-1}$) and low in September (about 2 $m \cdot s^{-1}$), indicating that strong wind-driven dispersion was unlikely to dominate particulate matter concentrations during the surveys.

Vegetation assessment

We quantified the potential of roadside vegetation to mitigate PM exposure using the LAI, which represents the total leaf area per unit of ground surface and serves as a key indicator of vegetation density and filtering capacity (Oguntunde et al., 2012). We measured LAI with the SunScan Canopy Analysis System at regular intervals along each route (approximately 30 m) to capture spatial variation in canopy cover. This allowed us to obtain detailed, segment-specific characterization of the vegetation children are exposed to during their commute.

Data analysis

We conducted statistical analysis in two steps. First, we calculated correlations between LAI and PM concentrations using Pearson's and Spearman's coefficients to capture both linear and monotonic relationships. The analysis was done in RStudio (R Core Team, 2025). To account for spatial heterogeneity, and potential modifiers of particulate matter concentrations, we used geospatial information from the BDOT10k topographic database (Head Office of Geodesy and Cartography [GUGiK], 2025). We assigned each PM measurement point a surrounding buffer (50 m radius) using GIS and quantified the proportion of built-up area. This variable reflects the surrounding urban structure, which can influence pollutant dispersion.

Trzeciak, M., Sikorska, D. (2026). The role of roadside vegetation near school in mitigating air pollution: an exploratory case study in Zielonka. *Sci. Rev. Eng. Env. Sci.*, *35* (2), 139–157. DOI 10.22630/srees.10965

The number of spatial measurement points per school route ranged from 6 to 11. These points represent distinct locations with different vegetation and built-environment characteristics and were analyzed as spatial gradients rather than independent replicates.

Points are spatially autocorrelated and were treated as exploratory observations rather than independent replicates.

Our analysis focused on identifying potential associations between vegetation density along school commuting routes and children's exposure to particulate matter, while acknowledging that other factors – such as wind, urbanization, traffic patterns, and species composition, which also influence pollutant concentrations.

Results and discussion

We observed pronounced differences between leaf-off and leaf-on conditions, reflected in both vegetation structure and particulate matter concentrations (Table 1).

TABLE 1. Seasonal variation of leaf area index (LAI) and particulate matter (PM_1, $PM_{2.5}$, PM_{10}) concentrations with descriptive statistics

Parameter	Unit	Minimum	Maximum	Mean ±*SD*
Measurement		leaf-off		
LAI	–	0.1	2.5	0.57 ±0.43
PM_1	$\mu g \cdot m^{-3}$	25	48	32.5 ±3.75
$PM_{2.5}$	$\mu g \cdot m^{-3}$	36	81	50.59 ±6.96
PM_{10}	$\mu g \cdot m^{-3}$	38	89	54.66 ±8.44
Measurement		leaf-on		
LAI	–	0.6	8.7	5.47 ±2.21
PM_1	$\mu g \cdot m^{-3}$	4	25	7.26 ±1.74
$PM_{2.5}$	$\mu g \cdot m^{-3}$	6	44	9.35 ±3.14
PM_{10}	$\mu g \cdot m^{-3}$	6	45	9.92 ±3.19

Source: own work.

Particulate matter concentrations were substantially lower during leaf-on compared to leaf-off, reflecting both increased canopy density and the expected mitigation effect of urban vegetation. LAI was several times higher during leaf-on conditions, consistent with full canopy development. These seasonal contrasts shaped the magnitude and detectability of vegetation–PM relationships across the study area (Przybysz et al., 2019; Hoppa et al., 2022). Interestingly, while mean PM levels

were consistently lower in leaf-on conditions, some maximum concentrations were actually higher than in leaf-off, indicating that dense vegetation can under certain conditions locally reduce airflow and enhance pollutant accumulation. This suggests that the effect of greenery is positive at low and moderate PM levels, but in episodes of extreme pollution, the vegetation can contribute to temporary local PM peaks.

Correlations between LAI and PM were weak but consistently negative (Table 2). This indicates a limited yet measurable influence of vegetation on reducing airborne particles. The strength of these relationships varied among the measurement points.

TABLE 2. Results of general Pearson's correlation analysis

Campaign	Size of particulates	r	p	R^2
Leaf-off	PM_1	−0.16	*	0.02
	$PM_{2.5}$	−0.15	*	0.02
	PM_{10}	−0.16	*	0.02
Leaf-on	PM_1	−0.08	*	0.01
	$PM_{2.5}$	−0.09	*	0.01
	PM_{10}	−0.09	*	0.01

Source: own work.

Correlations between LAI and particulate matter were consistently negative but weak in both seasons (Table 2). *P*-values are included for completeness but should be interpreted with caution due to spatial autocorrelation and the limited independence of measurement points.

Small effect sizes suggest that vegetation explains only a minor share of PM variability at the scale of our transects, although local differences between schools indicate that spatial configuration of greenery and airflow patterns may also play an important role. The slightly stronger correlations observed in leaf-off conditions can be attributed to higher background pollution, which increases the detectability of vegetation-related effects. Even under leaf-off conditions, evergreen species and woody surfaces contribute to particle deposition, making vegetation signals more discernible during periods of elevated emissions (Hoppa et al., 2022).

Correlations calculated separately for each school (Table 3) revealed clear local differences. While all relationships were generally negative, their magnitude varied across sites and seasons, suggesting that vegetation effects are strongly conditioned by urban form, canopy structure, and nearby emission sources.

Trzeciak, M., Sikorska, D. (2026). The role of roadside vegetation near school in mitigating air pollution: an exploratory case study in Zielonka. *Sci. Rev. Eng. Env. Sci.*, *35* (2), 139–157. DOI 10.22630/srees.10965

TABLE 3. Results of Pearson's correlation analysis for each school in leaf-off and leaf-on conditions

School	Leaf-off			Leaf-on			*n*
	size of particulates	*r*	*p*	size of particulates	*r*	*p*	
PS1	PM_1	−0.13	4.46×10^{-2}	PM_1	−0.19	*	
PS1	$PM_{2.5}$	−0.12	**6.91×10^{-2}**	$PM_{2.5}$	−0.20	*	7
PS1	PM_{10}	−0.01	**8.29×10^{-1}**	PM_{10}	−0.21	*	
PS2	PM_1	−0.28	*	PM_1	−0.38	*	
PS2	$PM_{2.5}$	−0.25	*	$PM_{2.5}$	−0.48	*	10
PS2	PM_{10}	−0.33	*	PM_{10}	−0.45	*	
PS3	PM_1	−0.35	*	PM_1	−0.01	**8.51×10^{-1}**	
PS3	$PM_{2.5}$	−0.32	*	$PM_{2.5}$	0.02	**6.14×10^{-1}**	11
PS3	PM_{10}	−0.31	*	PM_{10}	0.02	**5.60×10^{-1}**	
PS4	PM_1	−0.08	**1.97×10^{-1}**	PM_1	−0.15	6.21×10^{-3}	
PS4	$PM_{2.5}$	0.08	**1.87×10^{-1}**	$PM_{2.5}$	−0.15	6.19×10^{-3}	6
PS4	PM_{10}	0.06	**3.62×10^{-1}**	PM_{10}	−0.15	5.97×10^{-3}	

P-values are reported for completeness but should be interpreted with caution due to spatial autocorrelation and the lack of independent temporal replication. Please note that some values (marked in red) have $p \geq 0.05$.

Source: own work.

The highest correlations occurred for Primary Schools PS2 and PS3 in leaf-off conditions. In leaf-on conditions, correlations tended to strengthen, reflecting higher levels of vegetation. These findings highlight the context-dependent role of greenery, where vegetation effects on local air quality become more pronounced under higher pollution loads and in sheltered microenvironments.

Primary School 1 (PS1)

The PS1 route is dominated by low-density housing, wide streets, and sparse vegetation. PM concentrations were relatively uniform during leaf-off conditions, with minor increases near intersections, and decreased substantially during leaf-on conditions. Correlations between LAI and PM remained weak on both measurement days ($r \approx -0.13$ to -0.21). This may indicate that the limited and discontinuous canopy exerted only a small influence on local particulate levels.

Primary School 2 (PS2)

The PS2 route includes a forest edge, an open parking area, and a densely vegetated schoolyard. PM concentrations peaked over the parking zone in both measurement campaigns and declined sharply within the school grounds. This route showed some of the strongest correlations in the study ($r \approx -0.25$ to -0.48). This may suggest that where canopy cover is continuous and structurally diverse, vegetation is more closely associated with reductions in local particulate concentrations.

Primary School 3 (PS3)

The PS3 is situated within compact single-family housing with narrow streets and restricted airflow. In leaf-off conditions, PM concentrations were higher in areas with minimal greenery, yielding moderate negative correlations ($r \approx -0.31$ to -0.35). In leaf-on conditions, overall concentrations declined, likely because of low pollution levels and increased atmospheric mixing masked vegetation-related signals.

Primary School 4 (PS4)

The PS4 route follows a park boundary and passes through a railway underpass before continuing along low-density residential streets. PM concentrations were moderately high but spatially uniform in leaf-off conditions, likely due to effective ventilation provided by open park spaces. In leaf-on conditions, concentrations decreased and correlations remained weak ($r \approx -0.15$), indicating that vegetation effects were overshadowed by dispersion processes in this open setting.

Detailed comparison – individual school routes

Correlations between LAI and PM differed notably among the routes studied (Table 3), reflecting local variability in vegetation structure, built-up density, and microclimatic conditions observed on measurement days.

The PS1 route runs mainly through low-density residential areas with wide streets and sparse greenery. During leaf-off conditions, PM concentrations were relatively uniform, with slightly higher values near intersections (Fig. 2a). In leaf-on conditions, concentrations dropped considerably (Fig. 2b), mainly due to improved atmospheric dispersion and reduced emissions rather than vegetation

Trzeciak, M., Sikorska, D. (2026). The role of roadside vegetation near school in mitigating air pollution: an exploratory case study in Zielonka. *Sci. Rev. Eng. Env. Sci.*, *35* (2), 139–157. DOI 10.22630/srees.10965

effects. Correlations between LAI and PM were weak in both seasons ($r \approx -0.13$ to -0.21), indicating only a minor spatial association between canopy cover and particulate concentrations along this route.

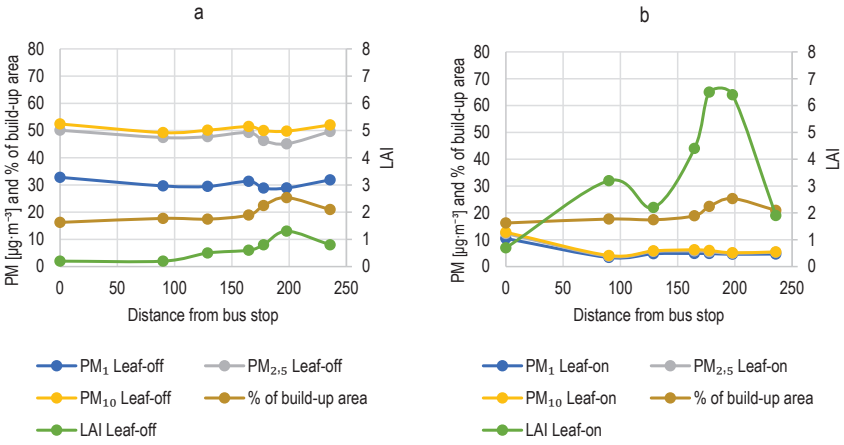

FIGURE 2. Leaf area index (LAI), percentage of build-up area and particulate matter (PM) concentrations across school route of Primary School 1 (detached housing, wide streets) in leaf-off (a) and leaf-on conditions (b)

Source: own work.

The PS2 route includes a mix of forest edge, open parking area, and vegetated schoolyard. In leaf-off conditions PM concentrations peaked over the parking zone and dropped sharply within the schoolyard (Fig. 3a). In leaf-on conditions, overall levels were lower but the spatial pattern remained similar (Fig. 3b). Here, correlations were one of the strongest among all schools ($r \approx -0.25$ to -0.48), suggesting that locations with denser and more continuous vegetation coincided with lower particulate matter concentrations, particularly where canopy continuity is high and air movement is unconstrained.

Primary School PS3 is located within a compact residential development characterized by narrow streets and limited air circulation. Leaf-off data (Fig. 4a) showed higher PM concentrations in zones with minimal greenery. The leaf-off relationship ($r \approx -0.31$ to -0.35) indicates a spatial co-occurrence of higher PM concentrations with areas of lower vegetation cover during a period of elevated background pollution. This is consistent with the role of evergreen vegetation in maintaining partial filtration capacity during periods of elevated emissions.

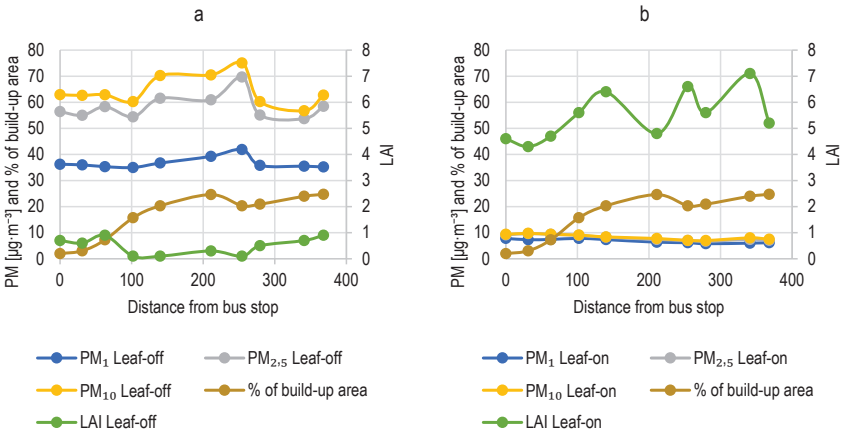

FIGURE 3. Leaf area index (LAI), percentage of build-up area and particulate matter (PM) concentrations across school route of Primary School 2 (mixed environment: forest, parking area, schoolyard) in leaf-off (a) and leaf-on conditions (b)

Source: own work.

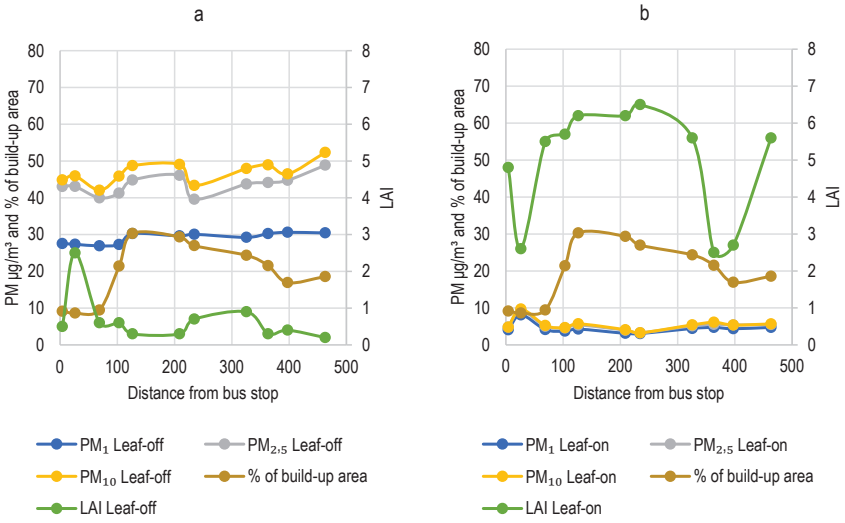

FIGURE 4. Leaf area index (LAI), percentage of build-up area and particulate matter (PM) concentrations across school route of Primary School 3 (narrow streets, compact single-family housing) in leaf-off (a) and leaf-on conditions (b)

The PS4 route follows a park boundary, passes through a railway underpass, and continues along the school fence near single-family homes. In leaf-off conditions, PM levels were moderately high but spatially uniform (Fig. 5a),

Trzeciak, M., Sikorska, D. (2026). The role of roadside vegetation near school in mitigating air pollution: an exploratory case study in Zielonka. *Sci. Rev. Eng. Env. Sci.*, *35* (2), 139–157. DOI 10.22630/srees.10965

likely due to efficient air mixing facilitated by open park spaces and tall trees. In leaf-on conditions (Fig. 5b), overall concentrations decreased, and correlations remained weak ($r \approx -0.15$), indicating that dispersion processes likely dominated over any direct vegetation-related spatial patterns.

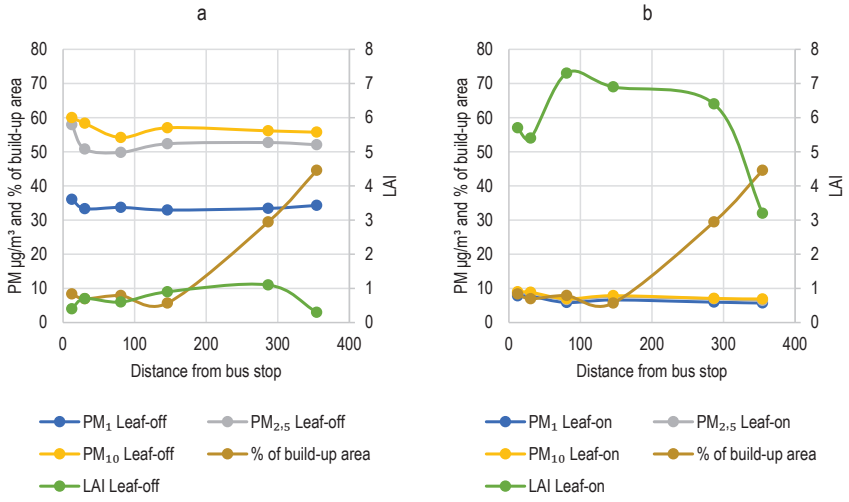

FIGURE 5. Leaf area index (LAI), percentage of build-up area and particulate matter (PM) concentrations across school route of Primary School 3 (route adjacent to park and railroad tracks) in leaf-off (a) and leaf-on conditions (b)

Source: own work.

Our results highlight three consistent patterns: (i) leaf-off conditions produced markedly higher PM concentrations, whereas leaf-on conditions produced higher LAI and lower pollution; (ii) vegetation–PM correlations were weak but consistently negative; and (iii) the strength of these relationships varied among school routes, reflecting differences in canopy continuity, street geometry, and local emissions.

These findings are broadly consistent with earlier work showing that urban vegetation can reduce airborne particle concentrations, but that such effects are typically localized and modest (Escobedo et al., 2011; Nowak et al., 2014; Janhäll, 2015). They also align with studies indicating that the influence of greenery becomes less detectable when emissions and meteorological conditions dominate the air-quality signal (Karagulian et al., 2015; Liu et al., 2025).

Seasonal patterns strongly shaped the relationship between vegetation and PM. During winter, PM concentrations were substantially higher due to residential

heating and reduced atmospheric dispersion, which is consistent with previous work documenting the dominant role of emission intensity and stagnant conditions in shaping urban air quality (Juda-Rezler et al., 2020; Hoppa et al., 2022). These elevated background levels increased the contrast between more and less vegetated segments, making vegetation-related spatial associations more apparent in the data. Even with low LAI during leaf-off conditions, evergreen species and the deposition of particles on woody plant surfaces may still support modest filtration (Beckett et al., 2000; Przybysz et al., 2019).

In contrast, September measurements were characterized by much lower PM concentrations and higher atmospheric mixing. While LAI increased severalfold compared to March campaign, the low pollution background introduced greater variability relative to the vegetation signal, which likely masked small spatial differences linked to vegetation. This interpretation aligns with studies showing that foliage effectiveness depends on both canopy density and pollutant load (Przybysz et al., 2014; Barwise & Kumar, 2020).

Spatial heterogeneity: influence of urban form, canopy continuity, and local emissions

The strength of LAI –PM relationships varied clearly across the four school routes, reflecting differences in vegetation structure, street geometry, and local emission sources. The strongest correlations ($r \approx -0.25$ to -0.48) occurred at Primary School PS2, where the route includes a forest edge, dense tree cover on the school grounds, and a notable share of evergreen species. On measurement days this continuous and structurally diverse canopy likely enhanced filtration and created more stable airflow conditions, which supports findings that vegetation effects increase when the canopy forms a coherent barrier (Janhäll, 2015; Barwise & Kumar, 2020). These results highlight PS2 as a setting where vegetation structure aligns well with mechanisms known to promote particulate matter removal.

The Primary School PS3 also showed relatively strong associations in leaf-off conditions ($r \approx -0.31$ to -0.35), suggesting that evergreen vegetation and woody surfaces contributed to local particle deposition during periods of elevated emissions (Beckett et al., 2000; Przybysz et al., 2019). This route is located within a compact residential area, where narrow streets and closely spaced buildings limit air movement. In such settings, the dominant aerodynamic effect is often the formation of street-canyon turbulence, which tends to reduce the filtering role of trees by trapping pollutants and altering airflow patterns (Vos et al., 2013;

Trzeciak, M., Sikorska, D. (2026). The role of roadside vegetation near school in mitigating air pollution: an exploratory case study in Zielonka. *Sci. Rev. Eng. Env. Sci.*, *35* (2), 139–157. DOI 10.22630/srees.10965

Vranckx et al., 2015). This mechanism may explain why leaf-on correlations at Primary School PS3 were nearly absent: with full foliage, vegetation contributes to the canyon-like structure, increasing turbulence and masking any direct filtering effect. In March campaign, when deciduous foliage was minimal, the few evergreen patches stand out more clearly in the signal, likely contributing to stronger correlations. These results reinforce the context dependency of vegetation and PM relationships in compact residential street networks.

The Primary Schools PS1 and the PS4 had weaker relationships in both measurement campaigns ($r \approx -0.13$ to -0.21, and $r \approx -0.15$, respectively). Primary School PS1 is characterized by wide streets and dispersed tree cover, conditions that promote rapid dilution of pollutants and reduce the influence of individual planting elements. Primary School PS4 borders an open park with tall deciduous trees but few shrubs or evergreens, and the adjacent railway corridor further increases ventilation. These open settings are known to disperse pollutants efficiently, diminishing the relative effect of vegetation (Hoppa et al., 2022), as also observed in studies of children's routes where greenery shapes exposure only in specific micro-environments (Khanian et al., 2024). Overall, Primary Schools PS4 and the PS1 may illustrate conditions where open urban form and strong airflow override potential PM reduction by vegetation.

Implications for designing vegetation along children's school routes

Our findings show that the benefits of roadside vegetation are strongly context-dependent. The effectiveness of trees in reducing particulate matter depends on the continuity of the canopy, the presence of evergreen species, street geometry, and background emissions. Routes where vegetation forms a connected structure provide more stable filtration than those with isolated trees, and evergreen patches play an important role during winter, when deciduous foliage is absent. At the same time, urban form can either enhance or suppress vegetation effects. Narrow streets or semi-enclosed spaces may trap pollutants and limit ventilation, meaning that "more trees" do not automatically translate into better air quality (Vos et al., 2013; Janhäll, 2015).

These patterns highlight the need for case-by-case planning that considers not only vegetation configuration but also local airflow and street-canyon effects, rather than uniform greening strategies. Local green buffers near emission sources, short stretches of continuous canopy, and mixed plantings that include evergreens can improve exposure conditions. This is especially important in micro-environments where children spend the most time. Designing vegetation with attention to airflow,

rather than relying solely on increasing tree density, appears essential in suburban settings like ours.

Beyond air-quality benefits, greenery along school routes provides additional psychological and behavioral advantages, supporting children's wellbeing, comfort, and walking experience (Lee et al., 2015; Khanian et al., 2024)the uneven distribution of greenery and route networks within cities results in varied opportunities for pedestrians, including children, to experience greenery. This study evaluates the urban heterogeneity of trade-offs between exposure to greenery and route length. We focus on the shortest and greenest hypothetical home–school routes for all children in the city. For this purpose, we conducted a spatial analysis using multiple spatially explicit data sets on primary schoolchildren, pedestrian street networks, and high-resolution urban green space maps, with Łódź (Poland. These broader gains reinforce the value of integrating vegetation strategically into the everyday mobility of young pupils.

Even small reductions in particulate matter can be meaningful for children's health, given their heightened vulnerability and the long-term consequences of early-life exposure (Kim et al., 2015; Roche et al., 2024). Our results contribute to the broader discussion on designing resilient urban environments that support safe and healthy school mobility. By showing where vegetation can offer benefits, and where its effect is constrained by urban form, we provide evidence that can inform planning decisions, from shaping pedestrian routes to prioritizing targeted greening. Strengthening green infrastructure along everyday walking paths has the potential to enhance both environmental conditions and children's wellbeing. In this sense, even modest effects of vegetation play an important role in creating healthier school surroundings.

Future studies could build on our findings by incorporating multi-season or multi-year measurements to capture a wider range of meteorological and vegetation conditions. Combining empirical transects with dispersion modeling would allow a more precise assessment of how street geometry and airflow shape children's exposure (Vranckx et al., 2015). Detailed species-level and structural analyses would help clarify which vegetation forms contribute most effectively to particulate removal. Integrating LAI with real-time traffic counts and emission inventories could further disentangle the relative influence of greenery and anthropogenic sources. These extensions align with calls to better integrate vegetation metrics with urban form when evaluating air-quality interventions (Barwise & Kumar, 2020).

Trzeciak, M., Sikorska, D. (2026). The role of roadside vegetation near school in mitigating air pollution: an exploratory case study in Zielonka. *Sci. Rev. Eng. Env. Sci.*, *35* (2), 139–157. DOI 10.22630/srees.10965

Limitations of the study

Our study has several limitations. We conducted only two measurement campaigns, effectively representing single-day snapshots for leaf-off and leaf-on conditions which means that short-term meteorological variability could not be fully controlled. Because measurements were collected along continuous routes at short spatial intervals, individual observation points are spatially autocorrelated and do not represent independent replicates.

LAI was measured along transects capturing horizontal leaf cover rather than a continuous vertical canopy profile, which may have limited our ability to assess the role of tree structure as a barrier for particulate matter. The Sniffer4D, like other optical particle counters, is affected by humidity and particle composition, which can introduce bias in absolute concentration values. We also lacked detailed information on traffic flow along the surveyed routes, even though vehicle emissions are a major driver of PM variability in suburban areas (Karagulian et al., 2015; Liu et al., 2025) it is important to know the sources contributing to human exposure. This study systematically reviewed and analysed available source apportionment studies on particulate matter (of diameter of 10 and 2.5 microns, PM_{10} and $PM_{2.5}$. While we selected measurement days with low to moderate wind to minimize dispersion effects, we did not explicitly measure local airflow, which may influence pollutant concentrations at micro-scales. Finally, our analysis relied on correlations, based on spatially structured data, without repeated measurements on multiple days, which cannot establish causality and can underestimate the influence of general factors affecting PM variability when the underlying signal is small or masked by meteorological noise. These constraints underline the need for cautious interpretation of the strength and direction of the observed relationships.

Conclusions

We found that roadside vegetation was modestly associated with lower PM concentrations along school routes in Zielonka, generally coinciding with several-fold reductions in PM. However, in some locations, vegetation coincided with local peaks, causing occasional increases in maximum PM values. Overall, the correlation between green cover and PM remained weak. Dense built-up areas showed little effect. PM levels were higher during leaf-off conditions, when vegetation impact was more detectable, while in leaf-on conditions, background PM was lower and vegetation effects harder to isolate.

Our results highlight that vegetation's air-quality benefits are context-dependent. Canopy continuity, local geometry and pollution background determine whether greenery acts as a net sink or, occasionally, as a factor that alters local dispersion.

We therefore caution against simple prescriptions such as "more trees always improve air quality."

We recommend further studies with multi-season or multi-year monitoring, concurrent meteorological measurements, and dispersion modeling. Species-level and structural analyses of vegetation should be included. Such work would better inform targeted greening strategies to reduce children's exposure near schools.

Acknowledgments

Map data copyrighted OpenStreetMap contributors and available from www.openstreetmap.org.

This research was funded by the National Science Centre (Poland) grant no. 2020/39/B/HS4/03240.

References

Barwise, Y., & Kumar, P. (2020). Designing vegetation barriers for urban air pollution abatement: A practical review for appropriate plant species selection. *npj Climate and Atmospheric Science*, *3*(1), 12. https://doi.org/10.1038/s41612-020-0115-3

Beckett, K. P., Freer-Smith, P., & Taylor, G. (2000). Effective tree species for local air-quality management. *Arboriculture & Urban Forestry*, *26*(1), 12–19. https://doi.org/10.48044/jauf.2000.002

Escobedo, F. J., Kroeger, T., & Wagner, J. E. (2011). Urban forests and pollution mitigation: Analyzing ecosystem services and disservices. *Environmental Pollution*, *159*(8–9), 2078–2087. https://doi.org/10.1016/j.envpol.2011.01.010

General Directorate for National Roads and Motorways [GDDKiA]. (2020). *General traffic measurement conducted by the General Directorate for National Roads and Motorways*. https://www.gov.pl/web/gddkia/generalny-pomiar-ruchu-20202021

Head Office of Geodesy and Cartography [GUGiK]. (2025). *BDOT10k: Database of topographic objects*. https://www.geoportal.gov.pl/

Health Effects Institute, & Institute for Health Metrics and Evaluation [HEI & IHME]. (2025). *State of Global Air 2025 report*. https://www.stateofglobalair.org/sites/default/files/documents/2025-10/soga-2025-report.pdf

Hoppa, A., Sikorska, D., Przybysz, A., Melon, M., & Sikorski, P. (2022). The role of trees in winter air purification on children's routes to school. *Forests*, *13*(1), 40. https://doi.org/10.3390/f13010040

Institute of Meteorology and Water Management [IMGW-PIB]. (2025). *Meteorological observations – synoptic daily data*. https://danepubliczne.imgw.pl/data/dane_pomiarowo_obserwacyjne/dane_meteorologiczne/dobowe/synop/2025/

Janhäll, S. (2015). Review on urban vegetation and particle air pollution – Deposition and dispersion. *Atmospheric Environment*, *105*, 130–137. https://doi.org/10.1016/j.atmosenv.2015.01.052

Juda-Rezler, K., Reizer, M., Maciejewska, K., Błaszczak, B., & Klejnowski, K. (2020). Characterization of atmospheric $PM_{2.5}$ sources at a Central European urban background site. *The Science of the Total Environment*, *713*, 136729. https://doi.org/10.1016/j.scitotenv.2020.136729

Karagulian, F., Belis, C. A., Dora, C. F. C., Prüss-Ustün, A. M., Bonjour, S., Adair-Rohani, H., & Amann, M. (2015). Contributions to cities' ambient particulate matter (PM): A systematic review of local source contributions at global level. *Atmospheric Environment*, *120*, 475–483. https://doi.org/10.1016/j.atmosenv.2015.08.087

Khanian, M., Łaszkiewicz, E., Kronenberg, J., & Sikorska, D. (2024). Urban heterogeneity of the trade-offs between exposure to greenery and walking distance in children's home–school routes. *Applied Geography*, *173*, 103437. https://doi.org/10.1016/j.apgeog.2024.103437

Kim, K. H., Kabir, E., & Kabir, S. (2015). A review on the human health impact of airborne particulate matter. *Environment International*, *74*, 136–143. https://doi.org/10.1016/j.envint.2014.10.005

Lee, A. C. K., Jordan, H. C., & Horsley, J. (2015). Value of urban green spaces in promoting healthy living and wellbeing: Prospects for planning. *Risk Management and Healthcare Policy*, *8*, 131–137. https://doi.org/10.2147/RMHP.S61654

Liu, Z., Qiu, Z., Yue, K., & Ren, F. (2025). Spatio-temporal characteristics and determining factors of traffic-related particulate matter in urban versus suburban areas. *Environmental Pollution*, *385*, 127127. https://doi.org/10.1016/j.envpol.2025.127127

McDonald, A. G., Bealey, W. J., Fowler, D., Dragosits, U., Skiba, U., Smith, R. I., Donovan, R. G., Brett, H. E., Hewitt, C. N., & Nemitz, E. (2007). Quantifying the effect of urban tree planting on concentrations and depositions of PM_{10} in two UK conurbations. *Atmospheric Environment*, *41*(38), 8455–8467. https://doi.org/10.1016/j.atmosenv.2007.07.025

Nowak, D. J., Hirabayashi, S., Bodine, A., & Greenfield, E. (2014). Tree and forest effects on air quality and human health in the United States. *Environmental Pollution*, *193*, 119–129. https://doi.org/10.1016/j.envpol.2014.05.028

Oguntunde, P. G., Olukunle, O. J., Fasinmirin, J. T., & Abiolu, O. A. (2012). Performance of the SunScan canopy analysis system in estimating leaf area index of maize. *Agricultural Engineering International: CIGR Journal*, *14*(3), 1–7. https://cigrjournal.org/index.php/Ejounral/article/view/1823

OpenStreetMap. (2025). *Planet dump*. https://planet.openstreetmap.org

Przybysz, A., Nersisyan, G., & Gawroński, S. W. (2019). Removal of particulate matter and trace elements from ambient air by urban greenery in the winter season. *Environmental Science and Pollution Research*, *26*(1), 473–482. https://doi.org/10.1007/s11356-018-3628-0

Przybysz, A., Sæbø, A., Hanslin, H. M., & Gawroński, S. W. (2014). Accumulation of particulate matter and trace elements on vegetation as affected by pollution level, rainfall and the passage of time. *Science of The Total Environment*, *481*, 360–369. https://doi.org/10.1016/j.scitotenv.2014.02.072

QGIS Development Team. (2023). *QGIS Geographic Information System* (Version 3.32) [Computer software]. Open Source Geospatial Foundation. http://qgis.org

R Core Team. (2025). *R: The R Project for Statistical Computing*. https://www.r-project.org/

Roche, I. V., Ubalde-Lopez, M., Daher, C., Nieuwenhuijsen, M., & Gascon, M. (2024). The health-related and learning performance effects of air pollution and other urban-related environmental factors on school-age children and adolescents − a scoping review of systematic reviews. *Current Environmental Health Reports*, *11*(2), 300–316. https://doi.org/10.1007/s40572-024-00431-0

Vos, P. E. J., Maiheu, B., Vankerkom, J., & Janssen, S. (2013). Improving local air quality in cities: To tree or not to tree? *Environmental Pollution, Selected Papers from Urban Environmental Pollution 2012*, *183*, 113–122. https://doi.org/10.1016/j.envpol.2012.10.021

Vranckx, S., Vos, P., Maiheu, B., & Janssen, S. (2015). Impact of trees on pollutant dispersion in street canyons: A numerical study of the annual average effects in Antwerp, Belgium. *Science of The Total Environment*, *532*, 474–483. https://doi.org/10.1016/j.scitotenv.2015.06.032

Summary

The role of roadside vegetation near school in mitigating air pollution: an exploratory case study in Zielonka. This study investigates the role of urban vegetation in mitigating particulate matter (PM_1, $PM_{2.5}$, PM_{10}) pollution along school routes in Zielonka, a small town near Warsaw. Measurements were collected during leaf-off (March) and leaf-on (September) conditions using a Sniffer4D mobile air quality monitor carried along pupils' commuting paths, alongside vegetation density estimates obtained with a SunScan Canopy Analysis System. Initial correlation analyses across the entire dataset revealed weak negative relationships between leaf area index (LAI) and particulate concentrations. To refine interpretation, the study introduced spatial stratification using built-up area percentages derived from the BDOT10k topographic database. While mean PM levels decreased with higher LAI, occasional local maxima were observed in dense canopy sections. The findings highlight that vegetation's effectiveness in improving air quality is highly context-dependent, shaped by urban form and season. Although the explanatory power was modest, the results emphasize the importance of integrating vegetation and built-environment interactions in air quality assessments. Further studies with broader spatial and temporal coverage are recommended to better characterize these relationships and guide targeted greening strategies along school routes.

Scientific Review Engineering and Environmental Sciences (2026), 35 (2), 158–183

Sci. Rev. Eng. Env. Sci. (2026), 35 (2) https://srees.sggw.edu.pl

ISSN 1732-9353 (suspended) eISSN 2543-7496 DOI 10.22630/srees.10366

Received: 15.03.2026
Accepted: 23.04.2026

Naama KHELIFA ✉
Moufida BOUKHABLA
Soumia BOUZAHER

University of Biskra, Department of Architecture, Laboratory of Design and Modelling of Architectural and Urban Forms and Ambiances (LACOMOFA), Algeria

✉naama.khelifa@univ-biskra.dz

Quantifying thermal comfort improvement by palm tree-based street greening, in hot and dry climate

Keywords: outdoor thermal comfort, OTC, palm tree, street greening, hot dry climate, sustainability

Introduction

Green spaces play an essential role in providing thermal comfort and mitigating the heat island effect, which leads to thermal discomfort due to rapid climate change. To reduce urban heat, green spaces contribute significantly to climate adaptation strategies, creating more sustainable and livable urban environments (Marando et al., 2022). Greening strategies, such as planting trees along streets, have been shown to improve urban thermal conditions by providing shade and enhancing evapotranspiration (Coccolo et al., 2018). Street greening involves incorporating various forms of green space, such as grass, shrubs, and trees, along streets to enhance outdoor thermal comfort, thereby improving the environmental

quality and aesthetic appeal of urban areas; this approach promotes sustainable urban development (Klemm et al., 2015). Innovative solutions, such as street greening, play a crucial role in improving living conditions in hot and dry climates. Among the different types of trees, palm trees represent a suitable choice due to their flexibility – they are particularly suitable for these climates due to their adaptive, drought-resistant properties and capacity to grow with minimal water – making them an ideal choice for street greening projects to improve thermal comfort. They also provide significant cooling benefits by offering shade, which directly influences surface temperatures and the surrounding environment. Additionally, the relative humidity produced by palm trees in the atmosphere contributes to local cooling effects (Gillner et al., 2015). This paper aims to measure the improvement in thermal comfort through street greening based on palm trees in a hot and dry climate. This study examines the city of Sidi Okba, located in the southeastern Algerian state of Biskra. It is one of the largest oases in Biskra and is famous for its vegetation, which mainly consists of local palm trees *Phoenix dactylifera*, distinguishing it from other southern cities (Farhi, 2002). In addition, there are trees planted along some streets, such as *Fucus retusa* and *Acacia*. Sidi Okba city is distinguished by the richness of its urban fabric, ranging from ancient traditional to modern contemporary.

This study examines the quantitative assessment of street greening based on palm trees. Two streets were selected for analysis. The first is located in the traditional individual residential fabric, which is protected and surrounded by palm groves on the northwestern and southern sides. Palm trees can be found behind some of the residential walls, while the streets themselves are winding and devoid of vegetation. The second street is situated in the collective housing fabric; it is bordered by two facades of similar residential blocks consisting of four stories and has sparse vegetation coverage (Fig. 1).

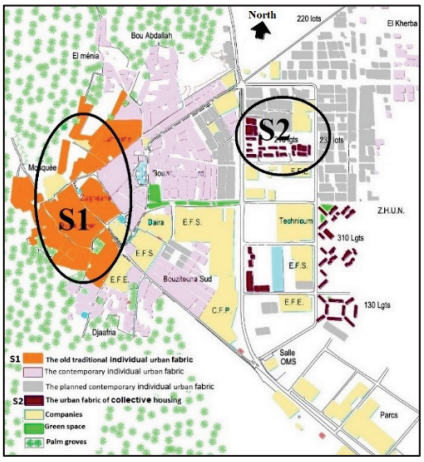

FIGURE 1. Study area: S1 – site of the traditional individual residential fabric, S2 – site of the collective housing fabric

Source: own work.

Khelifa, N., Boukhabla, M., Bouzaher, S. (2026). Quantifying thermal comfort improvement by palm tree-based street greening, in hot and dry climate. *Sci. Rev. Eng. Env. Sci.*, *35* (2), 158–183. DOI 10.22630/srees.10366

The study was conducted on the hottest days of July, the warmest month of summer (from July 10–12, 2024), according to data from the meteorological station closest to the study site. Measurements were collected over a 48-hour period, every 2 hours, using a comparative approach based on measurements and numerical simulation. The current scenario was then compared with the greening scenario. The research aims to provide urban planners, architects, landscape designers, and policymakers with concrete evidence of the palm trees' climatic benefits. The results will contribute to developing climate-responsive urban design and creating more resilient and comfortable cities in hot and dry climates.

Literature review

Palm trees characteristics

Palm trees were used for street greening in hot and dry climates due to their ability to withstand high temperatures and grow in arid conditions. They provide shade and reduce temperatures. When planted along streets, sidewalks, and other public places in urban areas, these trees are selected according to their type, shape, and size. In addition, palm trees have a high transpiration rate and enhance the cooling effect through evaporation, as they absorb solar radiation and use it to convert water into steam, thereby reducing air temperature (Bencheikh & Rchid, 2012).

Studies on the impact of street greening on outdoor thermal comfort

Many studies emphasize the importance of palm trees in enhancing outdoor thermal comfort, especially in hot and dry climates. Many studies have conducted field measurements and simulations to evaluate the impact of palm trees on local climatic conditions.

In a study by Teshnehdel et al. (2020), the results indicated that the presence of trees, including palm trees, significantly reduced air temperatures in urban areas. Under the palm tree canopy, temperatures decreased by 5°C compared to unshaded regions, which improves comfort for pedestrians and urban users, encouraging more outdoor activities during the hot months. A study by Bencheikh and Rchid (2012) stated that palm trees contribute to cooling by providing shade. They help reduce surface temperatures under their canopies, and their leaves can block sunlight, thereby lowering surface temperatures. Matallah et al. (2023) also stated that the process

of evaporation, by releasing water vapor from the leaves, leads to the cooling of the surrounding air. According to the study, palm trees can absorb carbon dioxide, improving air quality and quality of life (Audu & Lintoc, 2018; Boukhabla et al., 2022). In general, based on a review of the most important studies on greening with palm trees, we may conclude that planting palm trees in urban areas helps create cooler microclimates and improves outdoor thermal comfort in hot and dry climates.

Studies on the use of palm trees in urban greening

A study by Arab et al. (2016) stated that *Phoenix dactylifera* trees are distinguished by their ability to provide shade and their adaptability to hot, dry environments. This is due to their tall trunks, wide leaves, and expansive canopies, which reduce ground temperatures and enhance thermal comfort for pedestrians. A study by Youcef and Guedouh (2023) also indicated that palm trees reduce surface temperatures by 5°C under direct sunlight, increasing pedestrian comfort levels and enhancing city sustainability. Numerous studies have highlighted the significant role of palm trees in enhancing thermal comfort, maintaining environmental balance, promoting biodiversity, and absorbing pollutants, making them highly suitable for cities in arid climates and contributing to improve air quality. Research also emphasizes the psychological benefits of incorporating trees of all types into urban planning, as they foster relaxation and recreation while improving the outdoor climate (Elsadek et al., 2019).

Gaps in the current research and the need for further investigation

Although some research has addressed the effects of street planting with palm trees on thermal comfort, significant research gaps remain, as summarized further in the text.

Local climate influences

The influence of local wind patterns and incident sunlight on the effectiveness of trees in urban environments remains insufficiently explored and has not been studied. Research highlights that tree canopy characteristics, such as leaf area index (LAI) and crown density, significantly contribute to reducing stress and enhancing relative humidity levels (Geletič et al., 2022; Liu et al., 2023); however, no comprehensive analyses integrate these variables across different urban areas.

Khelifa, N., Boukhabla, M., Bouzaher, S. (2026). Quantifying thermal comfort improvement by palm tree-based street greening, in hot and dry climate. *Sci. Rev. Eng. Env. Sci.*, *35* (2), 158–183. DOI 10.22630/srees.10366

Seasonal changes

Current research has neglected seasonal changes in temperature and humidity, which are necessary to evaluate the impact of street planting with palm trees on outdoor thermal comfort across different seasons (moderate, cold, and hot). This neglect can lead to less accurate insights on the topic throughout the year.

The physiological effects of street trees on the urban environment appear significantly between summer and winter, influencing the level of general comfort experienced by pedestrians (Ren et al., 2022).

Geographical restrictions

The geographic focus of most studies on street greening limits their applicability to diverse urban settings. This geographical limitation restricts the generalizability of results across different climatic contexts, especially in hot climates and dry regions where local trees are commonly used for urban greening (Liu et al., 2023).

The sustainability of palm trees

Research has primarily focused on the cooling effects of palm trees, but little attention has been given to their long-term sustainability. This includes assessing their longevity and the resources required for their maintenance. While most studies have explored the role of palm trees in reducing temperatures, there is a notable gap in research evaluating their long-term viability and the requirements for their maintenance and care. Addressing this gap involves assessing the sustainability of palm trees in urban areas by examining their longevity and the resources needed for upkeep.

Quantifying thermal comfort improvement

Measuring the impact of street greening with palm trees on outdoor thermal comfort depends on a multifaceted approach that integrates various research methodologies. This strategy includes local climate analysis, measurement of thermal comfort indicators, numerical simulation, and surveys to comprehensively understand how urban greening enhances thermal comfort, especially in hot and dry climates.

Local climate analysis

Researchers analyze the local climate by measuring basic climatic parameters to evaluate the environmental conditions that affect thermal comfort, such as air temperature, relative humidity, wind speed, and solar radiation. In many measurement campaigns, climatic data is collected using portable weather stations and measuring instruments, as well as microelectronic devices such as Testo 480 (Jing et al., 2024).

Thermal comfort indicators

Thermal comfort indicators are standardized measures used to evaluate human thermal sensation and potential thermal stress. In this study, the analysis focuses on the fundamental climatic parameters (air temperature, relative humidity, wind speed) along with mean radiant temperature (*MRT*). To enhance the evaluation, two additional biometeorological indices, the physiological equivalent temperature (*PET*) and the new standard effective temperature (*SET**), are incorporated. These indices are calculated from measured climate data and modeling outputs, offering a more comprehensive understanding of how various environmental factors influence human comfort.

Digital simulation

Digital simulations often analyze the impact of palm trees on thermal comfort using two main strategies: shadow cooling and evaporation/conversion. These methods help researchers evaluate the benefits of palm trees and green infrastructure in urban environments (Bencheikh & Rchid, 2012).

Material and methods

Study objectives

This study aims to quantitatively assess the impact of street greening with palm trees on thermal comfort standards in hot and dry climates. Two streets in the city of Sidi Okba, one of the largest oases in Biskra, located 400 km southeast of Algiers (Fig. 2), were selected for analysis (in accordance with the above context). The methodology of the study was based on a comparative approach. First, field

Khelifa, N., Boukhabla, M., Bouzaher, S. (2026). Quantifying thermal comfort improvement by palm tree-based street greening, in hot and dry climate. *Sci. Rev. Eng. Env. Sci.*, *35* (2), 158–183. DOI 10.22630/srees.10366

measurements were conducted using the Testo 480 device to evaluate the outdoor thermal comfort of the current situation. Climatic parameters (air temperature, relative humidity, and wind speed), were recorded at two measurement stations on each street. Second, a greening scenario incorporating palm trees was proposed and simulated using the ENVI-met digital program and the RayMan (ver. 2017) software for Street Str2. The results of the field measurements were then compared with those of the proposed scenario.

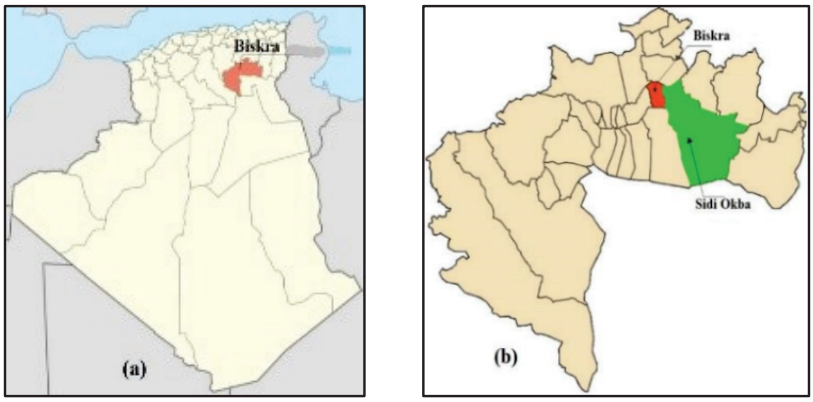

FIGURE 2. Location of the studied streets in Sidi Okba: a – macroscale of the country, b – microscale of Biskra Province

Source: own work.

On-site measurements

The study was conducted on two streets. The first street (Str1) is located within the traditional individual residential fabric and is surrounded on the northwestern and southern sides by palm forests of the local species *Phoenix dactylifera*. Most residences contain palm trees inside their homes, while the street itself is winding and devoid of vegetation. Its width varies between 2.50 m and 3.00 m. The second street (Str2) is located within the collective housing fabric and is wider, with a width of 7.00 m. Its vegetation cover is weak, and the buildings on both sides have uniform four-story blocks (height 12 m). Two fixed measuring points were chosen for the first street (Str1) – the first station (St1) at the beginning and the second (St2) in its middle. For the second street (Str2), two measuring points were chosen under a palm tree (St3) and under a tree of the local type (St4), which are located on both edges of the street (Table 1).

TABLE 1. Sites and measurement stations

Site	Street	Street trees number / type
S1 Traditional individual residential fabric	Str1  	
Section on the street (Str1) Measurement point (St1, St2)	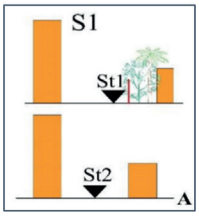 	
S2 Collective housing fabric Measurement point (St3, St4)	Str2  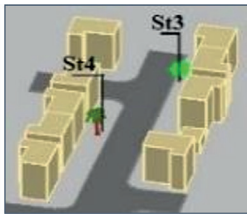	2 palm tree (*Phoenix dactylifera*) 1 berry tree 1 *Ficus retusa*
Section on the street (Str2)	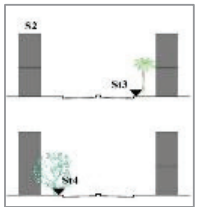 	

Source: own work.

We made a series of measurements every two hours for three consecutive days from 10 July to 12 July 2024, measuring the following climatic factors: air temperature (T_a), relative humidity (H_r), and wind speed (W_s), and using the multi-functional portable device Testo 480-AG 5011ST, 0563 4800 (Fig. 3). The one trip between the two streets took about 10 minutes by car, with readings taken in shaded areas and at an altitude of 1.40 m, to reduce the effect of heat reflected from the ground surface.

Khelifa, N., Boukhabla, M., Bouzaher, S. (2026). Quantifying thermal comfort improvement by palm tree-based street greening, in hot and dry climate. *Sci. Rev. Eng. Env. Sci.*, *35* (2), 158–183. DOI 10.22630/srees.10366

FIGURE 3. A multifunctional portable device Testo 480-AG 501 1ST, 0563 4800
Source: own work.

Atmospheric simulation

The atmosphere was simulated using the Envi-Met software, which required input data (Table 2) such as the simulation date, vegetation type, tree layout, and climatic parameters (air temperature, relative humidity, wind speed, and mean radiant temperature) were simulated and completed in two phases: (a) simulation of the current situation (Str1, Str2), and (b) scenario proposed for street greening simulation (Str2).

TABLE 2. Simulation's settings

Situation (geographic coordinates)	latitude: 34°75′, longitude: 5°57′
Simulation date	July 10–12, 2024
Simulation start time	06:00:00 a.m.
Initial temperature	31°C
Simulation duration	48 hours
Relative humidity at 2 m above ground [%]	20%
Wind speed at 10 m	2 $m \cdot s^{-1}$
Wind direction	135°
Specific humidity in 2,500 m	8.00 $g \cdot kg^{-1}$

Source: own work.

Current street greening scenario

This simulation was conducted to measure the improvement of thermal comfort for different scenarios under the pressure of summer heat, in a hot and dry climate. The experiment was carried out through the following stages:

1. The first simulation focuses on the current external environment of Street Str1, situated within the traditional individual residential fabric (S1). This area lacks vegetation but is encircled by palm forests dominated by *Phoenix dactylifera*. Two measurement points (St1 and St2) were selected to evaluate the environmental conditions (Fig. 4).

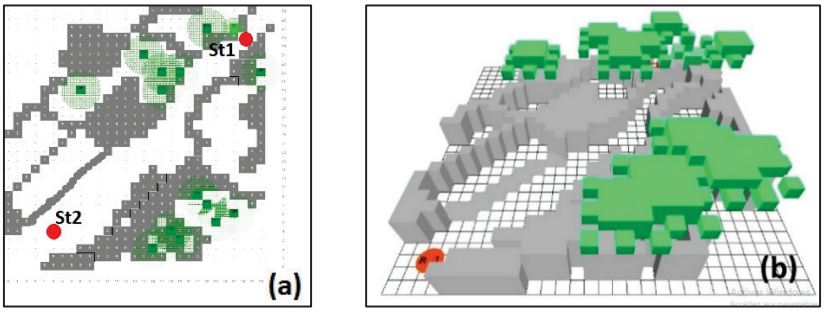

FIGURE 4. Model domain for the study in ENVI-met in current situation for Street Str1: a – 2D, b – 3D
Source: ENVI-met.

2. The second simulation examines the external environment of Street Str2, located within the collective housing fabric (S2), on the eastern side of the city. Measurements were conducted at two points: under a *Phoenix dactylifera* palm tree at Street St3, and beneath a mulberry tree at Street St4.
3. Street Str1, characterized by its narrow and winding layout, is situated within the traditional individual residential fabric (S1). It is naturally protected and bordered on the northwestern and southern sides by palm groves. Due to these existing conditions, no additional greening interventions were proposed for this street. In contrast, Street Str2 exhibits limited vegetation coverage. A greening proposal was developed to enhance its environment, utilizing local palm trees *Phoenix dactylifera* spaced at regular intervals of 5 m. The original measurement points, St3 and St4, were retained, but in the greening scenario, they were redesignated as St3′ and St4′ (Fig. 5).

The outcomes of the three scenarios were analyzed to assess the contribution of *Phoenix dactylifera* palm trees to improving thermal comfort in outdoor public spaces, particularly in cities experiencing hot and dry climatic conditions.

Khelifa, N., Boukhabla, M., Bouzaher, S. (2026). Quantifying thermal comfort improvement by palm tree-based street greening, in hot and dry climate. *Sci. Rev. Eng. Env. Sci.*, *35* (2), 158–183. DOI 10.22630/srees.10366

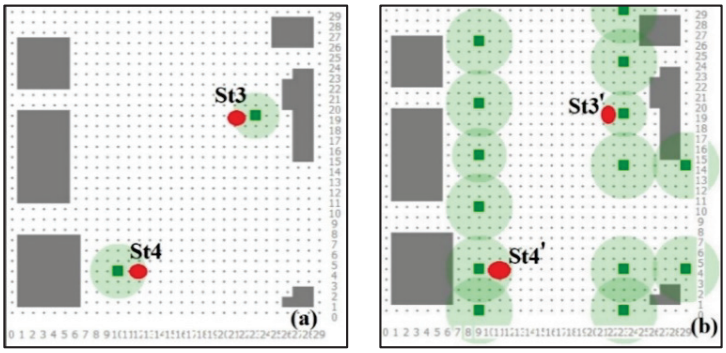

FIGURE 5. Model domain for the study in ENVI-met: a – current situation, b – proposed for Street Str2
Source: ENVI-met.

Results and discussion

Atmospheric model validation

To validate the ENVI-met model, we compared the simulated and recorded air temperature in Streets Str1 and Str2 during the period from July 10 to July 12, 2024. We calculated the correlation coefficient (*R*), the root mean square error (*RMSE*), the mean absolute error (*MAE*), and the root mean square percentage error (*RMSPE*), and then assessed the degree of agreement between the simulated and measured values (Table 3).

TABLE 3. Summary of the validation of simulated models for Street 1 (St1, St2) and Street 2 (St3, St4)

Station	Regression equation	R^2	*RMSE* [°C]	*MAE* [°C]	*RMSPE* [%]
St1	$y = 1.0164x + 0.3457$	0.8926	1.60	1.19	4.33
St2	$y = 1.2529x - 7.8296$	0.8931	2.15	1.74	5.79
St3	$y = 1.0676x - 2.5545$	0.9980	1.50	1.21	4.09
St4	$y = 0.9474x + 1.9583$	0.9990	1.42	1.14	3.87

Source: own work.

According to ASHRAE Guideline 14-2002 (American Society of Heating, Refrigerating and Air-Conditioning Engineers [ASHRAE], 2014), the correlation coefficient (*R*) should range from −1.0 to +1.0. In our review of previous studies,

we observed that only a limited number of works have validated their numerical models. It was also noted that the accuracy of simulation data becomes evident after the first four hours; therefore, the ENVI-met team recommends considering the simulation time to obtain reliable results.

In our study, we used air temperature to compare simulated data with measured data, and most validation results confirmed that the model maintains acceptable predictive accuracy (Fig. 6).

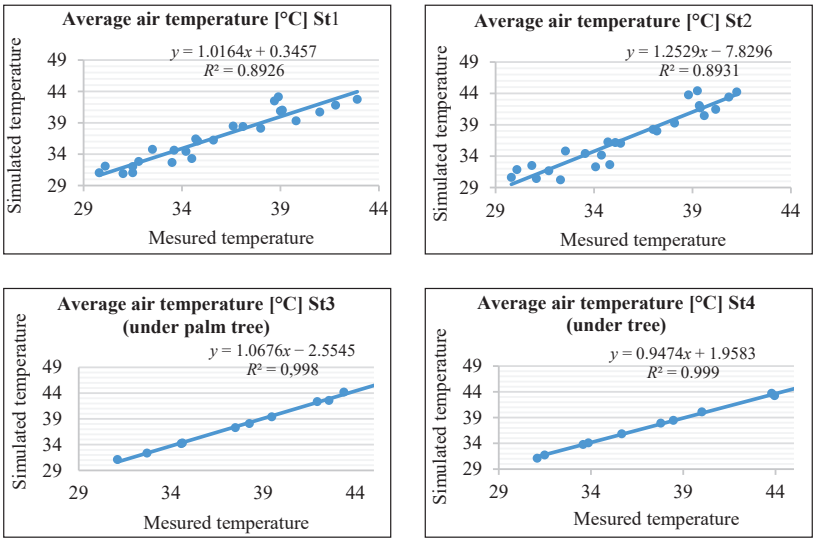

FIGURE 6. Validation of the simulation models on Street 1 (St1, St2) and Street 2 (St3, St4)
Source: own work.

For Station St2 the regression equation shows a deviation in slope of approximately 25% from unity and a negative intercept, which may indicate relative and systematic biases (Moriasi et al., 2007). To meet the need for additional statistical properties and significance testing, we calculated the root mean square error (*RMSE*), mean absolute error (*MAE*), and root mean square percentage error (*RMSPE*). These are standard metrics in hydrological and environmental modeling for assessing predictive accuracy beyond correlation alone, consistent with the findings of Jackson et al. (2019). Accordingly, we enhanced the regression analysis using supplementary validation measures, including *RMSE* of 2.15°C, *MAE* of 1.74°C, and *RMSPE* of 5.79%. These indicators are widely recognized in climate and environmental modeling as robust measures of model performance beyond the coefficient of determination (R^2). Willmott and Matsuura (2005) demonstrated that both *RMSE*

and *MAE* provide more accurate evaluations of predictive skill, particularly when regression parameters deviate from ideal values. *RMSPE* also assists in assessing relative deviations of observed values and is more sensitive to relative errors. Furthermore, the steep slope and negative intercept observed at Station St2 are likely influenced by local climatic effects or site-specific factors (the station is located on a street section where surrounding buildings were demolished).

Despite the high R^2 value, such deviations in slope and intercept are common in environmental datasets due to microclimatic fluctuations and urban infrastructure, all of which can affect temperature distribution. In this study, most of the additional validation metrics confirmed that the model maintains acceptable predictive accuracy.

Digital simulation results

Figure 7 presents the outputs generated by Leonardo through the ENVI-met simulation program. At 6:00 a.m., data were recorded for Street Str1, located within the traditional individual residential fabric (S1). The air temperature ranged from 28.40°C to 32.13°C, with relative humidity varying between 40.09% and 49.79%. Wind speed ranged from 0.00 $m \cdot s^{-1}$ to 1.89 $m \cdot s^{-1}$, while the mean radiant temperature ranged between 18.02°C and 23.54°C.

Figure 8 illustrates the outputs generated by Leonardo using the ENVI-met software, with respect to the street simulation scenario (Str2) under current conditions, within the collective housing fabric (S2) at 6:00 a.m. The air temperature ranged between 32.50°C and 33.61°C, the relative humidity varied between 29.63% and 32.93%, wind speed fluctuated between 0.02 and 1.96 $m \cdot s^{-1}$, and the mean radiant temperature ranged between 21.73 and 29.68°C.

Figure 9 presents the outputs generated by Leonardo through the ENVI-met simulation program. It displays the climatic values of the simulation at 6:00 a.m. for Street Str2, located within the collective housing fabric (S2). After proposing a scenario in which the street was planted with local palm trees (*Phoenix dactylifera*), the results indicated that the air temperature ranged between 32.11°C and 33.33°C, relative humidity varied between 29.45% and 32.77%, wind speed ranged from 0.02 $m \cdot s^{-1}$ to 1.97 $m \cdot s^{-1}$, while the mean radiant temperature ranged between 20.30°C and 27.28°C.

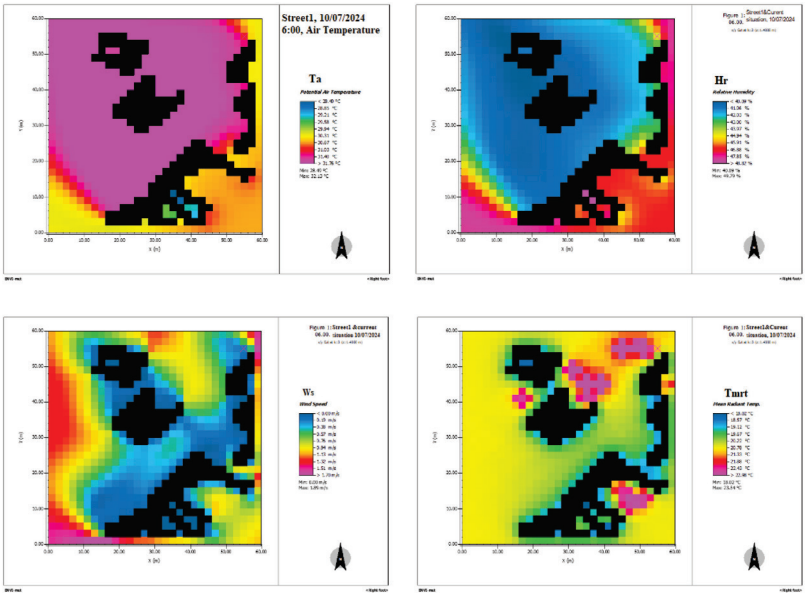

FIGURE 7. Visualization outputs generated by Leonardo's (Street 1) modeling software for the current situation

Source: Leonardo from the ENVI-met simulation program.

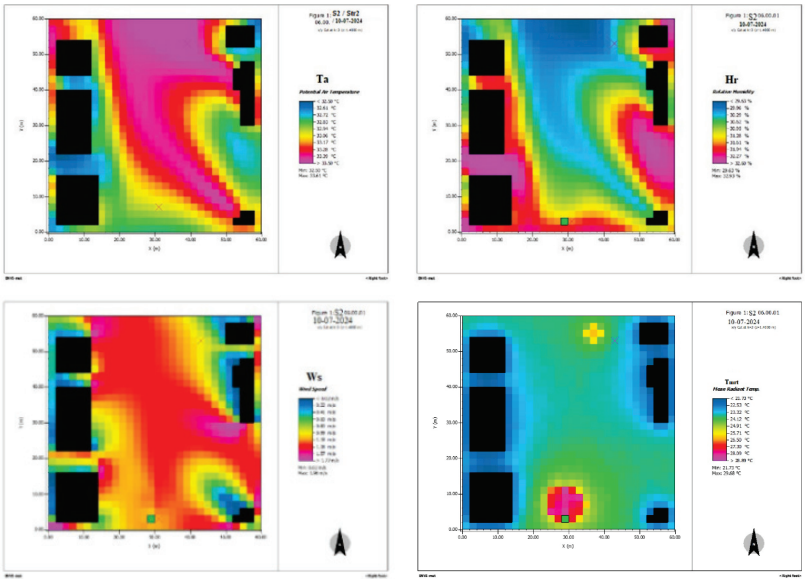

FIGURE 8. Visualization outputs generated by Leonardo's (Street 2) modeling software for the current simulation scenario

Source: Leonardo from the ENVI-met simulation program.

Khelifa, N., Boukhabla, M., Bouzaher, S. (2026). Quantifying thermal comfort improvement by palm tree-based street greening, in hot and dry climate. *Sci. Rev. Eng. Env. Sci.*, *35* (2), 158–183. DOI 10.22630/srees.10366

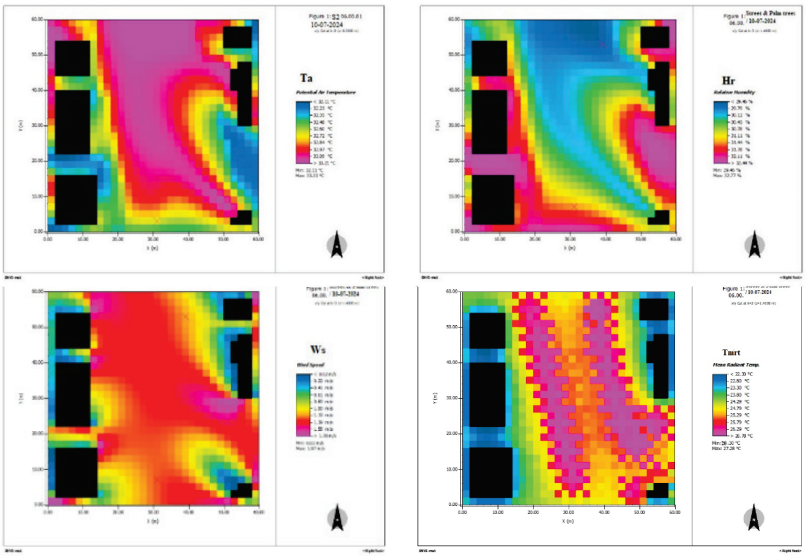

FIGURE 9. Visualization outputs generated by Leonardo's (Street 2) for the proposed simulation scenario

Source: Leonardo from the ENVI-met simulation program.

Comparing results before and after greening the streets with palm trees in terms of outdoor thermal comfort

Current situation

In the current condition of the two streets, it is observed that the air temperature in street Str1 was lower than that in street Str2, with a reduction ranging between 1.86 and 5.20°C. The lowest average temperature recorded was 30.53°C at 4:00 a.m. at Station St1 in Street Str1, compared to 32.39°C at Station St3 in Street Str2. The highest measurement reached 49.57°C at 2:00 p.m. at Station St4 in Street Str2, while the maximum recorded in Street Str1 was 44.37°C at 2:00 p.m. at Station St2. This indicates that Street Str1 provides better thermal comfort within the traditional individual residential fabric compared to Street Str2, which is located in the collective housing fabric. This difference can be explained by the location of Street Str1 within an urban fabric surrounded by palm groves, which contributed to the reduction of air temperatures (Table 4).

TABLE 4. Temperature for current situation scenario

Street	Station	Type	Min temperature [°C]	Max temperature [°C]
Str1	St1	field measurement	30.53	42.70
	St2		31.05	44.37
Str2	St3		32.39	47.82
	St4		32.96	49.57
	St3′	simulation (greening)	31.62	45.59
	St4′		31.85	47.13

Source: own work.

Proposed greening scenario for Str2 (St3' and St4')

In the proposed scenario, which involves the addition of palm trees along Street Str2 (St3′ and St4′), the average air temperature shows a reduction ranging between 0.77°C and 2.44°C compared to the current situation (St3 and St4). The lowest average temperature recorded was 32.39°C at 4:00 a.m. at Station St3 (beneath a palm tree). In the proposed scenario, this measurement decreased to 31.62°C at the same station. The maximum average temperature of 49.57°C was reached at 2:00 p.m., at Station St4 (under a tree), which subsequently decreased to 47.13°C at the same station following the greening intervention. It is noteworthy that the proposed greening of Street Str2, through the plantation of local palm trees *Phoenix dactylifera*, contributed significantly to enhancing thermal comfort (Fig. 10, Table 5).

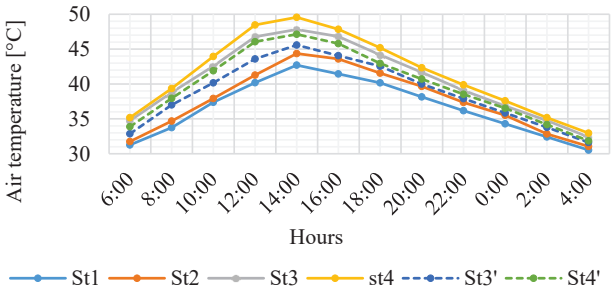

FIGURE 10. Comparison of the daily average air temperature in Streets Str1 and Str2: current versus proposed scenarios

Source: own work.

Khelifa, N., Boukhabla, M., Bouzaher, S. (2026). Quantifying thermal comfort improvement by palm tree-based street greening, in hot and dry climate. *Sci. Rev. Eng. Env. Sci.*, *35* (2), 158–183. DOI 10.22630/srees.10366

TABLE 5. Comparison of the daily average air temperature for Streets Str1 and Str2

Station	Hour											
	6:00	8:00	10:00	12:00	14:00	16:00	18:00	20:00	22:00	0:00	2:00	4:00
St1	31.26	33.75	37.38	40.19	42.70	41.44	40.16	38.16	36.18	34.29	32.42	30.53
St2	31.75	34.68	37.93	41.28	44.37	43.59	41.56	39.66	37.36	35.52	32.84	31.05
St3	34.75	38.79	42.56	46.78	47.82	46.82	44.17	41.67	39.07	36.86	34.77	32.39
st4	35.18	39.36	43.95	48.47	49.57	47.85	45.19	42.33	39.88	37.59	35.18	32.96
St3’	32.86	37.01	40.16	43.59	45.59	44.07	42.55	40.00	37.91	35.85	33.78	31.62
St4’	33.88	37.95	41.90	46.05	47.13	45.79	42.95	40.71	38.52	36.54	34.18	31.85

Source: own work.

When comparing the relative humidity levels of the current and proposed scenarios between Streets Str1 and Str2, we noticed the following (Fig. 11, Table 6):

– In the current scenario, Str1 (St1 and St2) exhibits higher and more stable relative humidity levels throughout the day compared to Str2 (St3 and St4), with a maximum value of 44.16% recorded at 6:00 a.m. at Station St1, and a minimum value of 26.77% recorded at 4:00 p.m. at Station St2. In contrast, Str2 in its current condition experiences greater fluctuations and lower relative humidity levels, with the highest value of 25.44% observed at 4:00 a.m. at station St3 (located beneath a palm tree), while the lowest value of 10.06% was recorded at 4:00 p.m. at station St4 (beneath a tree).
– In the proposed scenario for Str2 (St3′ and St4′), relative humidity levels improved significantly compared to the current situation (St3 and St4). The maximum recorded value reached 32.88% at 6:00 a.m. at Station St3′, while the minimum value of 15.90% was observed at 4:00 p.m. at Station St4′. Thus, the proposed greening of the street resulted in clear improvements in relative humidity levels, making them more comparable to those observed in Str1.

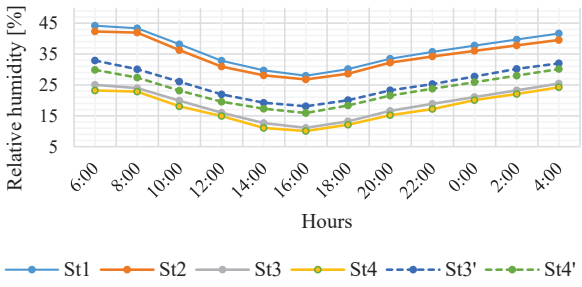

FIGURE 11. Comparison of the daily average relative humidity in Str1 and Str2: current versus proposed scenarios

Source: own work.

TABLE 6. Comparison of the daily average relative humidity for Streets Str1 and Str2

Station	Hour											
	6:00	8:00	10:00	12:00	14:00	16:00	18:00	20:00	22:00	0:00	2:00	4:00
St1	44.16	43.34	38.17	32.84	29.71	27.97	30.12	33.50	35.72	37.74	39.70	41.66
St2	42.30	41.95	36.26	30.94	28.08	26.77	28.62	32.21	34.23	36.04	37.79	39.54
St3	25.04	23.95	19.89	15.99	12.65	11.09	13.22	16.59	18.88	21.07	23.25	25.44
St4	23.18	22.82	18.06	14.91	11.05	10.06	12.11	15.19	17.18	20.07	22.05	24.23
St3’	32.88	30.07	26.05	21.93	19.23	18.08	20.06	23.25	25.27	27.73	30.18	31.98
St4’	29.87	27.39	23.16	19.55	17.28	15.90	18.34	21.54	23.75	25.88	28.00	30.13

Source: own work.

When comparing the wind speed levels of the current and proposed scenarios between Streets Str1 and Str2, we noticed the following (Fig. 12, Table 7):

– In the current scenario, Str1 (St1 and St2) exhibits relatively low wind speeds throughout the day, generally ranging from 0.14 to 0.49 $m \cdot s^{-1}$. In contrast, Str2 (St3 and St4) experiences higher wind speeds, with values ranging from approximately 0.79 $m \cdot s^{-1}$ to 1.12 $m \cdot s^{-1}$. These differences indicate that Str2, located within the collective housing fabric, is more exposed to wind compared to Str1, which is situated in the traditional individual residential fabric.
– In the proposed greening scenario for Str2 (St3′ and St4′), a slight increase in wind speed was observed, ranging from 1.06 to 1.30 $m \cdot s^{-1}$, compared to the current condition of the two streets. This improvement in airflow highlights the role of local palm trees in redirecting and stabilizing wind movement within contemporary urban fabrics, unlike the low wind conditions observed in Str1.

Overall, the analysis suggests that the proposed greening plan for Str2 could significantly enhance wind speeds in the area.

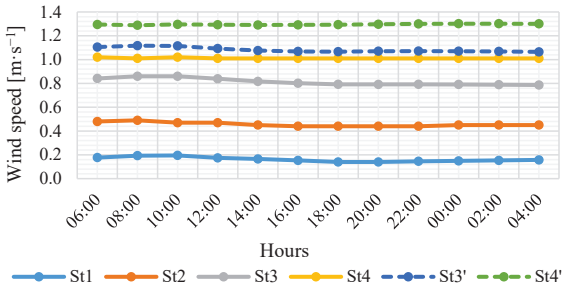

FIGURE 12. Comparison of the daily average wind speed in Streets Str1 and Str2: current versus proposed scenarios

Source: own work.

Khelifa, N., Boukhabla, M., Bouzaher, S. (2026). Quantifying thermal comfort improvement by palm tree-based street greening, in hot and dry climate. *Sci. Rev. Eng. Env. Sci.*, *35* (2), 158–183. DOI 10.22630/srees.10366

TABLE 7. Comparison of the daily average wind speed for Streets Str1 and Str2

Station	Hour											
	6:00	8:00	10:00	12:00	14:00	16:00	18:00	20:00	22:00	0:00	2:00	4:00
St1	0.18	0.19	0.19	0.17	0.17	0.15	0.14	0.14	0.15	0.15	0.15	0.16
St2	0.48	0.49	0.47	0.47	0.45	0.44	0.44	0.44	0.44	0.45	0.45	0.45
St3	0.84	0.86	0.86	0.84	0.82	0.80	0.79	0.79	0.79	0.79	0.79	0.79
St4	1.02	1.01	1.02	1.01	1.01	1.01	1.01	1.01	1.01	1.01	1.01	1.01
St3’	1.10	1.12	1.11	1.09	1.08	1.07	1.07	1.07	1.07	1.07	1.07	1.06
St4’	1.29	1.29	1.30	1.29	1.29	1.29	1.29	1.30	1.30	1.30	1.30	1.30

Source: own work.

When comparing the daily average mean radiant temperature (*MRT*) of the current and proposed scenarios in Streets Str1 and Str2, we noticed the following (Fig. 13, Table 8):

– In the current scenario, the average *(MRT*) of Str1 (St1 and St2) is consistently lower than that of Str2 (St3 and St4) throughout the day. Values for Str1 range from 25.20°C at 4:00 a.m. at Station St1 to 57.62°C at 2:00 p.m. at Station St2. In contrast, Str2 experiences greater fluctuations in *MRT*, with values ranging from approximately 36.11°C at 6:00 a.m. at Station St3 to 79.71°C at 2:00 p.m. at Station St4 during daytime hours.
– In the proposed greening scenario for Str2 (St3′ and St4′), there was a substantial reduction in average (*MRT*) compared to the current situation (St3 and St4). The difference between the minimum and maximum daily average values ranged from 5.94°C to 8.16°C during the day.

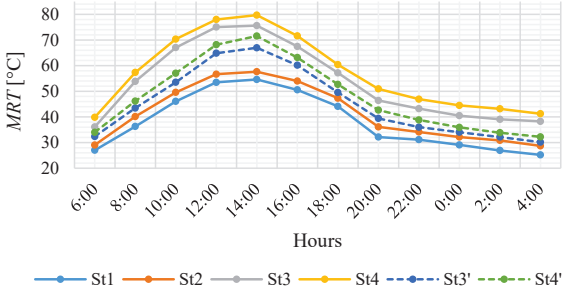

FIGURE 13. Comparison of the daily average mean radiant temperature (*MRT*) in Streets Str1 and Str2: current versus proposed scenarios

Source: own work.

This analysis indicates that the proposed greening measures effectively reduced (*MRT*) in Street Str2. However, the thermal conditions in Str1 within the traditional individual residential fabric remained lower, despite not being subjected to a greening scenario, benefiting instead from the cooling effect of the surrounding local palm groves.

TABLE 8. Comparison of the daily average mean radiant temperature for Streets Str1 and Str2

Station	Hour											
	6:00	8:00	10:00	12:00	14:00	16:00	18:00	20:00	22:00	0:00	2:00	4:00
St1	27.01	36.28	46.07	53.48	54.61	50.56	44.12	32.15	31.13	29.09	26.91	25.20
St2	29.04	40.14	49.57	56.68	57.62	54.01	47.30	36.11	34.12	32.16	30.86	28.70
St3	36.11	53.85	67.03	75.05	75.62	67.49	57.18	46.42	43.23	40.49	39.07	38.26
St4	39.85	57.36	70.33	77.99	79.71	71.61	60.40	50.94	46.93	44.49	43.15	41.25
St3’	32.36	43.46	53.50	64.83	66.98	60.16	49.56	39.41	36.02	34.03	32.17	30.17
St4’	34.00	46.19	57.05	68.16	71.55	63.15	52.68	42.67	38.84	35.92	33.85	32.24

Source: own work.

PET assessment revealed significant differences between the Street Str1, which is located in traditional individual residential fabric and the Street Str2 located in collective housing fabric. Street Str1 consistently maintains lower *PET* values throughout the day, with peak values at 14:00 reaching 60.7°C (St1) and 62.0°C (St2). In contrast, the current condition of Street Str2 exhibits higher thermal stress, with maximum *PET* values rising to 63.7°C (St3) and 64.9°C (St4). The measurement results of the current situation in both streets highlight the thermal resilience of traditional urban forms and the cooling effect of adjacent palm groves. This finding aligns with the conclusions of Abaas (2020) and Al-atrash and Al-ayyoub (2023), who emphasized the effectiveness of shading and urban form in reducing radiative exchange in hot and arid regions.

In the proposed simulation scenario of planting native palm trees along Street Str2, a clear improvement was observed, with *PET* values decreasing by 1.6°C (St3′) and 1.8°C (St4′) during solar peak hours (14:00). The cooling effect confirms the findings of Sayad et al. (2021) and Necira et al. (2024), who reported similar reductions in *PET* and *UTCI* following the implementation of linear afforestation in arid streets. Despite these improvements, *PET* values in all scenarios remain above 60°C in the afternoon (Fig. 14, Table 9). This suggests that while native palms effectively narrow the thermal performance gap between contemporary and traditional urban fabrics, additional mitigation strategies are required to achieve acceptable comfort levels in hot and dry climates. Such strategies may include increasing canopy density or integrating other tree species alongside palm trees (Ridha, 2017; Biqaraz et al., 2019).

Khelifa, N., Boukhabla, M., Bouzaher, S. (2026). Quantifying thermal comfort improvement by palm tree-based street greening, in hot and dry climate. *Sci. Rev. Eng. Env. Sci.*, *35* (2), 158–183. DOI 10.22630/srees.10366

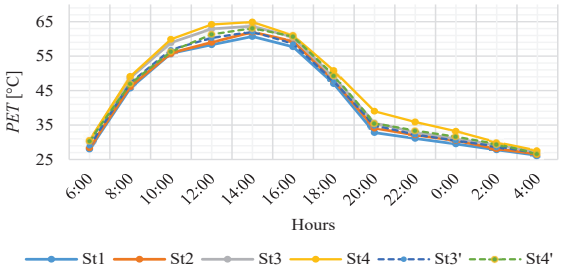

FIGURE 14. Comparison of the daily average physiological equivalent temperature (*PET*) in Streets Str1 and Str2: current versus proposed scenarios

Source: own work.

TABLE 9. Comparison of the daily average physiological equivalent temperature for Streets Str1 and Str2

Station	Hour											
	6:00	8:00	10:00	12:00	14:00	16:00	18:00	20:00	22:00	0:00	2:00	4:00
St1	28.00	45.70	55.80	58.30	60.70	57.70	47.00	32.80	31.10	29.50	27.80	26.20
St2	28.40	46.20	55.90	59.00	62.00	59.30	47.90	34.10	32.10	30.50	28.10	26.60
St3	30.30	48.70	58.90	62.90	63.70	60.50	48.80	35.60	32.90	31.00	29.20	27.10
St4	30.60	49.10	59.90	64.20	64.90	61.00	50.80	39.00	35.90	33.20	30.00	27.60
St3′	29.00	47.20	56.90	60.30	62.10	58.60	47.70	34.90	32.20	30.50	28.80	26.80
St4′	30.40	47.00	56.40	61.30	63.10	60.70	49.40	35.50	33.40	31.60	29.50	26.70

Source: own work.

When comparing the daily average new standard effective temperature (*SET**) between the current and proposed scenarios in Streets Str1 and Str2, we observed the following (Fig. 15, Table 10):

– In the current situation, the results showed clear differences between the two streets: Str1 in traditional individual residential fabric (S1), and Str2 in collective housing fabric (S2). We note that Street Str1, surrounded by palm groves, demonstrated better thermal performance than Street Str2. At peak heat hour (2:00 p.m.), *SET** values recorded at Stations St1 and St2 were 56.6°C and 57.9°C, respectively, while the *SET** measurements at Street Str2 were higher, 59.7°C at Station St3 and 61.0°C at Station St4. This variation in measurements underscores the thermal resilience and adaptability of the traditional urban fabric in hot, dry climates, as confirmed by a study of Ridha (2017), and Khalil and Wahhab (2020).

– In the proposed simulation scenario of planting native palm trees (*Phoenix dactylifera*) along Street Str2, we observed a clear improvement and a decrease in *SET** values: 1.6°C at Street St3′ (58.1°C) and 5.4°C at Street St4′ (55.6°C) at peak solar hour (14:00). This improvement highlights the lack of natural shading before the afforestation process.

The results are consistent with numerous previous studies conducted in hot and dry regions, which demonstrate that vegetation cover, particularly local palm trees, enhances the local climate by intercepting solar radiation (providing shading) and through transpiration.

Therefore, incorporating native palm trees into contemporary street design emerges as a vital strategy to bridge the thermal performance gap between contemporary and traditional urban fabrics in arid climates.

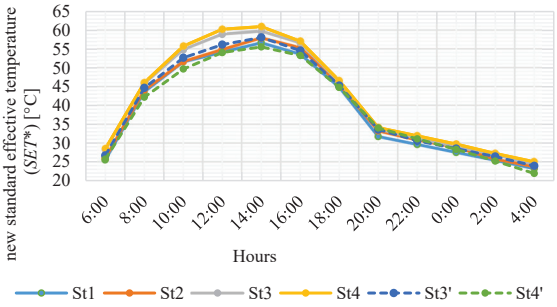

FIGURE 15. Comparison of the daily average new standard effective temperature in Streets Str1 and Str2: current versus proposed scenarios

Source: own work.

TABLE 10. Comparison of the daily average new standard effective temperature for Streets Str1 and Str2

Station	Hour											
	6:00	8:00	10:00	12:00	**14:00**	16:00	18:00	20:00	22:00	0:00	2:00	**4:00**
St1	25.50	43.60	51.50	54.10	56.60	53.60	44.80	31.70	29.60	27.50	25.40	23.20
St2	26.00	44.00	51.60	54.80	57.90	55.30	45.60	33.20	30.80	28.80	25.70	23.70
St3	28.2	45.8	54.8	58.9	59.7	56.6	46.2	33.7	31.2	29	26.9	24.30
St4	28.5	46.1	55.8	60.3	61.00	57.1	46.6	34.1	31.9	29.7	27.2	25.00
St3’	26.7	44.7	52.7	56.2	58.1	54.6	45.3	33.6	30.6	28.5	26.4	23.9
St4’	25.7	42.2	49.7	54.1	55.6	53.3	44.8	34	31.1	28.3	25.2	21.9

Source: own work.

Khelifa, N., Boukhabla, M., Bouzaher, S. (2026). Quantifying thermal comfort improvement by palm tree-based street greening, in hot and dry climate. *Sci. Rev. Eng. Env. Sci.*, *35* (2), 158–183. DOI 10.22630/srees.10366

Conclusions

This study concluded that planting palm trees along urban streets constitutes a climatically appropriate strategy and a sustainable solution for enhancing outdoor thermal comfort in hot and arid environments. The research employed an integrated methodology combining field measurements with computational simulations using Envi-Met and Rayman, thereby providing a deeper understanding of the influence of local vegetation on urban climatic performance.

A comparative analysis was conducted between two streets representing distinct urban fabrics. The first street, part of a traditional individual residential fabric, had not undergone tree planting but was surrounded by local palm groves. In contrast, the second street, belonging to a collective housing fabric designed for collective housing, was subjected to a palm tree planting proposal. This comparison revealed significant differences in climatic performance between the two cases.

The results indicate that Str1 demonstrated a remarkable advantage in thermal comfort levels both before and after the palm tree planting plan proposed for Str2. This superiority is attributed to the surrounding palm groves, which enhanced street-level shading, in addition to the influence of building design and street width. In contrast, the proposed palm tree planting along Str2 revealed a significant improvement across all thermal comfort indicators compared to pre-planting measurements. Notably, reductions were recorded in all measured parameters, including the *PET* and the *MRT*, accompanied by an improvement in relative humidity.

The findings confirmed the effectiveness of selecting local palm trees and their strong adaptability to hot and arid climatic conditions, particularly in regions suffering from water scarcity. This demonstrates the importance of carefully choosing appropriate tree species for street planting to maximize cooling efficiency and sustainability, in contrast to deciduous trees that may negatively affect thermal conditions during the winter season.

Methodologically, the results of this study contribute to validating the field measurement approach by comparing it with digital simulations, thereby strengthening the alignment between empirical data collection and computational modeling for assessing and proposing future design scenarios that support afforestation projects in hot and arid climates. Furthermore, the findings call upon local authorities and decision-makers to prioritize street planting programs using local palm trees, ensuring appropriate spacing and adequate maintenance to enhance outdoor thermal comfort. Urban planning and building regulations for new projects should also stipulate a minimum tree planting density,

with the possibility of verifying thermal comfort performance criteria through simulation tools such as Envi-Met.

This study examines two streets with contrasting characteristics, providing an opportunity to explore quantitative improvements within specific contexts. Nevertheless, conducting a broader spatial analysis that encompasses multiple neighborhoods with diverse architectural forms would enhance the generalizability of the findings and strengthen their reliability for applications in sustainable urban planning.

References

Abaas, Z. R. (2020). Impact of development on Baghdad's urban microclimate and human thermal comfort. *Alexandria Engineering Journal*, *59*(1), 275–290. https://doi.org/10.1016/j.aej.2019.12.040

Al-Atrash, F. Z., & Al-Ayyoub, A. (2023). Evaluating urban outdoor thermal comfort in Jabal Al Natheef Amman. *Sustainability*, *15*(5), 4092. https://doi.org/10.3390/su15054092

American Society of Heating, Refrigerating and Air-Conditioning Engineers [ASHRAE]. (2002). *Measurement of energy and demand savings* (ASHRAE Guideline 14-2002).

Arab, L., Kreuzwieser, J., Kruse, J., Zimmer, I., Ache, P., Alfarraj, S., Al-Rasheid, K. A. S., Schnitzler, J. P., Hedrich, R., & Rennenberg, H. (2016). Acclimation to heat and drought-Lessons to learn from the date palm (Phoenix dactylifera). *Environmental and Experimental Botany*, *125*, 20–30. https://doi.org/10.1016/j.envexpbot.2016.01.003

Audu, Y., & Lintoc, A. C. (2018). Inventory and assessment of carbon storage capacity of species of palms in Universiti Tun Husein Onn Malaysia, Main Campus, Batu Pahat, Johor Malaysia. *International Journal of Integrated Engineering*, *10*(9), 1–6. https://doi.org/10.30880/ijie.2018.10.09.001

Bencheikh, H., & Rchid, A. (2012). The effects of green spaces (palme trees) on the microclimate in arides zones, case study: Ghardaia, Algeria. *Energy Procedia*, *18*, 10–20. https://doi.org/10.1016/j.egypro.2012.05.013

Biqaraz, B., Fayaz, R., & Naeeni, G. H. (2019). A comparison of outdoor thermal comfort in historical and contemporary urban fabrics of Lar City. *Urban Climate*, *27*, 212–226. https://doi.org/10.1016/j.uclim.2018.11.007

Boukhabla, M., Femmam, N., Khelifa, N., Bouzaher, S., & Alkama, D. (2022). The climate of buildings: The pressure of CO_2 in the volume of the street and the role of the palm tree in its regulation. *International Journal of Innovative Studies in Sociology and Humanities*, *7*(9), 56–62. https://doi.org/10.20431/2456-4931.070906

Coccolo, S., Pearlmutter, D., Kaempf, J., & Scartezzini, J. L. (2018). Thermal Comfort Maps to estimate the impact of urban greening on the outdoor human comfort. *Urban Forestry and Urban Greening*, *35*, 91–105. https://doi.org/10.1016/j.ufug.2018.08.007

Elsadek, M., Liu, B., Lian, Z., & Xie, J. (2019). The influence of urban roadside trees and their physical environment on stress relief measures: A field experiment in Shanghai. *Urban Forestry and Urban Greening*, *42*, 51–60. https://doi.org/10.1016/j.ufug.2019.05.007

ENVI-Met GmbH. (2022). *Leonardo* (Computer software). ENVI-Met. https://www.envi-met.com

Farhi, A. (2002). Biskra: de l'oasis à la ville saharienne (Note). *Méditerranée*, *99*(3), 77–82. https://doi.org/10.3406/medit.2002.3264

Geletič, J., Lehnert, M., Resler, J., Krč, P., Middel, A., Krayenhoff, E. S., & Krüger, E. (2022). High-fidelity simulation of the effects of street trees, green roofs and green walls on the distribution of thermal exposure in Prague-Dejvice. *Building and Environment*, *223*, 109484. https://doi.org/10.1016/j.buildenv.2022.109484

Gillner, S., Vogt, J., Tharang, A., Dettmann, S., & Roloff, A. (2015). Role of street trees in mitigating effects of heat and drought at highly sealed urban sites. *Landscape and Urban Planning*, *143*, 33–42. https://doi.org/10.1016/j.landurbplan.2015.06.005

Jackson, E. K., Roberts, W., Nelsen, B., Williams, G. P., Nelson, E. J., & Ames, D. P. (2019). Introductory overview: Error metrics for hydrologic modelling – A review of common practices and an open source library to facilitate use and adoption. *Environmental Modelling & Software*, *119*, 32–48. https://doi.org/10.1016/j.envsoft.2019.05.001

Jing, W., Qin, Z., Mu, T., Ge, Z., & Dong, Y. (2024). Evaluating thermal comfort indices for outdoor spaces on a university campus. *Scientific Reports*, *14*(1), 1–16. https://doi.org/10.1038/s41598-024-71805-5

Khalil, H. I., & Wahhab, K. A. (2020). Investigation thermal comfort in urban environmental centres by combining traditional and modern principles. *Periodicals of Engineering and Natural Sciences*, *8*(3), 1674–1684. https://doi.org/10.21533/pen.v8.i3.1204

Klemm, W., Heusinkveld, B. G., Lenzholzer, S., & Hove, B. van (2015). Street greenery and its physical and psychological impact on thermal comfort. *Landscape and Urban Planning*, *138*, 87–98. https://doi.org/10.1016/j.landurbplan.2015.02.009

Liu, J., Zheng, B., & Yang, F. (2023). A simulation study of the impact of urban street greening on the thermal comfort in street canyons on hot and cold days. *Forests*, *14*(11), 2256. https://doi.org/10.3390/f14112256

Marando, F., Heris, M. P., Zulian, G., Udías, A., Mentaschi, L., Chrysoulakis, N., Parastatidis, D., & Maes, J. (2022). Urban heat island mitigation by green infrastructure in European Functional Urban Areas. *Sustainable Cities and Society*, *77*, 103564. https://doi.org/10.1016/j.scs.2021.103564

Matallah, M. E., Ahriz, A., Zitouni, D. C., Arrar, H. F., Ratmia, M. A. E. B., & Attia, S. (2023). A methodological approach to evaluate the passive cooling effect of Oasis palm groves. *Sustainable Cities and Society*, *99*, 104887. https://doi.org/10.1016/j.scs.2023.104887

Moriasi, D. N., Arnold, J. G., Van Liew, M. W., Bingner, R. L., Harmel, R. D., & Veith, T. L. (2007). Model evaluation guidelines for systematic quantification of accuracy in watershed simulations. *Transactions of the ASABE*, *50*(3), 885–900. https://doi.org/10.13031/2013.23153

Necira, H., Matallah, M. E., Bouzaher, S., Mahar, W. A., & Ahriz, A. (2024). Effect of street asymmetry, albedo, and shading on pedestrian outdoor thermal comfort in hot desert climates. *Sustainability*, *16*(3), 1291. https://doi.org/10.3390/su16031291

Ren, Z., Zhao, H., Fu, Y., Xiao, L., & Dong, Y. (2022). Effects of urban street trees on human thermal comfort and physiological indices: a case study in Changchun city, China. *Journal of Forestry Research*, *33*(3), 911–922. https://doi.org/10.1007/s11676-021-01361-5

Ridha, S. (2017). *Urban heat Island mitigation strategies in an arid climate. In outdoor thermal comfort reacheable* (doctoral dissertation). INSA de Toulouse.

Teshnehdel, S., Akbari, H., Di Giuseppe, E., & Brown, R. D. (2020). Effect of tree cover and tree species on microclimate and pedestrian comfort in a residential district in Iran. *Building and Environment*, *178*, 106899. https://doi.org/10.1016/j.buildenv.2020.106899

Willmott, C. J., & Matsuura, K. (2005). Advantages of the mean absolute error (MAE) over the root mean square error (RMSE) in assessing average model performance. *Climate research*, *30*(1), 79–82. https://doi.org/10.3354/cr030079

Youcef, K., & Guedouh, M. S. (2023). Effects of local trees on the environmental climate of urban outdoor spaces in arid and semi-arid regions. *International Conference on Applied Engineering and Natural Sciences*, *1*(1), 342–346. https://doi.org/10.59287/icaens.1019

Summary

Quantifying thermal comfort improvement by palm tree-based street greening, in hot and dry climate. This paper aims to quantify the improvement in outdoor thermal comfort through palm tree-based street greening in hot, dry regions affected by rapid urbanization and climate change. The study was conducted in Sidi Okba, one of the largest oases in Biskra, Algeria, during summer, characterized by its diverse urban housing fabric. Two streets were compared: Str1, located in a traditional vegetation-free urban fabric but surrounded by *Phoenix dactylifera* palm groves to the northwest and south, and Str2, situated in a contemporary urban fabric with minimal vegetation. The methodology combined field measurements and digital simulations using Envi-Met software to evaluate a greening scenario for Str2 involving palm tree integration. Results revealed that Str1 exhibited superior cooling effects due to its proximity to palm groves, while the proposed greening scenario for Str2 demonstrated significant thermal comfort improvement compared to its current state. Factors such as palm tree density, distribution, and the location of a street within the urban fabric influence microclimatic conditions. The study underscores the efficacy of local palm trees in providing sustainable cooling and their cultural-environmental suitability for hot, arid regions. It urges urban planners to prioritize native vegetation and integrate it into urban development strategies to enhance climate resilience.

Scientific Review Engineering and Environmental Sciences (2026), 35 (2), 184–198

Sci. Rev. Eng. Env. Sci. (2026), 35 (2) https://srees.sggw.edu.pl

ISSN 1732-9353 (suspended) eISSN 2543-7496 DOI 10.22630/srees.11106

Received: 01.02.2026
Accepted: 20.04.2026

Munaf Al-RAMAHEE[1]✉
Haider AMMASH[1]
Haider Al-JELAWY[1]
Sadjad HEMZAH[2]

[1] University of Al-Qadisiyah, College of Engineering, Iraq

[2] University of Kerbala, College of Engineering, Iraq

✉munaf.alramahee@qu.edu.iq

Behavior of self-compacted reinforced concrete deep beams using steel plates as shear reinforcement

Keywords: deep beam, self-compacting concrete, shear reinforcement, steel plate

Introduction

A reinforced concrete (RC) deep beam is one of the structural elements used in different structures, such as bridge bents, bridge girders, pile caps, and offshore structures. The shear deformation dominates the behavior of this element. Therefore, deep beams should be designed to have an acceptable level of shear strength by providing sufficient shear reinforcement. According to ACI 318-2014 (American Concrete Institute [ACI], 2014), the deep beam span should not exceed four times the overall depth. In addition, the shear span should be equal to or less than twice the beam depth. Different parameters play a significant role in controlling

the behavior of this type of structure, such as compressive strength of concrete, the shear span to depth ratio, the reinforcement ratio, and the arrangement of shear reinforcement.

Many studies have been conducted to investigate the role of the shear reinforcement type in reinforced concrete (RC) beams (Colajanni et al., 2014; Ombres, 2015; Ammash, 2017). It was shown experimentally that the shear strength of RC beams increases with the use of additional horizontal and independent bent-up bars (Hamid, 2005). A study was conducted to investigate different types of shear reinforcement that can be employed in RC beams. The obtained results showed that, when swimmer bars were used as shear reinforcement, an improvement was observed in the shear strength of RC beams compared with traditional stirrups (Al-Nasra & Asha, 2013).

Aziz and Yaseen (2013) studied the effect of the type and position of shear reinforcement on the behavior of high-strength deep beams. They showed experimentally that deep beams with a combination of inclined and vertical web reinforcement exhibited greater strength capacity than those with other shear reinforcement arrangements (Aziz & Yaseen, 2013). Ismail et al. (2017) conducted an experimental program to study the effect of different parameters on the behavior of RC deep beams, such as concrete strength, shear span to effective depth ratio, and shear reinforcement. They concluded that the concrete strength, the shear span-depth ratio, and the shear reinforcement need to be included in the current strength reduction factors used in design guidelines for inclined concrete struts (Ismail et al., 2017).

Self-compacting concrete (SCC) is considered an innovative solution for overcoming the challenges related to reinforcement congestion in deep beams. This type of concrete can spread into place, fill formwork, and encapsulate reinforcement due to its highly flowable properties, which eliminate the need for mechanical vibration and maintain homogeneity (EFNARC, 2005; Alkhattat & Al-Ramahee, 2021). SCC is suitable for deep beam applications due to its superior fresh properties, such as high deformability, adequate viscosity to resist segregation, and excellent passing ability through tight reinforcement spacing (Khayat & Mitchell, 2009). It was shown that the SCC deep beams exhibit comparable or superior structural performance compared with traditional concrete deep beams. SCC deep beams show improved concrete quality in congested regions, better bond characteristics between concrete and reinforcement, and enhanced construction efficiency (Hakeem et al., 2024).

Steel plates have recently been considered as an alternative shear reinforcement solution to reduce congestion while maintaining or enhancing structural

performance. They can be configured in many forms, such as perforated thin plates, solid plates, externally bonded plates, and internally embedded plate assemblies (Mhalhal & Al-Gasham, 2018). Different studies have shown varying degrees of success in the use of steel plate reinforcement systems. Chai et al. (2023) studied the use of perforated thin mild steel plates in deep beams and found that 2.0 mm plates with optimal perforation patterns achieved increases in the capacity of approximately 3% compared to the traditional reinforcement. Hamoda et al. (2024) have reported a 129% to 175% increase in ultimate shear capacity when externally bonded stainless-steel plates were used. The range of this increase depended on plate thickness and anchorage detailing.

The most common criterion for replacing traditional reinforcement with an alternative system is based on cross-sectional area equivalency, in which the total area of the traditional reinforcement is matched to the total area of the alternative reinforcement (Su et al., 2009). However, this criterion may not accurately represent the actual force transfer mechanisms in deep beams, where the strut-and-tie behavior and stress distribution differ significantly from those predicted by shallow beam theory. A rational approach would be based on the equivalency of the actual forces that shear reinforcement can carry, considering the specific load paths and stress field in deep beams according to strut-and-tie analysis and ACI 318 provisions. However, the validation of force-based procedure for designing steel plate replacement for shear reinforcement in deep beams is limited, despite the theoretical advantages of force-based equivalency. Moreover, most research has focused on replacing either the web reinforcement (stirrups) or the longitudinal skin reinforcement with steel plates, but studies have examined the simultaneous replacement of both reinforcement types, particularly in the SCC deep beams (Ibrahim et al., 2018; Qaddoory et al., 2021). Furthermore, there is a lack of experimental data on the effect of specific plate thickness on the comprehensive structural performance of SCC deep beams.

This study investigates an innovative approach for SCC deep beams by replacing, based on equivalency, both conventional vertical stirrups and longitudinal skin reinforcement with steel plates of varying thicknesses. Unlike previous studies that employed the area equivalency method, this study employs a force-based equivalency approach, in which the required force capacity of the traditional shear reinforcement is calculated based on strut-and-tie analysis and ACI 318 design provisions, and then used as the basis for determining the appropriate steel plate width replacement. Steel plates with different thicknesses were used (2 mm, 3 mm, and 4 mm) in this study as both vertical and longitudinal reinforcement to investigate the effect of these thicknesses on the structural performance of SCC deep beams.

Material and methods

The experimental program in this research consisted of manufacturing and testing seven self-compacting reinforced concrete deep beams. The dimensions of all specimens were 125 mm (width) and 400 mm (height) with a total length of 1,100 mm and 1,000 mm between supports length. The first specimen was considered a control specimen, where it was reinforced with conventional flexural and shear reinforcement. The control specimen (DB-control) was longitudinally reinforced with 4ø16 mm at bottom and 2ø10 mm at top. Also, it reinforced with 4ø10 mm for skin reinforcement and ø10 mm @ 100 mm c/c web reinforcement as shown in Figure 1. The remaining six specimens were divided into two groups with three specimens for each group. In the first group, comprising three deep beams (DB-web-2, DB-web-3, and DB-web-4), the web reinforcement was replaced with steel plates with a smooth surface finish and varying thicknesses (2 mm, 3 mm, and 4 mm) for each specimen, while the longitudinal and skin reinforcement were kept the same as in the control specimen. The width of each plate was determined based on the force transfer equivalency as 39 mm, 26 mm, and 19.5 mm for the 2 mm, 3 mm, and 4 mm plates' thickness, respectively. The details of the first group are shown in Figure 2 and Table 1. In the second group, comprising three specimens (DB-skn-2, DB-skn-3, and DB-skn-4), the skin reinforcement was also replaced by steel plates with smooth surface finish and a thicknesses of 2 mm, 3 mm, and 4 mm for each specimen, while the longitudinal and web reinforcement were kept the same as the control specimen. The width of each plate was calculated based on the same criteria to be 39 mm, 26 mm, and 19.5 mm for the 2 mm, 3 mm, and 4 mm plates' thicknesses, respectively. The details of skin reinforcement for this group were shown in Figure 3 and Table 1. All plate reinforcement, whether used as web or skin reinforcement, was tied to the traditional reinforcement using steel wire (binding wire) prior to casting to ensure proper positioning and mechanical connection within the concrete.

To ensure the concrete could spread in place, fill the formwork, and fill the gaps between plates, SCC was used in all specimens in this study. Different materials were used in this research, such as portland cement, fine and coarse aggregates, powder, superplasticizer, and steel plates. The proportions of the SCC mix were as follows: 446 $kg \cdot m^{-3}$ of cement, 759 $kg \cdot m^{-3}$ of fine aggregate, 831 $kg \cdot m^{-3}$ of coarse aggregate, 0.12 $kg \cdot m^{-3}$ of superplasticizer, and 132 $kg \cdot m^{-3}$ of limestone powder. The compressive strength at the age of 28 days for the SCC mixes used in the deep beams was determined to be 35 MPa in accordance with ASTM C192/C192M-19 (ASTM International [ASTM], 2019). The mechanical properties

Al-Ramahee, M., Ammash, H., Al-Jelawy, H., Hemzah, S. (2026). Behavior of self-compacted reinforced concrete deep beams using steel plates as shear reinforcement. *Sci. Rev. Eng. Env. Sci.*, *35* (2), 184–198. DOI 10.22630/srees.11106

of all reinforcement and steel plates are shown in Table 2. The tensile test was performed in accordance with ASTM-A370 (ASTM, 2016) and ASTM A615/A615M-20 (ASTM, 2020). All beams were tested under a four-point loading configuration, resulting in a shear span of approximately 333 mm and a shear span-to-effective depth ratio of approximately 1, as shown in Figure 4.

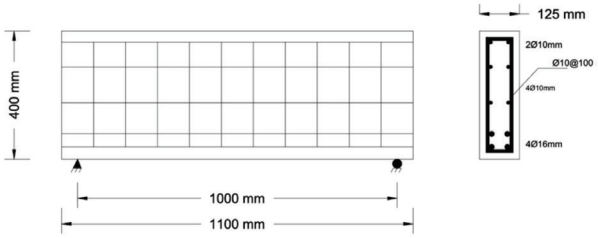

FIGURE 1. Details of the control self-compacting concrete deep beam
Source: own work.

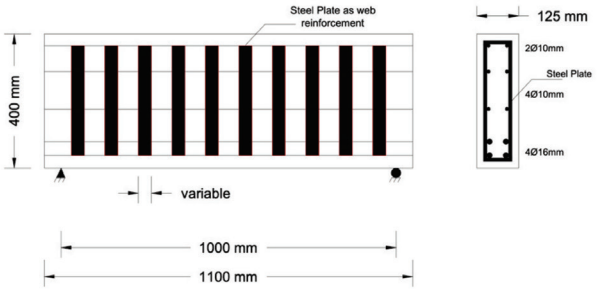

FIGURE 2. Details of self-compacting concrete deep beam with steel plate as web reinforcement
Source: own work.

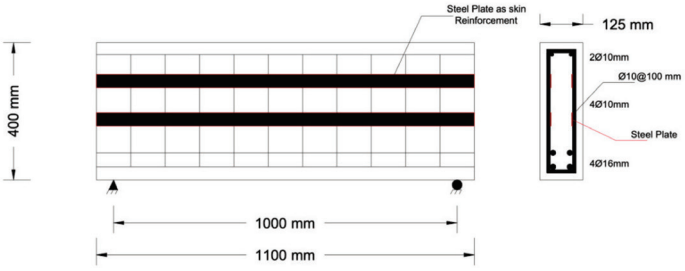

FIGURE 3. Details of self-compacting concrete deep beam with steel plate as skin reinforcement
Source: own work.

TABLE 1. Reinforcement details of self-compacting concrete deep beams

Beam ID	Group	Longitudinal reinforcement	Web reinforcement	Skin reinforcement	Steel plate width [mm]
DB-control	control	top 2ø10 mm bottom 4ø16 mm	ø10 mm @ 100	4ø10 mm	–
DB-web-2	1		2 mm steel plate	4ø10 mm	39
DB-web-3			3 mm steel plate	4ø10 mm	26
DB-web-4			4 mm steel plate	4ø10 mm	19.5
DB-skn-2	2		ø10 mm @ 100	2 mm steel plate	39
DB-skn-3			ø10 mm @ 100	3 mm steel plate	26
DB-skn-4			ø10 mm @ 100	4 mm steel plate	19.5

Source: own work.

TABLE 2. Mechanical properties of steel bars and plates

Property	ø10	ø16	2 mm steel plate	3 mm steel plate	4 mm steel plate
Yield strength [N·mm^{-2}]	520	563	390	320	250
Tensile strength [N·mm^{-2}]	610	682.94	440	380	340

Source: own work.

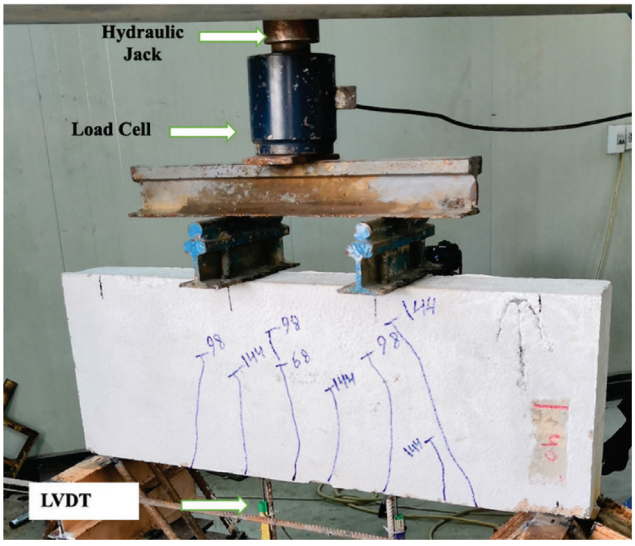

FIGURE 4. Universal testing machine

Source: own work.

Al-Ramahee, M., Ammash, H., Al-Jelawy, H., Hemzah, S. (2026). Behavior of self-compacted reinforced concrete deep beams using steel plates as shear reinforcement. *Sci. Rev. Eng. Env. Sci.*, *35* (2), 184–198. DOI 10.22630/srees.11106

Results and discussion

All specimens were initially cracked at a constant moment zone between loading points. The first crack was recorded in each beam at loads ranging from 40–60 kN, which represents 6–19% of the ultimate load of the SCC deep beams. With an increase in the applied load, inclined shear crack in the shear span zone has started to develop, while the existing flexural cracks propagated toward the compression zone and the applied load. Two failure modes were observed, as shown in Table 3.

TABLE 3. Summary of test results

Beam ID	First crack load [kN]	Ultimate load [kN]	(Pu–Pu control)/ /(Pu control) [%]	Failure mode
DB-control	50	425	1	strut compression failure
DB-web-2	55	312	−26	diagonal splitting failure
DB-web-3	55	344	−19	diagonal splitting failure
DB-web-4	40	470	11	strut compression failure
DB-skn-2	60	355	−16	diagonal splitting failure
DB-skn-3	50	418	−2	diagonal splitting failure
DB-skn-4	40	432	2	diagonal splitting failure

Source: own work.

The first one was the strut compression failure, observed in the control specimen and the DB-web-4 specimen. In these beams, the load was transferred through a path between the shear span area between the support and the point of loading. The second failure mode was a diagonal splitting failure in the remaining specimens. In this mode, the diagonal cracks propagated and extended in the shear span area between the support and the loading point. Examples of failure modes are shown in Figure 5.

The load versus mid-span displacement relationship curves are shown in Figures 6 and 7. These figures show comparison between the control specimen and the specimens in Group 1 (steel plates as web reinforcement) and Group 2 (steel plates as skin reinforcement), respectively. It can be seen from these figures that all specimens with steel plates as web and skin reinforcement had the same initial stiffness. This attribute can be related to the force-based equivalency method that was used in this research. However, Figures 6 and 7 show some differences in the ultimate load capacity compared to the control specimen. For beams with steel plates as web reinforcement, the ultimate load for the beam with a 4 mm

plate was 470 kN, which exceeded the ultimate load of the control beam by 11%. While for the beam with a 2 mm steel plate, a reduction in the ultimate load capacity of about 26% was recorded compared to the control specimen. For the beam with a 3 mm steel plate, the peak load decreased by 19% when compared to the control specimen. The observation of lower ultimate load-carrying capacity of the specimen with a 2 mm plate thickness compared to other specimens can be related to the reduced confinement effect provided by plates with lower flexural rigidity and the observed bond loss at the concrete-steel interface, especially over a larger contact surface, despite the increased contact area.

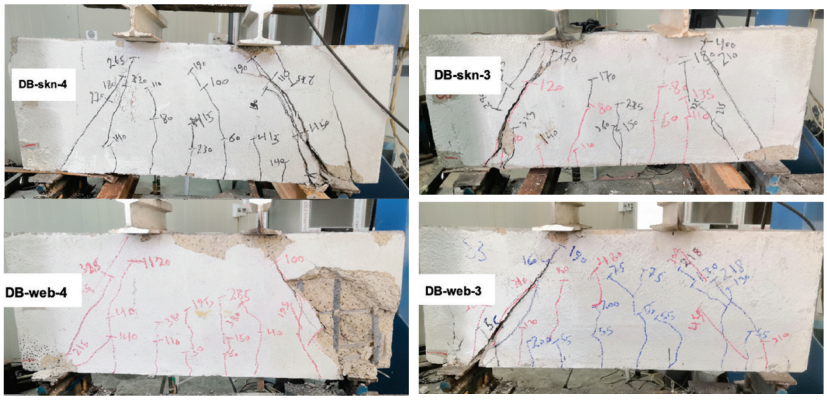

FIGURE 5. Samples of failure modes in self-compacting concrete deep beams
Source: own work.

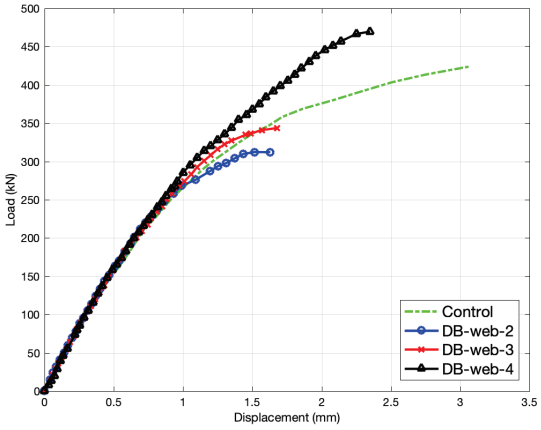

FIGURE 6. Load–displacement curve comparison for the equivalent steel plate as web reinforcement
Source: own work.

Al-Ramahee, M., Ammash, H., Al-Jelawy, H., Hemzah, S. (2026). Behavior of self-compacted reinforced concrete deep beams using steel plates as shear reinforcement. *Sci. Rev. Eng. Env. Sci.*, *35* (2), 184–198. DOI 10.22630/srees.11106

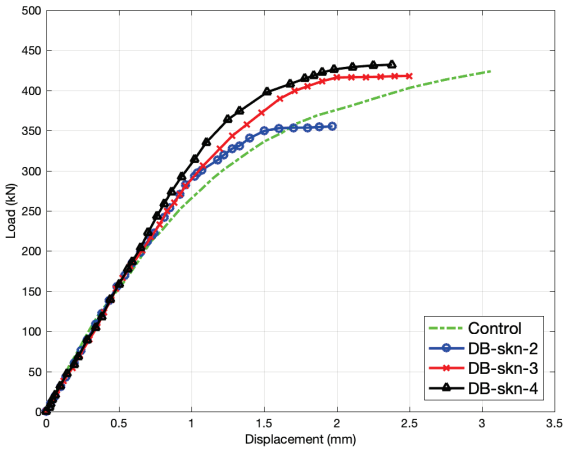

FIGURE 7. Load–displacement curve comparison for the equivalent steel plate as skin reinforcement
Source: own work.

For specimens with steel plates as skin reinforcement, more comparable results to the control beam in terms of ultimate load were achieved. The ultimate load for the beam with a 2 mm steel plate was 355 kN, which is less than the control beam's ultimate load by 16%. Moreover, the ultimate load for 3 mm and 4 mm steel plate beams was 418 kN and 432 kN, which represent 2% decrease and 2% increase compared to the control beam, respectively. Furthermore, it was shown that specimens DB-web-4 mm and DB-skn-4, compared to the control beam and beams with 2 mm and 3 mm, showed fewer cracks. In addition, these cracks were restricted and did not widen significantly. For these two specimens' reinforcement, the steel plates provide more confinement, which delayed the initiation of the first cracks and noticeably enhanced the failure loads compared with the other specimens. It is worth mentioning that local buckling of the steel plate was not observed in any specimens, as full concrete encasement provided continuous lateral restraint to the plates, significantly inhibiting out-of-plane deformation.

Numerical analysis

The numerical simulation was performed using the ABAQUS/Standard package to model and study the structural behavior of the adopted beams. The outcomes of this simulation were compared with and validated against

the corresponding experimental results. A three-dimensional finite element model (FEM) was created in which concrete was modeled using an eight-node linear brick element with reduced integration (C3D8R), and traditional steel reinforcement was modeled using a two-node linear truss element (T3D2). Moreover, the steel plates were represented using S4R shell elements due to their thin-walled nature, as the thicknesses were significantly smaller compared to the other plate dimensions. The nonlinear behavior of SCC was simulated using the concrete damage plasticity (CDP) model, including tensile cracking and compressive crushing. Both steel reinforcement and steel plates were modeled using a uniaxial stress-strain relationship to capture their elastic-plastic behavior.

Figures 8–10 show the comparison of the load mid-span displacement curves for the control beam, the beam with steel plates as web reinforcement, and the beams with steel plates as skin reinforcement, respectively. It can be seen from these figures that the experimental and numerical load versus mid-span displacement correlate well with each other, with a slightly stiffer numerical behavior compared to experimental results due to the assumed ideal connection between the concrete and the reinforcing steel in the numerical model. Table 4 shows the comparison of failure loads between the numerical and experimental results, where the maximum failure load difference between numerical and experimental results was around 9.3%.

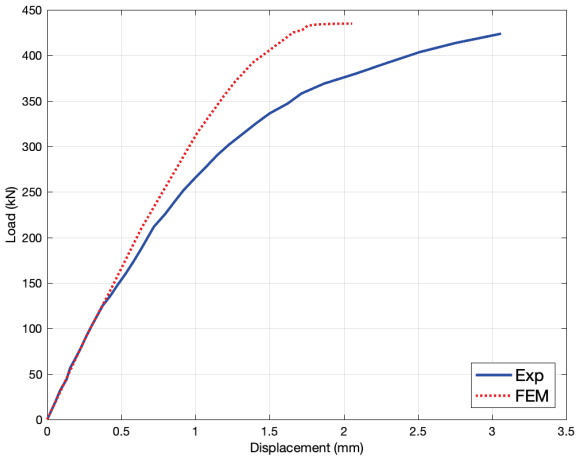

FIGURE 8. Comparison of experimental and numerical load–displacement curves for the control beam
Source: own work.

Al-Ramahee, M., Ammash, H., Al-Jelawy, H., Hemzah, S. (2026). Behavior of self-compacted reinforced concrete deep beams using steel plates as shear reinforcement. *Sci. Rev. Eng. Env. Sci.*, *35* (2), 184–198. DOI 10.22630/srees.11106

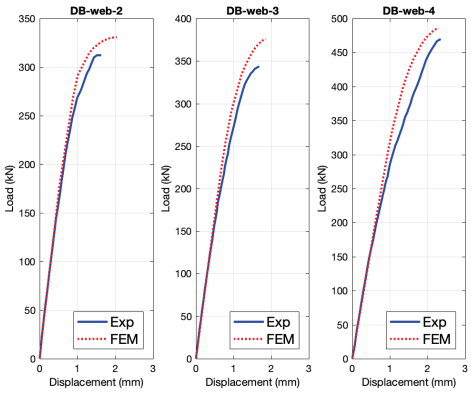

FIGURE 9. Load–displacement curves comparison for a beam with steel plates as web reinforcement
Source: own work.

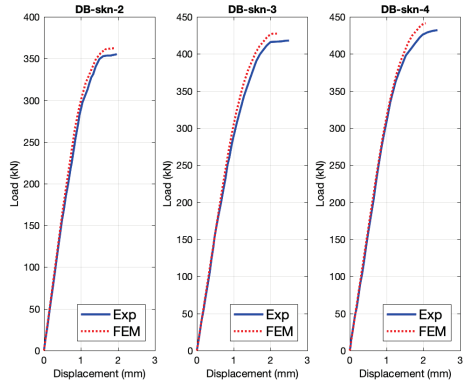

FIGURE 10. Load–displacement curves comparison for a beam with steel plates as skin reinforcement
Source: own work.

TABLE 4. Comparison of the ultimate load between the experimental test and the numerical simulation

Beam	Pu exp [kN]	Pu FEM [kN]	Increase in FEM over experimental [%]
DB-control	425	435	2.3
DB-web-2	312	330	5.7
DB-web-3	344	376	9.3
DB-web-4	470	486	3.4
DB-skn-2	355	362	1.9
DB-skn-3	418	427	2.1
DB-skn-4	432	441	2.0

Source: own work.

The validated numerical model was used to conduct another case where the steel plates were used as equivalent for skin and web reinforcement, which was not done experimentally. Based on the experiment, DB-web-4 showed the best structural performance based on ultimate load and crack pattern. This specimen was selected to perform additional analysis. Three new cases from DB-web-4 were simulated, which combine the 4 mm web steel plates reinforcement with 2 mm, 3 mm, and 4 mm as skin reinforcement. Figure 11 shows the load displacement curves for the new cases DB-web4-skn2, DB-web4-skn3, and DB-web4-skn4. From this figure, there is no significant difference among these cases. It can be concluded that web reinforcement is governing the behavior of the deep beam over the skin reinforcement.

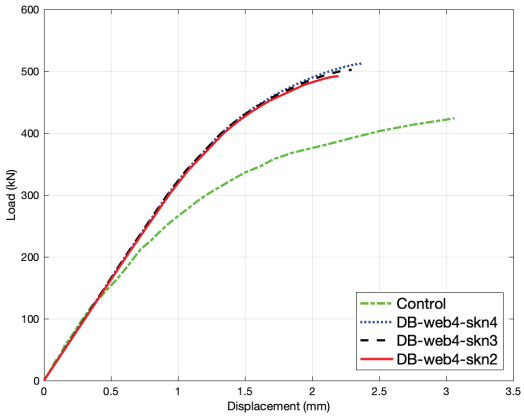

FIGURE 11. Load–displacement curves for a combination of web and skin reinforcement
Source: own work.

Conclusions

This research investigated the structural behavior and shear efficiency of self-compacted reinforced concrete deep beam incorporating steel plates as an alternative to conventional stirrups and skin reinforcement. The following conclusions can be drawn from the research:

– The experimental results showed that the effectiveness of replacing traditional shear reinforcement with steel plates is highly dependent on plate thickness.
– The use of 4 mm-thick steel plates as web reinforcement resulted in an 11% increase in ultimate capacity compared with the control.

- The beams with a 2 mm and a 3 mm steel plates as web reinforcement exhibited decreases in the ultimate load of 26% and 19% respectively, compared to the control specimen.
- The incorporation of steel plates with varying thicknesses as skin reinforcement yielded results comparable to those of the control beam, suggesting that structural integrity was maintained without significant degradation.
- The finite element analysis showed good agreement with experimental data, confirming the reliability of the proposed reinforcement technique.
- This study concludes that steel plates serve as a viable and effective alternative to conventional shear reinforcement in SCC reinforced deep beams, with optimal structural performance achieved through the implementation of 4 mm-thick web plates.

References

American Concrete Institute [ACI]. (2014). *Building code requirements for structural concrete and commentary* (ACI 318-14).

Alkhattat, S. S., & Al-Ramahee, M. A. (2021). Shear performance of reinforced self-compacting concrete beams incorporating steel and polypropylene fibers. *Scientific Review Engineering and Environmental Sciences*, *30*(4), 537–551. https://doi.org/10.22630/PNIKS.2021.30.4.45

Al-Nasra, M., & Asha, N. M. (2013). Shear reinforcements in the reinforced concrete beams. *American Journal of Engineering Research (AJER)*, *2*(10), 191–199.

Ammash, H. (2017). Behavior of reinforcement concrete beams using steel strips as a shear reinforcements. *International Journal of Applied Engineering Research*, *12*(19), 8681–8688.

ASTM International [ASTM]. (2016). *Standard test methods and definitions for mechanical testing of steel products 1* (ASTM-A370). ASTM. https://doi.org/10.1520/A0370-16

ASTM International [ASTM]. (2019). *Practice for making and curing concrete test specimens in the laboratory* (ASTM C192/C192M-19). https://doi.org/10.1520/C0192_C0192M-19

ASTM International [ASTM]. (2020). *Specification for deformed and plain carbon-steel bars for concrete reinforcement* (ASTM A615/A615M-20). https://doi.org/10.1520/A0615_A0615M-20

Aziz, O. Q., & Yaseen, S. A. (2013). Effect of type and position of shear reinforcement of high-strength reinforced concrete deep beams. *AL Rafdain Engineering Journal*, *21*(5), 69–79.

Chai, K. F., Woon, K. S., Wong, J. K., Lim, J. H., Lee, F. W., & Lee, Y. L. (2023). Experimental and numerical study of the strength performance of deep beams with perforated thin mild steel plates as shear reinforcement. *Applied Sciences*, *13*(14), 8217. https://doi.org/10.3390/app13148217

Colajanni, P., La Mendola, L., Mancini, G., Recupero, A., & Spinella, N. (2014). Shear capacity in concrete beams reinforced by stirrups with two different inclinations. *Engineering Structures*, *81*, 444–453. https://doi.org/10.1016/j.engstruct.2014.10.011

Dassault Systèmes (n.d.). *ABAQUS*. Dassault Systèmes.

European Federation of Specialist Building Products for Concrete [EFNARC]. (2005). *The European guidelines for self-compacting concrete.*

Hakeem, I., Mansour, W., Li, W., & Badawi, M. (2024). Analyze the potential for employing internally welded steel plates to improve the shear response of high-strength self-compacting concrete-encased steel beams with large web openings. *Engineering Structures*, *304*, 117636. https://doi.org/10.1016/j.engstruct.2024.117636

Hamid, N. (2005). *The use of horizontal and inclined bars as shear reinforcement*. Universiti Teknologi Malaysia.

Hamoda, A., Yehia, S., Ahmed, M., Sennah, K., Abadel, A. A., & Shahin, R. I. (2024). Experimental and numerical investigation of shear strengthening of simply supported deep beams incorporating stainless steel plates. *Buildings*, *14*(11), 3680. https://doi.org/10.3390/buildings14113680

Ibrahim, A., Mansor, A., Salman, W. D., & Hamood, M. J. (2018). Strength and ductility of bubbled wide reinforced concrete beams with diverse types of shear steel plates. *International Journal of Engineering & Technology*, *7*(4.2), 502–506.

Ismail, K. S., Guadagnini, M., & Pilakoutas, K. (2017). Shear behavior of reinforced concrete deep beams. *ACI Structural Journal*, *114*(1), 87–99. https://doi.org/10.14359/51689151

Khayat, K., & Mitchell, D. (2009). *Self-consolidating concrete for precast, prestressed concrete bridge elements*. Transportation Research Board. https://doi.org/10.17226/14188

Mhalhal, J., & Al-Gasham, T. (2018). New technique to enhance the shear performance of RC deep beams using mild steel plates. *International Journal of Engineering & Technology*, *7*(4.2), 86–94.

Ombres, L. (2015). Structural performances of reinforced concrete beams strengthened in shear with a cement based fiber composite material. *Composite Structures*, *122*, 316–329. https://doi.org/10.1016/j.compstruct.2014.11.059

Qaddoory, K. I., Mansor, A. A., Mohammed, A. S., & Noman, B. J. (2021). Effect of using different aspect ratio of longitudinal steel plates in reinforced concrete beams. *E3S Web of Conferences*, *318*, 03016. https://doi.org/10.1051/e3sconf/202131803016

Su, R. K. L., Lam, W. Y., & Pam, H. J. (2009). Experimental study of plate-reinforced composite deep coupling beams. *Structural Design of Tall and Special Buildings*, *18*(3), 235–257. https://doi.org/10.1002/tal.407

Summary

Behavior of self-compacted reinforced concrete deep beams using steel plates as shear reinforcement. This research studies the structural behavior of self-compacted reinforced concrete deep beams by using steel plates as an alternative to traditional shear reinforcement. Seven specimens were fabricated and tested to evaluate the effectiveness of steel plate substitution based on force equivalency principles. The experimental program

Al-Ramahee, M., Ammash, H., Al-Jelawy, H., Hemzah, S. (2026). Behavior of self-compacted reinforced concrete deep beams using steel plates as shear reinforcement. *Sci. Rev. Eng. Env. Sci.*, *35* (2), 184–198. DOI 10.22630/srees.11106

includes one specimen with traditional stirrup reinforcement as a control specimen and six specimens divided into two groups. The first group included three beams with web reinforcement substituted with 2 mm, 3 mm, and 4 mm steel plates. The second group included three beams with skin reinforcement replaced by steel plates of the same varying thicknesses. Experimental results showed that using 4 mm-thick web steel plates enhances the load-carrying capacity by 11% compared to the control specimen. Other specimens, especially those with skin reinforcement steel plates, showed comparable performance to the control beam, suggesting that steel plate substitution maintains structural integrity without significant strength degradation. Finite element analysis was carried out using ABAQUS software to validate the experimental results. The numerical outcomes showed good agreement with those from the experimental program in terms of ultimate load capacity. The study concludes that steel plates can serve as a viable alternative to traditional shear reinforcement in self-compacting concrete deep beams, with optimal performance achieved using 4 mm-thick web steel plates.

Scientific Review Engineering and Environmental Sciences (2026), 35 (2), 199–218

Sci. Rev. Eng. Env. Sci. (2026), 35 (2) https://srees.sggw.edu.pl

ISSN 1732-9353 (suspended) eISSN 2543-7496 DOI 10.22630/srees.11113

Received: 05.02.2026
Accepted: 20.04.2026

Okan ŞIMŞEK

Adana Alparslan Türkeş Science and Technology University, Faculty of Architecture and Design, Turkey

✉osimsek@atu.edu.tr

Auditory comfort and noise perception under thermal and visual conditions in urban parks

Keywords: auditory comfort, noise perception, thermal comfort, urban spaces, visual comfort

Introduction

Environmental comfort in open urban spaces is of great significance for urban quality of life and human health. Noise, considered the most serious environmental problem after air pollution, can negatively affect user comfort in outdoor areas (European Environment Agency [EEA], 2019). In this context, auditory comfort is an important dimension of comfort, defined as the perception of a sound environment in a space as non-disturbing and pleasant. Traditionally, auditory comfort evaluations have mostly relied on quantitative noise metrics such as sound pressure level (Vardaxis & Bard, 2018; Torresin et al., 2019). However, in recent years, the "soundscape" approach has emphasized that not only the numerical level of the acoustic environment but also the contextual perception of individuals is important (Zhao et al., 2018; Mascolo et al., 2020; Jo & Jeon, 2021; Mancini et al., 2021). Previous research indicates that higher noise levels in an environment do not automatically lead to poorer perceived acoustic quality. This outcome highlights

that auditory comfort depends on more than just sound pressure level; it is also shaped by qualitative and contextual attributes − such as the spectral composition of sounds, their origin, suitability to the setting, and their interaction with other environmental factors (Cureau et al., 2022; Yang et al., 2024). Human perception is inherently multisensory, meaning that people respond to their surroundings through the combined action of several senses. Consequently, outdoor comfort cannot be interpreted through a single physical stimulus alone. The perception of auditory comfort is closely intertwined with visual and thermal aspects of the environment (Yang & Moon, 2019; Nitidara et al., 2022; Zeng et al., 2024).

Growing evidence in the literature further supports that distinct comfort domains influence one another. A doctoral study, for example, emphasized that thermal, acoustic, and visual comfort parameters are interrelated, although the specific direction or strength of these relationships remains uncertain (Şimşek, 2024). On university campuses, enhancing visual comfort in outdoor settings has been observed to simultaneously improve perceptions of thermal comfort (Lam et al., 2020). Similarly, research in dense urban environments reported that greater thermal discomfort tends to amplify sensitivity to noise, thereby reducing overall acoustic comfort (Lau & Choi, 2021). Climatic characteristics, such as ambient temperature and relative humidity, also play a key role in how individuals perceive both the acoustic landscape and the general outdoor experience (D'Alessandro et al., 2018).

Investigations focusing on the visual–auditory relationship have revealed that visual qualities substantially affect how people judge the acoustic environment of a space. The integration of natural components, in particular, appears to foster positive auditory evaluations. Studies conducted in urban parks confirmed that areas with greenery or water features promote both visual and auditory satisfaction among visitors (Cohen et al., 2014). Conversely, visually monotonous or poorly maintained areas – those lacking natural elements – tend to make existing noise sources feel more intrusive and unpleasant. A study around a university campus similarly showed that as the proportion of natural elements (green areas, water features, etc.) increased, participants' perceptions of acoustic comfort and overall environmental satisfaction also improved (Cureau et al., 2022). Accordingly, higher visual environmental quality can soften the perception of noise and thereby improve auditory comfort.

Evidence on light–sound interactions remains mixed. Early work suggested that very bright conditions may slightly increase noise annoyance relative to typical illumination (Shigehisa & Gunn, 1978), whereas other studies reported negligible effects of illuminance changes on annoyance judgments (Yang & Moon, 2018).

At the same time, improving perceived visual quality has been argued to indirectly support acoustic appraisal; for instance, enhanced lighting quality was associated with reduced annoyance in indoor settings (Ma & Nie, 2014). Overall, the influence of illuminance on auditory outcomes appears subtle and context dependent.

The connection between thermal and auditory comfort has also gained growing attention in recent years. Scholars have examined how air temperature and other climatic variables affect individuals' reactions to noise, and empirical work supports the existence of such cross-modal effects. In a field investigation conducted in a university campus in China, Chen et al. (2022) reported that participants exposed to cold winter temperatures experienced a marked decline in auditory comfort, particularly when unpleasant sounds were present. Interestingly, the introduction of pleasant background sounds – such as soft music or birdsong – counteracted this negative perception, helping participants feel more thermally comfortable even under cool conditions. By contrast, in areas dominated by mechanical or crowd noise, both thermal and auditory comfort ratings deteriorated notably (Chen et al., 2022).

The literature collectively underlines that outdoor comfort is inherently multisensory. Because people interpret environmental stimuli holistically, assessing comfort based solely on a single physical factor offers an incomplete understanding. For this reason, studies increasingly adopt multidimensional frameworks that integrate thermal, visual, and acoustic parameters (Kousis & Pisello, 2020). In public open spaces such as parks and plazas, such integrative research has revealed that comfort ratings across different sensory domains are mutually dependent. For instance, a study by Cureau et al. (2022) found that subjective survey responses provided a more accurate prediction of overall comfort than physical measurements alone, demonstrating the importance of multisensory evaluation (Cureau et al., 2022). Consequently, outdoor environmental design should move beyond isolated interventions − such as noise reduction or shading − and instead aim for strategies that comprehensively address user experience.

Within this context, the present study seeks to explore auditory comfort in outdoor environments by concurrently considering visual and thermal influences. Previous research indicates that auditory comfort is affected not only by sound levels but also by the visual and climatic qualities of the setting. However, the specific mechanisms underlying these multisensory relationships in open public spaces remain insufficiently defined. To fill this gap, the current study employs simultaneous survey and environmental measurements conducted during the autumn season in two major urban parks in Adana, Turkey (Merkez Park and Atatürk Park), which represent the Mediterranean climate and host dense public

use. By integrating subjective and objective data, this research aims to identify the key environmental parameters that shape auditory comfort in outdoor settings. The findings underscore that urban noise management and environmental design must account not only for acoustic variables but also for visual configurations and microclimatic enhancements to foster holistic user comfort.

Material and methods

Study area and participants

The fieldwork took place in two large urban parks − Merkez Park (36°59′44″ N, 35°20′06″ E) and Atatürk Park (36°59′49″ N, 35°19′24″ E) − situated in the city center of Adana, a city characterized by a Mediterranean climate, marked by long hot summers, mild winters, and high annual sunshine duration (Fig. 1). Both parks are important public spaces that function as hubs for social interaction and recreation, attracting residents and visitors throughout the day.

FIGURE 1. Field studies conducted at Merkez Park and Atatürk Park
Source: own work.

Data collection was conducted in October, representing typical autumn conditions. Environmental measurements and on-site surveys were administered at three different times of day: morning (09:00–10:00), midday (12:00–13:00), and afternoon (16:00–17:00). Within each park, four distinct observation points were chosen to reflect variations in surface materials (grass, soil, and pavement), spatial orientation (north and south), and shading conditions (open, tree-shaded, and semi-shaded areas). This sampling strategy ensured that the dataset

captured the micro-environmental diversity present within the parks, enhancing the representativeness of the results. This study was conducted in accordance with institutional ethical guidelines. Ethical approval was obtained from the relevant ethics committee prior to data collection. All participants were informed about the purpose and scope of the study, and written informed consent was obtained through a voluntary participation form.

In total, 202 volunteers of different ages and genders participated in the study. While the participants completed a concise questionnaire describing their immediate perceptions of the surrounding physical environment, simultaneous environmental measurements were taken at the corresponding observation sites.

Data collection process

Two main categories of data were collected in the present research. The first consisted of subjective responses obtained through questionnaires that recorded participants' perceptual evaluations, while the second comprised objective environmental data gathered from physical measurements conducted at the same times and locations as the surveys.

The questionnaire was designed in a structured format with four main sections:

1. Demographic information. This part included basic socio-demographic characteristics such as participants' age, gender, and duration of residence in the region.
2. Immediate auditory perception and comfort evaluation. Participants were invited to assess the sound environment through two key questions: their perception of the noise level and their degree of auditory comfort. Noise perception was rated on a seven-point Likert scale ranging from "very noisy" (−3) to "very quiet" (+3), whereas auditory comfort was evaluated on an equivalent scale from "very uncomfortable" (−3) to "very comfortable" (+3).
3. Perception and preference regarding the sound environment. Respondents identified the types of sounds present in their surroundings − such as traffic, human activity, natural sources, or others − and indicated which sound categories they preferred to hear.
4. Strategies for improving auditory comfort. In this final section, participants selected from a list of potential interventions aimed at enhancing auditory comfort, including the addition of vegetation, installation of noise barriers, or introduction of pleasant natural sound sources.

At the same time as the surveys, seven environmental parameters were measured at each participant's location (Fig. 2): air temperature [°C], relative humidity [%], wind speed [m·s^{-1}], mean radiant temperature [°C], sound pressure level [dBA], horizontal illuminance [klx], and vertical illuminance [klx].

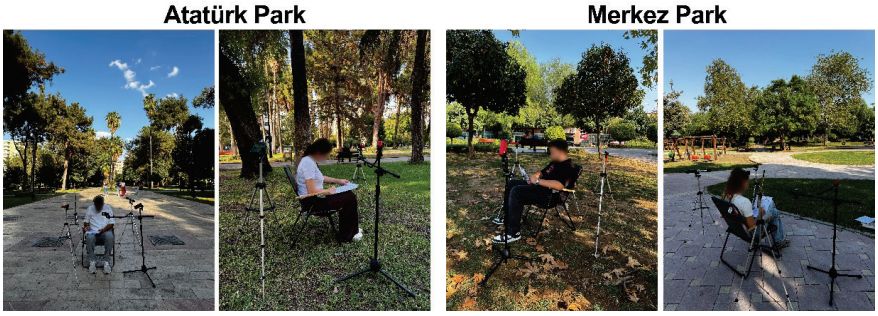

FIGURE 2. Measurement and survey studies
Source: own work.

These measurements were obtained using portable monitoring devices. Each participant's subjective evaluations were directly paired with the corresponding environmental data collected at that moment, yielding an integrated dataset that allowed for detailed comparative analysis.

Measurement devices and parameters

Physical environmental data were collected on site during each survey session to correspond precisely with participants' subjective evaluations. The instruments and parameters used in the measurements are summarized below:

– Air temperature [°C], relative humidity [%], and mean radiant temperature [°C] were obtained with a portable Extech HT200 instrument, which provided real-time readings of microclimatic conditions. The device has an accuracy of approximately ±1°C for air temperature and ±3% for relative humidity.
– Wind speed [m·s^{-1}] was monitored using a wireless anemometer specifically designed for field assessment of local air movement. The instrument is suitable for low air velocity measurements and has an accuracy of approximately ±0.1 m·s^{-1}.
– Sound pressure level [dBA] measurements were performed with a sound level meter compliant with IEC 61672 standards (International Electrotechnical Commission [IEC], 2013) and operating under the A-weighting curve. The device operates within a measurement range of approximately

30–130 dBA and uses a fast response setting to capture short-term fluctuations in the acoustic environment.

– Horizontal and vertical illuminance [klx] were recorded with a portable luxmeter meeting ISO/CIE 19476 requirements (International Organization for Standardization & International Commission on Illumination [ISO & CIE], 2014). Measurements were taken at users' seating height, parallel to the ground for horizontal illuminance, and perpendicular to the line of sight for vertical illuminance. The luxmeter has an accuracy of approximately ±3% and is suitable for outdoor daylight measurements.

All measurements were conducted at approximately 1.1 m above ground level, representing the average seated human position in outdoor environments. All instruments were carefully calibrated before the field campaign. Measurements were conducted simultaneously with the questionnaire surveys, ensuring that environmental data and perceptual responses were precisely synchronized and directly comparable within the integrated dataset.

Data analysis process

The analytical procedure was carried out in three main stages using IBM SPSS Statistics 25. At the first stage, bivariate associations among participants' evaluations of auditory comfort, perceived noise levels, and the measured physical parameters were explored using Pearson's correlation analysis. This approach was selected to identify both the direction and magnitude of linear relationships among variables. Because all variables were measured on continuous scales and met the assumptions required for parametric testing, Pearson's r was considered the most appropriate technique. Accordingly, correlations were calculated between auditory comfort and noise perception scores and the environmental indicators, including air temperature, relative humidity, wind speed, mean radiant temperature, sound pressure level, and both horizontal and vertical illuminance.

The second stage involved assessing whether these relationships remained significant when considered together. To this end, a multiple linear regression analysis was employed, enabling the simultaneous evaluation of several predictors on a single dependent variable. Beyond examining individual influences, this method provides insight into the combined and potentially suppressive or mediating effects among predictors (Lu et al., 2025; Muniz & MacKinnon, 2025). For this reason, multiple regression was adopted as a rigorous tool to elucidate the multifactorial nature of environmental comfort phenomena.

Finally, the third stage focused on aspects of perception extending beyond measured physical factors. Participants' qualitative responses regarding perceived sound types, preferences, and their proposed strategies for improving auditory comfort were systematically analyzed. They identified prevalent sound categories in their surroundings − such as human activity, natural elements, and traffic noise − and expressed their expectations concerning an ideal acoustic environment.

Results and discussion

Correlation analysis

Pearson's correlation analysis results revealed a strong and statistically significant positive relationship between auditory comfort and participants' perceived quietness ($r = 0.772$, $p < 0.001$). In other words, the quieter an environment was perceived to be, the higher the reported level of auditory comfort. Conversely, sound pressure level exhibited a significant negative correlation with auditory comfort ($r = -0.520$, $p < 0.001$), indicating that rising noise levels were consistently associated with reduced comfort ratings.

Regarding the other physical parameter (air temperature, relative humidity, wind speed, mean radiant temperature, and both horizontal and vertical illuminance) no statistically significant relationships with auditory comfort were observed ($p > 0.05$). These outcomes suggest that within the scope of this study, participants' auditory comfort was primarily influenced by noise-related factors rather than by thermal or visual environmental variables. Details of these bivariate relationships are summarized in Table 1.

For participants' subjective noise perception, Pearson's analyses revealed a strong negative correlation with sound pressure level ($r = -0.687$, $p < 0.001$). This indicates that higher measured sound levels led to the environment being perceived as noisier. Another noteworthy finding is that participants' noise perception was not only associated with auditory sources but also significantly related to other environmental stimuli. Specifically, significant correlations were identified with air temperature ($r = 0.155$, $p = 0.034$), relative humidity ($r = -0.202$, $p = 0.005$), and wind speed ($r = -0.185$, $p = 0.011$). These findings suggest that auditory perception can be influenced not only by acoustic properties of the environment but also by thermal comfort parameters through multisensory pathways. An increase in temperature tended to be associated with perceiving the environment as quieter, while higher humidity and wind speed negatively influenced quietness perception. However,

mean radiant temperature, horizontal illuminance, and vertical illuminance did not show significant correlations with noise perception ($p > 0.05$). The details of these bivariate relationships are presented in Table 2.

TABLE 1. Relationships between auditory comfort and other variables

Variable	Pearson's *r*	Significance (*p*)	Interpretation
Noise perception	0.772	0.000	positive and significant: as the environment is perceived quieter, comfort increases
Air temperature	0.070	0.341	weak and non-significant
Relative humidity	−0.119	0.103	weak and non-significant
Wind speed	−0.092	0.207	weak and non-significant
Mean radiant temperature	0.033	0.657	negligible, non-significant
Sound pressure level	−0.520	0.000	negative and significant, higher sound levels reduce comfort
Horizontal illuminance	−0.106	0.148	weak and non-significant
Vertical illuminance	−0.039	0.591	negligible, non-significant

Source: own work.

TABLE 2. Relationships between noise perception and other variables

Variable	Pearson's *r*	Significance (*p*)	Interpretation
Auditory comfort	0.772	0.000	strong positive correlation: as noise decreases, comfort increases
Air temperature	0.155	0.034	significant positive relationship
Relative humidity	−0.202	0.005	significant negative relationship
Wind speed	−0.185	0.011	significant negative relationship
Mean radiant temperature	0.066	0.372	no relationship
Sound pressure level	−0.687	0.000	strong negative correlation: higher levels reduce quietness perception
Horizontal illuminance	−0.117	0.109	no relationship
Vertical illuminance	0.008	0.914	no relationship

Source: own work.

Multiple linear regression analysis

To examine the extent to which environmental variables explained variations in auditory comfort, a multiple linear regression analysis was performed. In this model, participants' subjective auditory comfort ratings served as the dependent variable, while air temperature, relative humidity, wind speed, mean radiant

temperature, sound pressure level, horizontal illuminance, and vertical illuminance were entered as predictors (Table 3).

TABLE 3. Significant predictors from the multiple linear regression analysis

Variable	Coefficient β	Significance (p)	Interpretation
Sound pressure level	−0.103	0.000	strongest and most significant negative predictor: as sound levels increase, auditory comfort decreases
Vertical illuminance	−0.020	0.040	statistically significant negative predictor: higher vertical illuminance reduces auditory comfort

Source: own work.

The overall regression model was statistically significant (F = 11.959, $p < 0.001$), indicating that the selected environmental variables collectively provide a meaningful explanation of auditory comfort. The model demonstrated a moderate explanatory power, accounting for approximately 29.1% of the variance in auditory comfort (adjusted $R^2 = 0.291$).

The regression results demonstrated that sound pressure level exerted a significant negative influence on auditory comfort ($\beta = -0.103$, $p < 0.001$), confirming that higher noise levels correspond to lower perceived comfort. Among all predictors, sound pressure level emerged as the dominant variable in the model, exhibiting the strongest standardized effect, indicating that acoustic intensity remains the primary determinant of auditory comfort when multiple environmental variables are considered simultaneously. This outcome is consistent with prior findings emphasizing the detrimental impact of excessive sound exposure on users' acoustic satisfaction. Interestingly, vertical illuminance also appeared as a statistically significant predictor, though with a smaller negative coefficient ($\beta = -0.020$, $p = 0.040$). In practical terms, this means that greater vertical brightness was associated with slightly reduced auditory comfort ratings, whereas lower levels seemed to enhance perceived comfort.

One possible explanation is that elevated vertical illuminance can create a sense of glare or visual distraction, which in turn heightens sensitivity to unwanted sounds. This interpretation underscores the subtle yet meaningful cross-influences between visual and auditory domains. The results further demonstrate that auditory comfort is shaped by a combination of environmental factors rather than isolated variables, highlighting the importance of evaluating environmental conditions within a holistic, multisensory framework.

A noteworthy finding is that vertical illuminance, which did not show a significant relationship in correlation analysis, became significant in regression

analysis. This finding indicates the presence of a suppressor effect within the multivariate structure of the data. While vertical illuminance alone does not exhibit a direct relationship with auditory comfort, its influence becomes apparent when the shared variance with other environmental variables is controlled. This difference stems from the fact that correlation only assesses pairwise linear relationships, whereas regression accounts for the simultaneous contribution of all variables, controlling for interrelations. Thus, the significance of vertical illuminance in regression suggests that its effect on auditory comfort is shaped through suppressor relationships with other environmental variables (Fig. 3). Air temperature, relative humidity, wind speed, mean radiant temperature, and horizontal illuminance were not statistically significant predictors ($p > 0.05$). Nevertheless, the inclusion of these variables in the model contributes to a more comprehensive understanding of the environmental system, suggesting that their effects may be indirect or mediated through interactions with other variables.

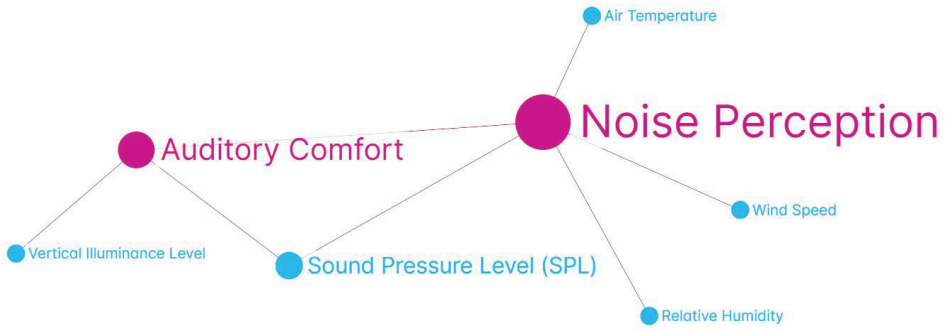

FIGURE 3. Parameters influencing auditory comfort and noise perception
Source: own work.

Collinearity diagnostics indicated varying levels of interdependence among the predictors, which is expected given the complex interactions between environmental parameters in outdoor environments. Despite this, the model remained statistically robust, and key predictors retained their significance.

Perceived and preferred sound types

Participants' evaluations of the outdoor acoustic environment reflected not only their perceptions of existing sound sources but also their personal preferences and expectations. To analyze these responses, the perceived and preferred sound

types were grouped into four main categories: traffic-related, human-related, natural, and other (Fig. 4).

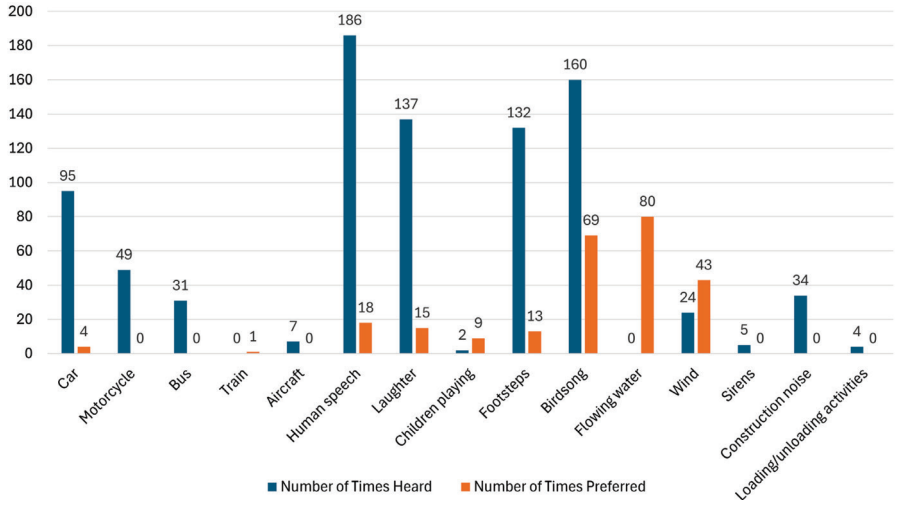

FIGURE 4. Perceived and preferred sound types in outdoor spaces
Source: own work.

The results reveal a noticeable mismatch between what participants heard most frequently and what they actually preferred to hear. Human-related sounds were the most commonly perceived yet among the least favored. For instance, 186 participants reported hearing speech, but only 18 identified it as a sound they enjoyed. Laughter and footsteps followed a similar pattern, commonly noticed but seldom appreciated. This pattern suggests that although human sounds dominate the outdoor soundscape, they are generally perceived as intrusive background noise rather than sources of comfort.

Traffic-related sounds, such as those from cars, motorcycles, buses, and airplanes, ranked low both in perception frequency and in preference. In particular, sounds generated by motorcycles, buses, and construction activities were never listed as desirable, emphasizing that high-decibel mechanical noise was consistently associated with disturbance and reduced auditory comfort.

By contrast, natural sounds emerged as distinctly preferred. Birdsong was perceived by 160 participants and actively preferred by 69, while flowing water – although absent in the physical setting − was identified as a desirable sound by 80 respondents. This finding clearly positions natural sounds like the most positively valued auditory stimuli in outdoor spaces. Even wind

sounds, though less frequently perceived, were relatively well-liked compared to anthropogenic noises.

Overall, these outcomes indicate that the enhancement of outdoor auditory environments should extend beyond mere noise reduction. Urban soundscape design would benefit from strategies that amplify the presence and perceptibility of natural acoustic elements, thereby fostering more restorative and comfortable outdoor experiences.

Strategies for improving auditory comfort

Participants were also invited to propose strategies that, in their view, could enhance auditory comfort in outdoor environments. They were free to choose multiple options from a predefined list. The results indicate that users tend to associate auditory comfort not merely with the absence of unwanted noise but with a more comprehensive sense of environmental quality (Fig. 5).

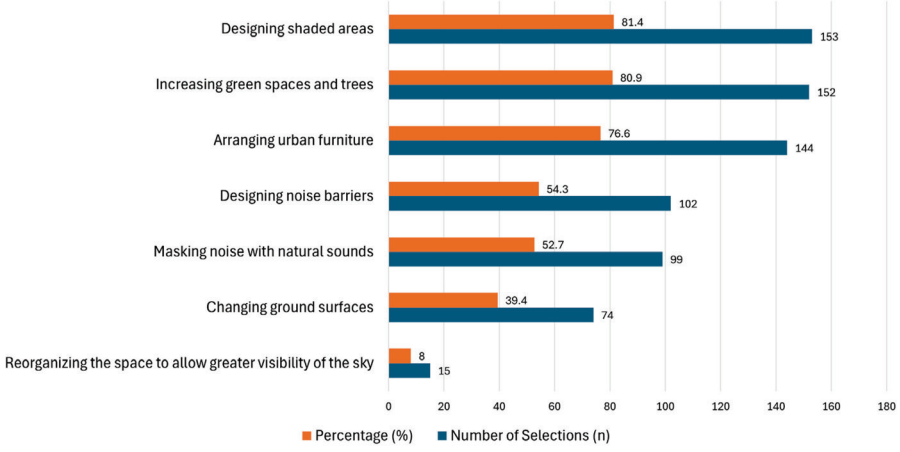

FIGURE 5. Strategies for improving auditory comfort in outdoor spaces
Source: own work.

Among the proposed strategies, creating shaded areas (81.4%) and increasing greenery and tree density (80.9%) were most frequently selected. These preferences suggest that participants value integrated design solutions capable of simultaneously improving auditory, visual, and thermal comfort. Shaded zones and vegetation not only act as natural sound barriers but also enrich the overall soundscape by accentuating desirable natural sounds.

A similarly high level of agreement was observed for the arrangement of urban furniture (76.6%), emphasizing the influence of spatial organization on acoustic experience. Adjustments in seating orientation, spacing, or surface materials may subtly shape how users perceive the surrounding sound environment.

Direct acoustic interventions were also well received: more than half of the respondents supported the installation of noise barriers (54.3%) and the masking of unwanted noise with natural sounds (52.7%). These preferences show that participants favor a dual approach − reducing unpleasant sounds while amplifying positive auditory cues − which is consistent with contemporary soundscape design principles.

By contrast, strategies such as increasing sky visibility or modifying ground surfaces received comparatively lower support, likely because their influence on perceived auditory comfort is indirect.

Taken together, these findings reinforce the notion that auditory comfort in outdoor public spaces extends beyond physical sound levels. It can be enhanced holistically through the integration of natural elements, thoughtful spatial organization, and the deliberate inclusion of positive auditory features.

Discussion

This research adopted a multidimensional framework to examine how environmental variables influence users' auditory comfort in outdoor settings. The findings demonstrate that auditory perception is not determined by sound pressure levels alone but emerges from complex interactions among acoustic, thermal, and visual conditions. While confirming several well-established relationships frequently discussed in prior studies, the results also shed light on the subtle, indirect ways in which thermal and visual factors can shape auditory comfort.

The observed negative association between auditory comfort and sound pressure level aligns closely with the broader literature. In the present study, higher measured sound levels corresponded to a marked decrease in participants' reported comfort, reaffirming the detrimental impact of noise intensity on human well-being. At the same time, the strong positive link between perceived quietness and auditory comfort underscores the dual importance of objective and subjective dimensions of acoustic evaluation ($r = 0.772$, $p < 0.001$) (Taghipour et al., 2020; Liang et al., 2021; Ratcliffe, 2021).

Thermal factors (namely air temperature, relative humidity, wind speed, and mean radiant temperature) displayed limited yet noteworthy associations with auditory comfort. Although these variables did not show statistically significant relationships with auditory comfort ($p > 0.05$), they exhibited significant correlations with noise perception, particularly for air temperature ($r = 0.155$, $p = 0.034$), relative humidity ($r = –0.202$, $p = 0.005$), and wind speed ($r = –0.185$, $p = 0.011$). Such findings strengthen multisensory interpretations of outdoor experience, emphasizing that environmental sensations are typically perceived as an integrated whole. Prior studies have shown, for example, that higher temperatures may reduce noise tolerance and amplify annoyance (Zhang et al., 2020). Likewise, the interplay of wind and humidity has been suggested to influence auditory comfort indirectly by affecting neural excitability and levels of attention (Wang et al., 2021).

Although the correlations between illuminance and auditory comfort were modest, the regression results indicated that vertical illuminance acted as a significant negative predictor. Specifically, vertical illuminance, which was not significant in correlation analysis ($r = −0.039$, $p = 0.591$), became statistically significant in the regression model ($\beta = −0.020$, $p = 0.040$). This observation supports the view that excessive brightness or glare, particularly at eye level, can lead to distraction and mild environmental stress (Williamson et al., 2023). In practical terms, increased vertical illuminance may draw visual attention away from the acoustic environment, thereby diminishing auditory comfort.

Participants' responses concerning perceived and preferred sound types further confirm that comfort depends not only on intensity but also on the qualitative nature of sounds. Natural sounds − such as birdsong, wind rustling, and flowing water − were consistently preferred, whereas anthropogenic sounds from vehicles, construction, or sirens were largely rejected. This pattern supports the concept of positive soundscapes, which recognize natural sounds as restorative and emotionally beneficial (Davies et al., 2009). Beyond acoustic comfort, exposure to natural sounds has also been linked to psychological relaxation and stronger place attachment (Yang & Zhang, 2024).

Finally, participants' suggested strategies reveal that improving auditory comfort involves both acoustic management and spatial design considerations. The most frequently preferred strategies included increasing shaded areas (81.4%), enhancing vegetation density (80.9%), and improving urban furniture arrangement (76.6%), while direct acoustic interventions such as noise barriers (54.3%) and sound masking (52.7%) were also widely supported. Commonly endorsed measures − including the use of vegetation, noise barriers, and natural sound masking − reflect a preference for holistic soundscape design approaches that seek

to attenuate undesirable sounds while enhancing pleasant ones (Fei et al., 2025). From this perspective, effective outdoor design should move beyond conventional noise control, integrating multisensory principles that simultaneously support acoustic, visual, and thermal well-being.

Conclusions

The results indicate that the acoustic environment remains the most influential factor in shaping outdoor auditory comfort. Lower sound pressure levels and stronger perceptions of quietness consistently contributed to higher comfort ratings. At the same time, the observed negative association between vertical illuminance and comfort implies that lighting conditions, particularly brightness in the field of view, may subtly influence how soundscapes are perceived. Although thermal variables such as air temperature, humidity, and wind speed did not directly predict auditory comfort, they affected participants' perception of noise intensity, suggesting that thermal sensations can modulate how auditory stimuli are cognitively processed. Together, these outcomes point to the inherently multisensory nature of outdoor comfort. Participants' soundscape preferences further enrich this interpretation. Natural sounds like birdsong, flowing water, and wind were rated as the most pleasant and desirable, whereas human-related (speech, laughter) and mechanical sounds (traffic, construction) were typically disliked. This finding underscores that a comfortable sound environment depends not only on quietness but also on the quality and diversity of sounds present. The strategies most often proposed by participants − including expanding green areas, introducing shaded structures, reorganizing urban furniture, and masking unwanted sounds with natural ones − illustrate a clear preference for environments that balance sensory richness with tranquility. Overall, the study demonstrates that improving auditory comfort in public open spaces requires an integrated design perspective. Beyond traditional noise control, planners should adopt multidimensional strategies that enhance natural sound presence, strengthen visual quality, and ensure favorable microclimatic conditions. Further research conducted across different seasons, climatic zones, and demographic groups will be essential for deepening the understanding of these multisensory comfort interactions and refining soundscape-oriented urban design practices.

References

Chen, H., Hong, B., Qu, H., Geng, Y., & Su, M. (2022). Effects of acoustic perception on outdoor thermal comfort in campus open spaces in China's cold region. *Buildings*, *12*(10), 1518. https://doi.org/10.3390/buildings12101518

Cohen, P., Potchter, O., & Schnell, I. (2014). The impact of an urban park on air pollution and noise levels in the Mediterranean city of Tel-Aviv, Israel. *Environmental Pollution*, *195*, 73–83. https://doi.org/10.1016/j.envpol.2014.08.015

Cureau, R. J., Pigliautile, I., Kousis, I., & Pisello, A. L. (2022). Multi-domain human-oriented approach to evaluate human comfort in outdoor environments. *International Journal of Biometeorology*, *66*(10), 2033–2045. https://doi.org/10.1007/s00484-022-02338-7

D'Alessandro, F., Evangelisti, L., Guattari, C., Grazieschi, G., & Orsini, F. (2018). Influence of visual aspects and other features on the soundscape assessment of a university external area. *Building Acoustics*, *25*(3), 199–217. https://doi.org/10.1177/1351010X18778759

Davies, W. J., Adams, M. D., Bruce, N. S., Marselle, M., Cain, R., Jennings, P., Poxon, J., Carlyle, A., Cusack, P., Hall, D. A., Irwin, A., Hulme, K. I., & Plack, C. J. (2009, August 23–26). The positive soundscape project: a synthesis of results from many disciplines. In *Internoise 2009, Ottawa, Canada*.

European Environment Agency [EEA]. (2019). *Environmental noise in Europe – 2020* (EEA Report 22/2019). https://www.eea.europa.eu/en/analysis/publications/environmental-noise-in-europe/environmental-noise-in-europe/@@download/file

Fei, X., Wu, Y., Dong, J., & Kong, D. (2025). The effects of soundscape interactions on the restorative potential of urban green spaces. *Sustainability*, *17*(6), 2674. https://doi.org/10.3390/su17062674

IBM Corp. (2017). *IBM SPSS Statistics 25*.

International Electrotechnical Commission [IEC]. (2013). *Electroacoustics – sound level metrics* (IEC 61672).

International Organization for Standardization, & International Commission on Illumination [ISO& CIE]. (2014). *Characterization of the performance of illuminance meters and luminance meters* (ISO/CIE 19476). International Organization for Standardization, International Commission on Illumination.

Jo, H. I., & Jeon, J. Y. (2021). Compatibility of quantitative and qualitative data-collection protocols for urban soundscape evaluation. *Sustainable Cities and Society*, *74*, 103259. https://doi.org/10.1016/J.SCS.2021.103259

Kousis, I., & Pisello, A. L. (2020). For the mitigation of urban heat island and urban noise island: two simultaneous sides of urban discomfort. *Environmental Research Letters*, *15*(10), 103004. https://doi.org/10.1088/1748-9326/abaa0d

Lam, C. K. C., Yang, H., Yang, X., Liu, J., Ou, C., Cui, S., Kong, X., & Hang, J. (2020). Cross-modal effects of thermal and visual conditions on outdoor thermal and visual comfort perception. *Building and Environment*, *186*, 107297. https://doi.org/10.1016/j.buildenv.2020.107297

Lau, K. K. L., & Choi, C. Y. (2021). The influence of perceived aesthetic and acoustic quality on outdoor thermal comfort in urban environment. *Building and Environment*, *206*, 108333. https://doi.org/10.1016/j.buildenv.2021.108333

Liang, P., Guan, H., Wang, Y., Chen, H., Song, P., Ma, H., & Hu, S. (2021). The effect of music tempo and volume on acoustic perceptions under the noise environment. *Sustainability*, *13*(7), 4055. https://doi.org/10.3390/su13074055

Lu, X., Teh, S. Y., Tay, C. J., Abu Kassim, N. F., Fam, P. S., & Soewono, E. (2025). Application of multiple linear regression model and long short-term memory with compartmental model to forecast dengue cases in Selangor, Malaysia based on climate variables. *Infectious Disease Modelling*, *10*(1), 240–256. https://doi.org/10.1016/j.idm.2024.10.007

Ma, H., & Nie, W. (2014). Influence of visual factors on noise annoyance evaluation caused by road traffic noise in indoor environment. *INTER-NOISE and NOISE-CON Congress and Conference Proceedings*, *249*(1), 6308–6315.

Mancini, S., Mascolo, A., Graziuso, G., & Guarnaccia, C. (2021). Soundwalk, questionnaires and noise measurements in a university campus: A soundscape study. *Sustainability*, *13*(2), 841. https://doi.org/10.3390/su13020841

Mascolo, A., Mancini, S., Graziuso, G., Quartieri, J., & Guarnaccia, C. (2020). Comparison between sound pressure levels and perception: a soundscape application in a university campus. *Journal of Physics: Conference Series*, *1603*(1), 012026. https://doi.org/10.1088/1742-6596/1603/1/012026

Muniz, F. B., & MacKinnon, D. P. (2025). Three approaches to testing for statistical suppression. *Multivariate Behavioral Research*, *60*(4), 817–839. https://doi.org/10.1080/00273171.2025.2483245

Nitidara, N. P. A., Sarwono, J., Suprijanto, S., & Soelami, F. X. N. (2022). The multisensory interaction between auditory, visual, and thermal to the overall comfort in public open space: A study in a tropical climate. *Sustainable Cities and Society*, *78*, 103622. https://doi.org/10.1016/J.SCS.2021.103622

Ratcliffe, E. (2021). Sound and soundscape in restorative natural environments: A narrative literature review. *Frontiers in Psychology*, *12*, 570563. https://doi.org/10.3389/fpsyg.2021.570563

Shigehisa, T., & Gunn, W. J. (1978). Annoyance response to recorded aircraft noise. II. Effect of intensity of illumination in relation to noise spectrum. *The Journal of Auditory Research*, *18*(3), 183–190.

Şimşek, O. (2024). *General comfort prediction model recommendations on the combined effects of thermal, auditory and visual comfort on urban public open space users*. Eskişehir Technical University.

Taghipour, A., Athari, S., Gisladottir, A., Sievers, T., & Eggenschwiler, K. (2020). Room acoustical parameters as predictors of acoustic comfort in outdoor spaces of housing complexes. *Frontiers in Psychology*, *11*, 504736. https://doi.org/10.3389/fpsyg.2020.00344

Torresin, S., Albatici, R., Aletta, F., Babich, F., & Kang, J. (2019). Assessment methods and factors determining positive indoor soundscapes in residential buildings: A systematic review. *Sustainability*, *11*(19), 5290. https://doi.org/10.3390/su11195290

Vardaxis, N. G., & Bard, D. (2018). Review of acoustic comfort evaluation in dwellings. Part III: airborne sound data associated with subjective responses in laboratory tests. *Building Acoustics*, *25*(4), 289–305. https://doi.org/10.1177/1351010X18788685

Wang, S., Liu, Y., & Corcoran, J. (2021). A season for complaints: how does weather affect noise complaints between neighbors? *Weather, Climate, and Society*, *13*(4), 753–768. https://doi.org/10.1175/WCAS-D-21-0020.1

Williamson, C. A., Morganti, J. J., & Smithson, H. E. (2023). Bright-light distractions and visual performance. *Frontiers in Psychology*, *14*, 1088975. https://doi.org/10.3389/fpsyg.2023.1088975

Yang, H., & Zhang, S. Q. (2024). Impact of rural soundscape on environmental restoration: An empirical study based on the Taohuayuan Scenic Area in Changde, China. *PLOS ONE*, *19*(3), e0300328. https://doi.org/10.1371/journal.pone.0300328

Yang, W., & Moon, H. J. (2018). Combined effects of sound and illuminance on indoor environmental perception. *Applied Acoustics*, *141*, 136–143. https://doi.org/10.1016/j.apacoust.2018.07.008

Yang, W., & Moon, H. J. (2019). Combined effects of acoustic, thermal, and illumination conditions on the comfort of discrete senses and overall indoor environment. *Building and Environment*, *148*, 623–633. https://doi.org/10.1016/j.buildenv.2018.11.040

Yang, X., Zhang, G., Lu, X., Zhang, Y., & Kang, J. (2024). Contribution of soundscape appropriateness to soundscape quality assessment in space: A mediating variable affecting acoustic comfort. *Journal of Environmental Management*, *372*, 123321. https://doi.org/10.1016/j.jenvman.2024.123321

Zeng, F., Liang, S., Zhang, J., Chen, Y., Feng, S., Mo, Q., Zhou, T., Lai, Y., Liu, T., & Wang, S. (2024). The effects of acoustic-light-thermal environment quality parameters on pedestrians' overall comforts in residential districts. *Scientific Reports*, *14*(1), 1–16. https://doi.org/10.1038/s41598-024-70227-7

Zhang, X., Zhou, S., Kwan, M. P., Su, L., & Lu, J. (2020). Geographic Ecological Momentary Assessment (GEMA) of environmental noise annoyance: the influence of activity context and the daily acoustic environment. *International Journal of Health Geographics*, *19*(1), 50. https://doi.org/10.1186/s12942-020-00246-w

Zhao, X., Zhang, S., Meng, Q., & Kang, J. (2018). Influence of Contextual Factors on Soundscape in Urban Open Spaces. *Applied Sciences*, *8*(12), 2524. https://doi.org/10.3390/app8122524

Summary

Auditory comfort and noise perception under thermal and visual conditions in urban parks. This study investigates auditory comfort in outdoor urban environments by examining the combined influence of visual and thermal factors. Field research was conducted in two major urban parks in Adana, Turkey, representing the Mediterranean climate, where simultaneous environmental measurements and surveys were performed

during the autumn season. The collected data included air temperature, relative humidity, wind speed, mean radiant temperature, sound pressure level, and both horizontal and vertical illuminance. Correlation and regression analyses revealed that sound pressure level was the most influential parameter, showing a strong negative association with auditory comfort, while higher vertical illuminance slightly decreased comfort levels. Thermal variables exhibited indirect effects on noise perception rather than on comfort itself. Participants expressed a strong preference for natural sounds such as birdsong and flowing water, while human and mechanical sounds were generally disliked. The findings highlight that auditory comfort is a multisensory phenomenon shaped by both acoustic and contextual environmental qualities.

Scientific Review Engineering and Environmental Sciences (2026), 35 (2), 219–238

Sci. Rev. Eng. Env. Sci. (2026), 35 (2) https://srees.sggw.edu.pl

ISSN 1732-9353 (suspended) eISSN 2543-7496 DOI 10.22630/srees.10984

Received: 08.12.2025
Accepted: 23.02.2026

Miriam Kattyuska CARASSAS ROSALES

Sleyther Arturo De La CRUZ VEGA✉

Universidad Nacional de Barranca, Faculty of Engineering, Peru

✉sdelacruz@unab.edu.pe

Clay masonry units with variation in construction and demolition waste (CDW) particle size

Keywords: waste, brick, aggregate, sustainability

Introduction

Clay masonry units have been essential building materials for centuries in the construction of homes and infrastructure (Gallegos & Casabonne, 2005), not only due to their availability, ease of molding, and mechanical strength after firing (Uribe et al., 2021) but also because these properties have allowed ceramic bricks to become one of the most widely used and fundamental products in traditional masonry (Muñoz Pérez et al., 2021). This effectiveness continues to be observed in the use of these ceramic building units in many parts of the world, such as Latin America, Asia, and Africa, where their use remains predominant (Rotaondaro, 2007) in both artisanal processes and semi-industrialized systems that supply the growing urban demand (UN Environment et al., 2018), particularly in areas where self-construction is common (Tam et al., 2018).

Carassas Rosales, M. K., De La Cruz Vega, S. A. (2026). Clay masonry units with variation in construction and demolition waste (CDW) particle size. *Sci. Rev. Eng. Env. Sci.*, *35* (2), 219–238. DOI 10.22630/srees.10984

At the same time, rapid urban growth has led to a significant increase in the generation of construction and demolition waste (CDW), which refers to waste or refuse generated from building, remodeling, and demolition work (Kofoworola & Gheewala, 2009) and generally consists of a mixture of leftover materials from these processes (Chi et al., 2020). Globally, this waste represents one of the largest volumes of solid waste streams, reaching over 30% of total solid waste in several cities (Lu et al., 2017). In Latin America, the limited infrastructure for its management means that a large portion of CDW is disposed of in informal landfills, causing negative environmental impacts, additional cleanup costs, and deterioration of the urban landscape (Oviedo Cogollo & Vega Suárez, 2021).

Given this scenario, the valorization of CDW has gained relevance as a strategy to promote more sustainable construction, with its incorporation into the production of building materials being one of the most researched alternatives (Sieffert et al., 2014). Some previous research has shown that CDW could be partially incorporated into the production of these units, provided that the dosage and corresponding particle size are controlled (Robayo et al., 2016). Bektas et al. (2007) highlight that both crushed stone and ceramic waste can function as the granular skeleton, improving internal stability and increasing brick density.

For instance, research has evaluated the incorporation of recycled concrete and brick powder in the production of geopolymeric mortars and bricks, demonstrating the potential of these residues to produce resistant and functional materials through alkaline activation processes and modifications in particle size distribution (Rahimpour et al., 2024; Capasso et al., 2025). Similarly, a study published in 2024 on geopolymers incorporating brick and concrete demolition waste explored mixtures with different percentages of CDW, highlighting the effects of waste composition and processing on the mechanical properties of the resulting materials (Parra et al., 2024). Furthermore, recent review studies have analyzed the use of recycled CDW aggregates in concrete, illustrating how variations in treatment and aggregate characteristics influence the final performance of construction products (Luo et al., 2024). Overall, these recent publications (2024–2025) demonstrate a growing research trend toward the valorization of construction and demolition waste with different particle sizes and processing methods, aiming to reduce waste generation, promote circular economy strategies, and develop more sustainable building materials.

An important aspect of this research lies in the particle size of the CDW, as this determines crucial properties such as compaction, porosity, and the final mechanical strength of the brick. Evidence suggests that fine fractions of ceramic waste or pulverized brick can act as micro-fillers, reducing porosity and modifying

water absorption by filling the voids in the clay matrix (Rahhal et al., 2019). Zanelli et al. (2021) show that the incorporation of fine and very fine fractions of CDW is technically viable as long as there is an adequate granulometric classification, noting that particles with a size less than 0.6 mm can be incorporated without affecting the physical-mechanical behavior of the brick.

Other studies reveal that coarser particle sizes, or excessive substitution percentages, tend to increase porosity and absorption, while decreasing density and compressive strength if firing conditions are not controlled (Gencel et al., 2022). Similarly, recent research confirms that there is an optimal incorporation range depending on the type of waste and the firing temperature. Cases such as Dubale et al. (2023) report that substitutions between 10% and 25% of crushed CDW make it possible to obtain bricks that meet the established strength criteria when fired at temperatures between 850°C and 900°C.

In Peru, a similar situation exists. Brick production plays a dominant role in urbanized areas, while the generation of CDW is increasing due to the rapid growth of the construction sector. However, this waste is not receiving adequate attention from the authorities because a management and treatment plan has not been implemented to allow access to all the potential benefits that could be obtained from it (Bazán, 2018). This is because reuse strategies are needed to reduce clay extraction and promote more sustainable practices (Kumar et al., 2021).

However, there is still little evidence regarding how the particle size variation of CDW influences the physical and mechanical properties of clay units produced under local conditions (Torres, 2024). Therefore, this study aims to evaluate the influence of different CDW particle sizes (3/4″, 1/2″, 3/8″, and No. 4) on the physical and mechanical properties of clay masonry units, considering parameters such as absorption, dimensional variation, and compressive strength. The results are intended to establish technical criteria to guide the optimal incorporation of CDW in the sector.

The use of CDW in the production of clay masonry units represents a natural, technical, and sustainable alternative to the challenges of overexploitation of resources and poor waste management in construction (Pacheco-Torgal, 2014). The relevance of this research lies in the problems generated by environmental degradation, the increase in informal dumps, and the need for affordable construction materials, while simultaneously promoting the circular economy and the efficient use of local resources (Lieder & Rashid, 2016). This fosters the production of more sustainable, safe, and durable bricks by combining technical innovation with responsible, low-environmental-impact construction practices (Tejada, 2025).

Carassas Rosales, M. K., De La Cruz Vega, S. A. (2026). Clay masonry units with variation in construction and demolition waste (CDW) particle size. *Sci. Rev. Eng. Env. Sci.*, *35* (2), 219–238. DOI 10.22630/srees.10984

From a social perspective, this research proposes the reuse of CDW in clay bricks as an alternative for producing accessible and safe building materials for communities where debris accumulation and a lack of local resources are significant concerns (Santana et al., 2024). This allows for the production of affordable units with adequate mechanical properties, which helps improve the structural safety of homes and enhances the quality of life in communities, while also promoting more sustainable construction practices (Vega Garcia, 2024).

Theoretically, the study is supported by scientific documentation on the incorporation of construction and demolition waste as part of ceramic materials (Al-Fakih et al., 2018) and the effects of particle size on the physical and mechanical properties of bricks. It also draws on evidence of how the particle size of construction and demolition waste can act as a micro filler or granular structure, influencing absorption, dimensional variation, and compressive strength. Furthermore, it expands the knowledge applied to civil engineering and sustainable construction technologies (Junior et al., 2022).

From a methodological standpoint, the research presents a quasi-experimental and quantitative design that allows for the evaluation of how variations in particle size of CDW of 3/4″, 1/2″, 3/8″, and No. 4 influence the performance of clay bricks. Laboratory tests, conducted under current technical standards, ensure valid and reliable results, providing information to promote sustainable alternatives in the brickmaking industry (Xiao et al., 2022). From an environmental perspective, the research encourages the reuse of CDW, which reduces the extraction of virgin clay and the amount of waste in landfills (Padmalosan et al., 2023). This practice contributes to the circular economy and opens up possibilities that will lead to the production of more sustainable bricks, in line with ecological construction strategies and impact mitigation values associated with traditional materials (Zhang, 2013).

The main objective of this research was to evaluate the influence of the particle size of CDW on the physical-mechanical properties of clay bricks.

Material and methods

The research conducted is applied because it aims to obtain scientific results with practical applications (Quintero, 2007), allowing theoretical knowledge to be translated into feasible solutions that address the needs of the sector and society (Mayz & Pérez, 2002). In this sense, the research seeks to evaluate the influence of CDW size on the properties of clay bricks, providing technical criteria that promote more efficient and environmentally responsible production processes (Fig. 1).

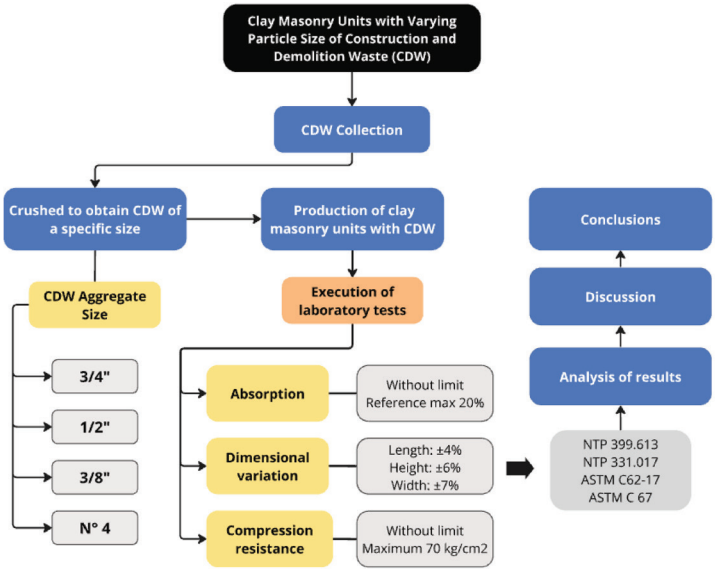

FIGURE 1. Investigation process

Source: own work.

The design is quasi-experimental because the independent variable is manipulated while total control of all external conditions is not achieved, allowing observation of its effects on the properties of the bricks produced (Shadish et al., 2002). This type of design allows, through the control of laboratory conditions and the application of technical evaluation protocols (Manterola & Otzen, 2015), the comparison of groups being subjected to different particle sizes. In this case, the research analyzes how the particle sizes 3/4″, 1/2″, 3/8″, and No. 4 influence the physical-mechanical performance of masonry units.

This research is quantitative because it focuses on the measurement and analysis of numerically obtained data to answer the research questions (Creswell & Creswell, 2018). It contributes to the application of standardized and objective procedures (Cárcamo Vásquez et al., 2009) for evaluating the physical-mechanical properties of clay bricks made with different particle sizes of CDW, such as water absorption, dimensional variation, and compressive strength. The application of precise measurements will yield replicable results that can be statistically verified, thus ensuring the validity and reliability of the analysis (Hernández et al., 2014).

The total number of clay bricks manufactured constituted the research population. The sample consisted of 75 bricks, comprising a control group without the addition of CDW and four experimental groups. Each experimental group was

Carassas Rosales, M. K., De La Cruz Vega, S. A. (2026). Clay masonry units with variation in construction and demolition waste (CDW) particle size. *Sci. Rev. Eng. Env. Sci.*, *35* (2), 219–238. DOI 10.22630/srees.10984

made with a different particle size, allowing for a comparative analysis of the effect of particle size on the aforementioned brick properties. The CDW was extracted from a landfill where this material had been present for extended periods, ensuring that the material obtained was representative. The aggregates were then processed through crushing and grinding to obtain the particle size fractions required for the study (3/4″, 1/2″, 3/8″, and No. 4).

The clay masonry units were handcrafted using molds measuring 20 × 11 × 9 cm (Fig. 2), classified as solid bricks Type II according to NTP 331.017 (Instituto Nacional de Calidad [INACAL], 2015). Five test groups were formed, each consisting of 15 specimens: one control group without added waste and four experimental groups with the different fractions of construction and demolition waste mentioned, allowing the tests to be organized in a controlled manner for subsequent evaluation.

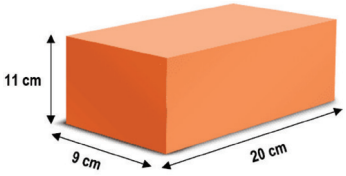

FIGURE 2. Clay brick unit dimensions
Source: own work.

Water absorption, dimensional variation, and compressive strength tests were conducted in accordance with the limits and procedures established by NTP 399.613 (INACAL, 2017), ASTM C62-17 (ASTM International, 2017), and ASTM C67-14 (ASTM International, 2014). For the water absorption test, the bricks were first dried to a constant mass, then fully immersed in water for a specified period, and the increase in mass was measured to determine the absorption percentage. Dimensional variation was evaluated by measuring the length, width, and height of the bricks before and after water immersion to quantify expansion or shrinkage (Fig. 3). Compressive strength tests were carried out using a universal testing machine, applying a gradually increasing load until failure and recording the maximum load sustained by each specimen. In addition, chemical composition data from previous studies on CDW were incorporated to assess their potential influence on the physical and mechanical behavior of the bricks. This combined approach ensures methodological rigor and provides a comprehensive understanding of how the characteristics of the recycled material affect key properties such as strength, durability, and water absorption.

FIGURE 3. View of the manufactured masonry units
Source: own photos.

Results and discussion

Construction and demolition waste

This composition of CDW shows that the majority consists of concrete, bricks, tiles, and slabs. These materials, which possess medium strength, represent the largest fraction of the waste, while other components appear in smaller proportions (Table 1). In this context, it can be interpreted that CDW has the potential to provide granular structure and some mechanical reinforcement to clay bricks, especially when appropriate particle sizes are used (Chica & Beltrán, 2018). Furthermore, the presence of ceramic and stone materials could influence water absorption and internal cohesion, which are key aspects for ensuring the durability of the final product.

However, it is also important to note that CDW does not have a uniform or identical composition everywhere, as this depends on factors such as the type of structure demolished, the demolition procedure, and the environmental management systems employed. For this reason, the behavior of the waste can vary between different collection areas (Suárez-Silgado et al., 2019). This justifies the need to carry out a proper classification before incorporating them into construction materials.

Carassas Rosales, M. K., De La Cruz Vega, S. A. (2026). Clay masonry units with variation in construction and demolition waste (CDW) particle size. *Sci. Rev. Eng. Env. Sci.*, *35* (2), 219–238. DOI 10.22630/srees.10984

TABLE 1. Mean composition of construction and demolition waste

Element	% by mass [%]
Concrete	63.67
Solid bricks	17.98
Tiles/Slabs	11.11
Mortar	4.23
Concrete block	0.11
Concrete tiles	0.39
Stones	1.38
Asbestos-cement	0.38
Wood	0.11
Organic matter	0.20

Source: Chávez Porras et al. (2013).

The analysis was performed using X-ray fluorescence spectrometry, a technique that, as explained by Torres-Rodríguez et al. (2022), identifies elements by exciting atoms with X-rays and then detecting the characteristic emissions, thus revealing the mineral composition of the CDW. The results, quantified in the following table, show the chemical components of the CDW and give us an idea of their potential role in the properties of the brick (Table 2).

TABLE 2. Elemental composition of construction and demolition waste by X-ray fluorescence spectrometry assay

Element	Result [%]	Oxides	Result [%]
Calcium (Ca)	36.839	Silicon oxide (SiO_2)	36.852
Silicon (Si)	29.509	Calcium oxide (CaO)	30.089
Aluminum (Al)	14.126	Aluminum oxide (Al_2O_3)	15.581
Iron (Fe)	10.202	Iron oxide (Fe_2O_3)	8.515
Magnesium (Mg)	4.477	Magnesium oxide (MgO)	4.334
Potassium (K)	2.069	Potassium oxide (K_2O)	1.455
Sulfur (S)	1.199	Sulfur oxide (SO_3)	1.748
Titanium (Ti)	1.066	Titanium oxide (TiO_2)	1.038
Manganese (Mn)	0.218	Manganese oxide (MnO)	0.164
Strontium (Sr)	0.197	Strontium oxide (SrO)	0.136
Zirconium (Zr)	0.057	Zirconium oxide (ZrO_2)	0.045
Vanadium (V)	0.041	Vanadium oxide (V_2O_5)	0.043

Source: Vega Neyra and Hizo Celestino (2025).

X-ray fluorescence analysis demonstrated that demolition waste contains components such as minerals and oxides, which are almost identical to those found in traditional fired bricks, with abundant silica, alumina, and calcium and iron oxides, all of which are active in the material's behavior (Saíz et al., 2023). This similarity in chemical structure suggests the potential use of this waste as a material that could partially and adequately replace the traditional components of concrete masonry units, promoting compatibility with cementitious materials and the internal cohesion of the mixture.

In the present study, no presence of asbestos, asbestos-containing materials, or paints with heavy metals was detected in the construction and demolition waste evaluated; the materials were subjected to inspection and chemical characterization, which showed that their composition mainly consists of typical mineral phases from concrete and ceramics (such as silica, alumina, and calcium oxides), with no hazardous or toxic compounds identified, nor significant concentrations of contaminating elements that could pose a risk to human health or the environment. Therefore, the recycled material can be considered safe and suitable for use in the production of masonry units. Furthermore, the bricks produced with this material will be completely encapsulated by mortar during the plastering process, remaining fully covered, which serves as an additional physical barrier that limits any potential particle release and enhances the safety and stability of the material in its final application.

Absorption

The water absorption results reveal slight variations (small percentages) as CDW is incorporated in different particle sizes, ranging from 10.7% for the control brick to values between 11.7% and 13.0% for mixtures with recycled aggregate (Fig. 4). However, these variations remain within technically acceptable limits for masonry units. This slight increase can be attributed to the increased porosity generated by the incorporation of CDW particles, which allows for greater water retention without compromising the brick's internal structure. This effect is more noticeable in fine-grained residues, while coarser sizes tend to decrease absorption. Although NTP 399.613 (INACAL, 2017) does not establish a maximum absorption limit for this type of brick, a reference value of no more than 22% is considered to ensure adequate performance in bricks fired under this standard. From this perspective, all the values obtained are below the estimated threshold, with residue No. 4 registering the lowest absorption values, indicating better performance against moisture, while the 3/8″ residues showed the highest absorption, showing that

Carassas Rosales, M. K., De La Cruz Vega, S. A. (2026). Clay masonry units with variation in construction and demolition waste (CDW) particle size. *Sci. Rev. Eng. Env. Sci.*, *35* (2), 219–238. DOI 10.22630/srees.10984

the granulometry of the CDW influences the absorption capacity, suggesting that there is an optimal residue size range that allows maintaining controlled porosity and ensuring the durability of the brick, but showing that the incorporation of CDW does not affect the absorption capacity or the hygroscopic condition of the brick.

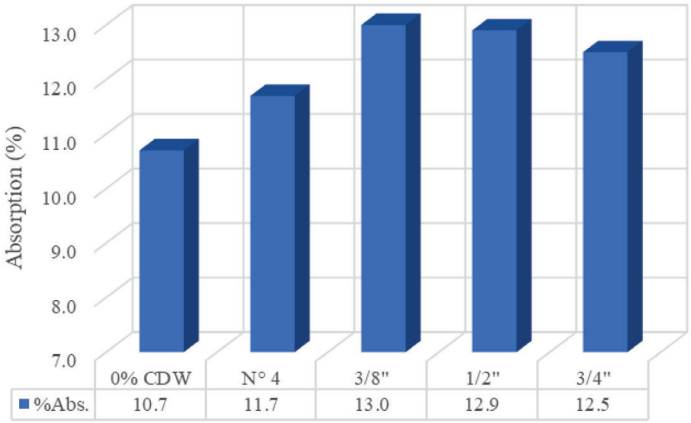

FIGURE 4. Average absorption of clay bricks with construction and demolition waste
Source: own work.

Dimensional variation

The dimensional variation reflected in the bricks incorporated with CDW is within the limits allowed by the national technical standard NTP 331.017 (INACAL, 2015), which stipulates tolerances in length of ±4%, in height of ±6%, and ±7% for the width of units such as those in this study. Regarding dimensional variations, height showed the greatest variation (102.7%), while length and width showed slight reductions, remaining close to the standard dimension. The 3/8″ waste best preserved its dimensions, while the No. 4 waste exhibited the greatest deviations (Fig. 5). This suggests that proper control of waste size can minimize deformations and promote a more uniform distribution of internal stresses during the drying and firing process. None of these variations exceeded regulatory limits, and no significant deformations were observed. Therefore, it can be concluded that the inclusion of CDW waste would not compromise the dimensional uniformity of the produced units. Furthermore, these results confirm that, with good control of dosage and particle size distribution, bricks can maintain high dimensional consistency, which is crucial for their correct placement and structural performance on site.

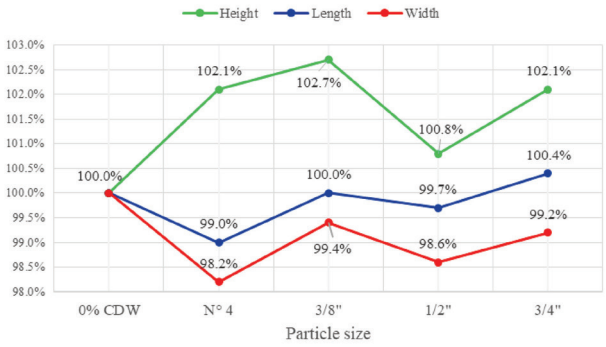

FIGURE 5. Average dimensional variation of clay bricks with construction and demolition waste
Source: own work.

Compressive strength

The compressive strength results for the unit groups show significant variations depending on the size of the incorporated CDW residue. While bricks with 3/4″ and No. 4 residue achieved the highest values, 65 kg·cm^{-2} and 64 kg·cm^{-2}, respectively, even surpassing the control brick (55 kg·cm^{-2}), bricks with 3/8″ residue exhibited the lowest strength, and those with 1/2″ residue showed intermediate performance (Fig. 6). This behavior reflects that coarser residue allows for better compaction and internal densification of the brick, favoring the development of its internal structure during firing. This indicates that the selection of residue size is crucial for ensuring structural strength, with coarser residue offering better performance in bricks incorporating CDW. Therefore, the appropriate choice of residue size not only improves strength but also contributes to the uniformity and durability of the units in practical applications.

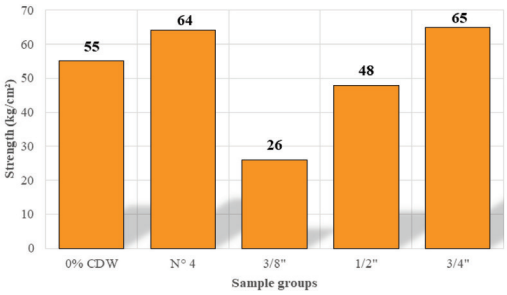

FIGURE 6. Average compressive strength of clay bricks with construction and demolition waste
Source: own work.

Carassas Rosales, M. K., De La Cruz Vega, S. A. (2026). Clay masonry units with variation in construction and demolition waste (CDW) particle size. *Sci. Rev. Eng. Env. Sci.*, *35* (2), 219–238. DOI 10.22630/srees.10984

Discussion

Regarding water absorption, a progressive increase was observed with the incorporation of CDW, particularly with 3/8″ particles, which reached 12.9%. This behavior is consistent with Voišnienė et al. (2019), who indicated that certain waste particle sizes can increase porosity. Similarly, Gencel et al. (2022) reported values up to 17.5% for particles smaller than 2 mm, noting that an unsuitable particle size distribution may influence the material's hygroscopic response. Cruzado (2018) also obtained absorption values around 12.79%, reinforcing the relationship between finer particles and higher voids. A notable finding of the current study is that waste No. 4 showed the lowest absorption, suggesting an optimal particle size range that allows improved compaction and reduced porosity. Dos Reis et al. (2019) indicate that a moderate particle size in CDW can densify the material and decrease absorption. Similar results were reported by Gutiérrez and Miranda (2025), with absorptions as low as 4.93%, demonstrating that relatively coarse particles can enhance moisture resistance, while Peña and Rincón (2018) found absorption values of 3.63% for particle sizes around 2.5 mm, showing that fine particles, if properly controlled, also reduce absorption. Other studies, however, show that absorption depends on both the amount and type of residue. Gutiérrez and Oyarce (2021) reported values as high as 24.8%, while Raini et al. (2025) observed 20%, indicating that particle shape and incorporation percentage influence absorption as much as size. Finally, Torres (2024) reported 3.6% for mixtures with controlled granulometry, highlighting that a uniform and well-processed particle size limits absorption even in the presence of CDW (Fig. 7).

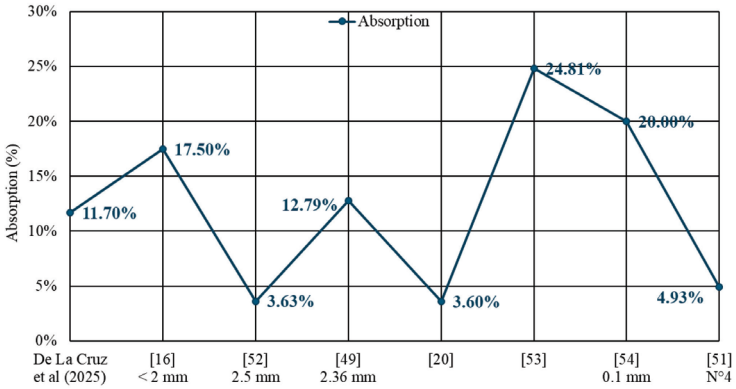

FIGURE 7. Absorption of bricks with construction and demolition waste according to different authors
Source: own work.

Continuing with the dimensional variation, no significant deformation was observed, as all bricks remained within the limits established by the standard. This is consistent with Cruzado (2018), who also reported that the incorporation of CDW did not produce significant deformations, observing a variation of 4.41% in height and noting that the greatest fluctuations occur in this dimension. Similarly, Torres (2024) found the greatest variation in height at 1.77%, and Gutiérrez and Oyarce (2021) recorded their most notable variation in thickness at 2.68%, although all values remained within the standard limits. In the present study, height showed the highest percentage of variation (102.7% relative to the nominal height), while bricks made with 3/8″ residues better preserved their dimensions, and those made with No. 4 residues exhibited the most noticeable deviations, indicating that CDW granulometry has a stronger influence on the geometric stability of bricks than commonly considered (Fig. 8).

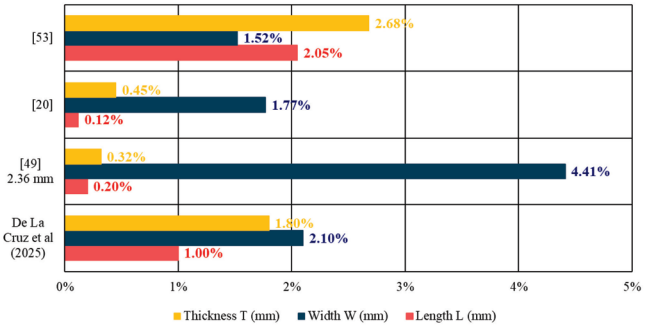

FIGURE 8. Dimensional variation of bricks with construction and demolition waste according to different authors

Source: own work.

Finally, regarding compressive strength, the highest values were obtained with the coarse waste (No. 4 and 3/4″), even surpassing the standard brick. This behavior aligns with the findings of dos Reis et al. (2019) and Vega Neyra and Hizo Celestino (2025), who demonstrated that using optimal CDW particle sizes achieves better compaction and improves the internal structure of fired bricks. This is consistent with studies showing that coarse particles, such as 3/4″, allow for higher strengths by generating a denser matrix with lower porosity. Similarly, Gutiérrez and Oyarce (2021) indicated that adequate strength is achieved with small dosages of waste, but progressive increases in the proportion of incorporation can lead to a decrease, highlighting the existence of an optimal substitution limit, as also noted by Raini et al. (2025). In contrast, the 3/8″ residues exhibited

Carassas Rosales, M. K., De La Cruz Vega, S. A. (2026). Clay masonry units with variation in construction and demolition waste (CDW) particle size. *Sci. Rev. Eng. Env. Sci.*, *35* (2), 219–238. DOI 10.22630/srees.10984

the lowest strengths, reflecting the same behavior described by Gencel et al. (2022) and Cruzado (2018), who stated that fine particles (smaller than 2 mm or close to 2.36 mm) increase porosity, resulting in lower mechanical strength due to greater void occupancy within the matrix. Even studies with ultrafine particles, such as 0.25 mm (Voišnienė et al., 2019) or 0.125 mm (Reis et al., 2019), show that although considerable strength values can be achieved in specific contexts, performance depends heavily on the proportion and compaction process, and excessive use can lead to less dense structures. The results of the present study are also partially related to those of Torres (2024), who indicated that CDW can slightly decrease compressive strength compared to conventional bricks, without compromising their structural performance (Fig. 9).

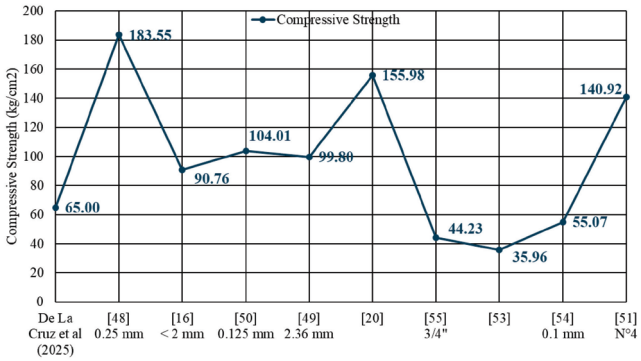

FIGURE 9. Compressive strength of bricks with construction and demolition waste according to other authors

Source: own work.

Conclusions

The properties of the standard clay bricks, without the incorporation of CDW, showed an absorption of 10.7%, a dimensional variation within acceptable limits, and a compressive strength of 55 kg·cm^{-2}. These values constitute the baseline for evaluating the effect of incorporating construction and demolition waste, allowing for clear identification of the changes generated by each recycled particle size compared to the conventional material.

Water absorption increased with the incorporation of CDW, reaching up to 13.0% in 3/8″ particles, while residues with a CDW aggregate size of No. 4 registered lower absorption (11.7%), demonstrating that fine particles increase

porosity and facilitate water capture, while intermediate granulometries allow maintaining good performance against humidity and preserve the durability of the unit.

Regarding dimensional variation, all units with CDW remained within the limits established by standard NTP 331.017. Height showed variations of up to 102.7% with 3/8″ waste, while waste with a No. 4 CDW aggregate size showed a 102.1% fluctuation in height and smaller deviations in length and width. This demonstrates that the CDW particle size influences the geometric stability of the bricks, making it important to select appropriate sizes to maintain the required uniformity on site. Overall, the dimensional performance obtained demonstrates that the incorporation of waste is compatible with regulatory requirements, provided that adequate control of the production process and the particle size distribution used is ensured.

Regarding compressive strength, the CDW bricks with an aggregate size of No. 4 and those of 3/4″ reached 64 and 65 $kg \cdot cm^{-2}$, respectively, surpassing the standard brick, while the 3/8″ waste bricks registered only 26 $kg \cdot cm^{-2}$. This reflects that coarse particles favor compaction and, therefore, the development of the brick's internal structure, improving its mechanical capacity, while the use of fine particles can generate greater porosity and significantly reduce the strength of the units. Taken together, all this evidence confirms that strength depends not only on the presence of CDW but also on particle size.

Acknowledgements

The authors gratefully acknowledge Universidad Nacional de Barranca for the financial support provided for the development of this research.

References

Al-Fakih, A., Mohammed, B., Liew, M., & Nikbakht, E. (2018). Incorporation of waste materials in the manufacture of masonry bricks: An update review. *Journal of Building Engineering*, *21*, 37–54. https://doi.org/10.1016/j.jobe.2018.09.023

ASTM International. (2014). *Standard test methods for sampling and testing brick and structural clay tile* (ASTM C67-14). https://www.astm.org/c0067-14.html

ASTM International. (2017). *Standard specification for building brick (solid masonry units made from clay or shale)* (ASTM C62-17). https://www.astm.org/c0062-17.html

Bazán, I. (2018). *Caracterización de residuos de construcción de Lima y Callao (estudio de caso)* [*Characterization of construction waste in Lima and Callao (case study)*] (Bachelor's thesis). Pontificia Universidad Católica del Perú. http://hdl.handle.net/20.500.12404/10189

Bektas, F., Turanli, L., Wang, K., & Ceylan, H. (2007). Comparative performance of ground clay brick in mitigation of alkali–silica reaction. *Journal of Materials in Civil Engineering*, *19*(12), 1070–1078. https://doi.org/10.1061/(ASCE)0899-1561(2007)19:12(1070)

Capasso, I., D'Angelo, G., del Río Merino, M., Campanile, A., Caputo, D., & Liguori, B. (2025). CDW-based geopolymers: Pro and cons of using unselected waste. *Polymers*, *17*(5), 570. https://doi.org/10.3390/polym17050570

Cárcamo Vásquez, H., Méndez Bustos, P., & Rebolledo Carreño, A. (2009). Tendencias de los enfoques cualitativos y cuantitativos en artículos publicados en scientific library on line (scielo). *Paradígma*, *30*(2), 179–200. http://ve.scielo.org/scielo.php?script=sci_arttext&pid=S1011-22512009000200012&lng=es&tlng=es

Chávez Porras, Á., Guarín Cortes, N. L., & Cortes Duarte, M. C. (2013). Determinación de propiedades físico-químicas de los materiales agregados en muestra de escombros en la ciudad de Bogotá D.C. [Determination of physical-chemical properties of the materials added in sample debris in the city of Bogota] *Revista Ingenierías Universidad De Medellín*, *12*(22), 45–58. https://doi.org/10.22395/rium.v12n22a4

Chi, B., Lu, W., Ye, M., Bao, Z., & Zhang, X. (2020). Construction waste minimization in green building: A comparative analysis of LEED-NC 2009 certified projects in the US and China. *Journal of Cleaner Production*, *256*, 120749. https://doi.org/10.1016/j.jclepro.2020.120749

Chica, L., & Beltrán, J. (2018). Caracterización de residuos de demolición y construcción para la identificación de su potencial de reúso. *DYNA*, *85*(206), 338–347. https://doi.org/10.15446/dyna.v85n206.68824

Creswell, J., & Creswell, J. (2018). *Research design: Qualitative, quantitative, and mixed methods approaches.* SAGE.

Cruzado, J. (2018). *Elaboración de ladrillos de 18 huecos tipo IV con residuos de demolición y cemento* [*Production of 18-hole type IV bricks using demolition waste and cement*] (Bachelor's thesis). Universidad Nacional Agraria La Molina. https://hdl.handle.net/20.500.12996/3544

Dos Reis, G. S., Cazacliu, B. G., Cothenet, A., & Torrenti, J. M. (2019). Valorization of inert part of construction and demolition wastes for the production of fired bricks. *Proceedings*, *34*(1), 8. https://doi.org/10.3390/proceedings2019034008

Dubale, M., Vasić, M. V., Goel, G., Kalamdhad, A., & Singh, L. B. (2023). Utilization of Construction and Demolition Mix Waste in the Fired Brick Production: The Impact on Mechanical Properties. *Materials*, *16*(1), 262. https://doi.org/10.3390/ma16010262

Gallegos, H. & Casabonne, C. (2005). *Albañilería estructural*. Fondo Editorial PUCP. https://doi.org/10.18800/9789972427541

Gencel, O., Kizinievič, O., Erdoğmuş, E., Kizinievič, V., Sutcu, M., & Muñoz, P. (2022). Manufacturing of fired bricks derived from wastes: utilization of water treatment sludge and concrete demolition waste. *Archives of Civil and Mechanical Engineering*, *22*(2), 78. https://doi.org/10.1007/s43452-022-00396-7

Gutiérrez, A., & Oyarce, G. (2021). *Adición de residuos sólidos al ladrillo de arcilla artesanal para mejorar sus propiedades en función a la norma E-070 – Cajamarca, 2019* [*Addition of solid waste to handmade clay brick to improve its properties according to standard E-070 – Cajamarca, 2019*] (Bachelor's thesis). Universidad Privada del Norte. https://hdl.handle.net/11537/28124

Gutiérrez, B., & Miranda, J. (2025). *Ladrillos ecológicos elaborados con concreto de demolición y polvo de vidrio reciclado* [*Ecological bricks made with demolition concrete and recycled glass powder*] (Bachelor's thesis). Universidad San Ignacio de Loyola. https://hdl.handle.net/20.500.14005/15583

Hernández, R., Fernández, C., & Baptista, P. (2014). *Metodología de la investigación* (6th ed.). McGraw-Hill.

Instituto Nacional de Calidad [INACAL]. (2015). *Unidades de albañilería – Ladrillos de arcilla usados en albañilería – Requisitos* (NTP 331.017) (2nd ed.).

Instituto Nacional de Calidad [INACAL]. (2017). *Unidades de albañilería – Métodos de muestreo y ensayo de ladrillos de arcilla usados en albañilería* (NTP 399.613) (2nd ed.).

Junior, A. C. P., Jacinto, C., Turco, C., Fernandes, J., Teixeira, E., & Mateus, R. (2022). Analysis of the effect of incorporating construction and demolition waste on the environmental and mechanical performance of earth-based mixtures. *Construction and Building Materials*, *330*, 127244. https://doi.org/10.1016/j.conbuildmat.2022.127244

Kofoworola, O. F., & Gheewala, S. H. (2009). Estimation of construction waste generation and management in Thailand. *Waste Management*, *29*(2), 731–738. https://doi.org/10.1016/j.wasman.2008.07.004

Kumar, R., Kumar, M., Kumar, I., & Srivastava, D. (2021). A review on utilization of plastic waste materials in bricks manufacturing process. *Materials Today: Proceedings*, *46*(6), 6775–6780. https://doi.org/10.1016/j.matpr.2021.04.337

Lieder, M., & Rashid, A. (2016). Towards circular economy implementation: a comprehensive review in context of manufacturing industry. *Journal of Cleaner Production*, *115*, 36–51. https://doi.org/10.1016/j.jclepro.2015.12.042

Lu, W., Webster, C., Peng, Y., Chen, X., & Zhang, X. (2017). Estimating and calibrating the amount of building-related construction and demolition waste in urban China. *International Journal of Construction Management*, *17*(1), 13–24. https://doi.org/10.1080/15623599.2016.1166548

Luo, H., Aguiar, J., Wan, X., Wang, Y., Cunha, S., & Jia, Z. (2024). Application of aggregates from construction and demolition wastes in concrete: Review. *Sustainability*, *16*(10), 4277. https://doi.org/10.3390/su16104277

Manterola, C., & Otzen, T. (2015). Estudios experimentales 2 Parte: Estudios cuasi-experimentales [Experimental studies 2nd part. Quasi-experimental studies]. *International Journal of Morphology, 33*(1), 382–387. https://doi.org/10.4067/S0717-95022015000100060

Mayz, J., & Pérez, J. (2002). ¿Para qué hacer investigación científica en las universidades venezolanas? *Investigación y Postgrado*, *17*(1), 159–171. http://ve.scielo.org/scielo.php?script=sci_arttext&pid=S1316-00872002000100007&lng=es&tlng=es

Muñoz Pérez, S. P., Delgado Sánchez, J. L., & Facundo, L. E. F. (2021). Elaboración de ladrillos ecológicos en muros no estructurales: una revisión. *Cultura Científica y Tecnológica*, *18*(1), 1–9. https://doi.org/10.20983/culcyt.2021.1.3.1

Oviedo Cogollo, A. R., & Vega Suárez, J. C. (2021). Construction and demolition waste management and circular economy: A narrative review. *Lámpsakos*, *26*, 41–51. https://doi.org/10.21501/21454086.4232

Pacheco-Torgal, F. (2014). Eco-efficient construction and building materials research under the EU Framework Programme Horizon 2020. *Construction and Building Materials*, *51*, 151–162. https://doi.org/10.1016/j.conbuildmat.2013.10.058

Padmalosan, P., Vanitha, S., Kumar, V. S., Anish, M., Tiwari, R., Dhapekar, N. K., & Yadav, A. S. (2023). An investigation on the use of waste materials from industrial processes in clay brick production. *Materials Today: Proceedings.* https://doi.org/10.1016/j.matpr.2023.01.238

Parra, C., Miñano, I., Calabuig, M., Benito, F., Mateo, J. M., Carrión, E., & Ruiz, C. (2024). Geopolymer with brick and concrete demolition construction waste. *Materiales de Construcción*, *74*(356), e361. https://doi.org/10.3989/mc.2024.392424

Quintero, A. (2007). ¿Es necesario hacer ciencia básica? *Revista Científica*, *17*(5), 431–432. http://ve.scielo.org/scielo.php?script=sci_arttext&pid=S0798-22592007000500001&lng=es&tlng=es

Rahhal, V. F., Trezza, M., Tironi, A., Castellano, C. C., Pavlíková, M., Pokorný, J., Irassar, E. F., Jankovský, O., & Pavlík, Z. (2019). Complex characterization and behavior of waste fired brick powder-Portland cement system. *Materials*, *12*(10), 1650. https://doi.org/10.3390/ma12101650

Rahimpour, H., Amini, A. B., Sharifi, F., Fahmi, A., & Zinatloo-Ajabshir, S. (2024). Facile fabrication of next-generation sustainable brick and mortar through geopolymerization of construction debris. *Scientific Reports*, *14*, 10914. https://doi.org/10.1038/s41598-024-61688-x

Raini, I., Imad, R., El Asmi, H., Obda, I., Mesrar, L., & Jabrane, R. (2025). Production of eco-friendly clay bricks from municipal construction and demolition waste. *Journal of Ecological Engineering*, *26*(3), 296–308. https://doi.org/10.12911/22998993/199456

Robayo, R., Mejía, R., & Mulford, A. (2016). Production of building elements based on alkali-activated red clay brick waste. *Revista Facultad de Ingeniería*, *25*(43), 21–30. http://www.scielo.org.co/scielo.php?script=sci_arttext&pid=S0121-11292016000300002&lng=en&tlng=es

Rotaondaro, R. (2007). Arquitectura de tierra contemporánea: tendencias y desafíos. *Apuntes: Revista de Estudios sobre Patrimonio Cultural – Journal of Cultural Heritage Studies*, *20*(2), 342–353. http://www.scielo.org.co/scielo.php?script=sci_arttext&pid=S1657-97632007000200014&lng=en&tlng=es

Santana, I. S. A., Novaes, M. D. P., Araújo, R. C. C. D., & Batalha-Vieira, L. (2024). Exposed clay bricks made with waste: An analysis of research and technological trends. *Sustainability*, *16*(24), 11274. https://doi.org/10.3390/su162411274

Shadish, W. R., Cook, T. D., & Campbell, D. T. (2002). *Experimental and quasi-experimental designs for generalized causal inference.* Houghton Mifflin.

Sieffert, Y., Huygen, J., & Daudon, D. (2014). Sustainable construction with repurposed materials in the context of a civil engineering–architecture collaboration. *Journal of Cleaner Production*, *67*, 125–138. https://doi.org/10.1016/j.jclepro.2013.12.018

Suárez-Silgado, S. S., Betancourt-Quiroga, C., Molina Benavides, J., & Mahecha Vanegas, L. (2019). La gestión de los residuos de construcción y demolición en Villavicencio: estado actual, barreras e instrumentos de gestión. *Entramado*, *15*(1), 224–244. https://doi.org/10.18041/1900-3803/entramado.1.5408

Tam, V. W., Soomro, M., & Evangelista, A. C. J. (2018). A review of recycled aggregate in concrete applications (2000–2017). *Construction and Building materials*, *172*, 272–292. https://doi.org/10.1016/j.conbuildmat.2018.03.240

Tejada, M. (2025). *Análisis de la implementación de ladrillos ecológicos para una viabilidad económica y ambiental en el sector de la construcción*. Universidad Privada del Norte. https://hdl.handle.net/11537/44568

Torres, A. (2024). *Fabricación de ladrillos ecológicos con residuos de construcción y demolición para su empleo en la mampostería ordinaria [Manufacturing ecological bricks from construction and demolition waste for use in ordinary masonry]*. Universidad Continental. https://hdl.handle.net/20.500.12394/15962

Torres-Rodríguez, D., Marcó, L. M., Gómez, C., & García-Orellana, Y. (2022). Total X-Ray Fluorescence (TXRF) as an alternative method for the determination of micronutrients in soils of the Quíbor depression (Venezuela). *TecnoLógicas*, *25*(53), e203. https://doi.org/10.22430/22565337.2195

UN Environment, Scrivener, K. L., John, V. M., & Gartner, E. (2018). Eco-efficient cements: Potential economically viable solutions for a low-CO_2 cement-based materials industry. *Cement and Concrete Research*, *114*, 2–26. https://doi.org/10.1016/j.cemconres.2018.03.015

Uribe, R., Camillo, F., & Lascano, L. (2021). Clay minerals specialized ceramic categorization protocol: A review. *infoANALÍTICA*, *9*(2), 15–57. https://doi.org/10.26807/ia.v9i2.202

Vega Garcia, F. J. (2024). *Influencia de la adición de residuos de construcción y demolición (RCD) en las propiedades mecánicas del ladrillo artesanal* [*Influence of the addition of construction and demolition waste (CDW) on the mechanical properties of handmade brick]*. Universidad Peruana Los Andes. https://hdl.handle.net/20.500.12848

Vega Neyra, C. S., & Hizo Celestino, C. N. (2025). *Propiedades fisicas-mecánicas de ladrillos macizos de concreto producidos a través de residuos de demolición, Barranca* [*Physical-mechanical properties of solid concrete bricks produced from demolition waste, Barranca*]. Universidad Nacional de Barranca. https://repositorio.unab.edu.pe/item/5d76817c-946e-467e-b18b-178dbfd379c1

Voišnienė, V., Kizinievič, O., Kizinievič, V., & Malaiškienė, J. (2019, May 16–17). *Production of fired clay brick from municipal solid waste incinerator fly ash. 13th International Conference Modern Building Materials, Structures and Techniques, Vilnius, Lithuania.* https://doi.org/10.3846/mbmst.2019.149

Xiao, Y., Kong, K., Aminu, U. F., Li, Z., Li, Q., Zhu, H., & Cai, D. (2022). Characterizing and predicting the resilient modulus of recycled aggregates from building demolition waste with breakage-induced gradation variation. *Materials*, *15*(7), 2670. https://doi.org/10.3390/ma15072670

Zanelli, C., Marrocchino, E., Guarini, G., Toffano, A., Vaccaro, C., & Dondi, M. (2021). Recycling construction and demolition residues in clay bricks. *Applied Sciences*, *11*(19), 8918. https://doi.org/10.3390/app11198918

Zhang, L. (2013). Production of bricks from waste materials – A review. *Construction and Building Materials*, *47*, 643–655. https://doi.org/10.1016/j.conbuildmat.2013.05.043

Summary

Clay masonry units with variation in construction and demolition waste (CDW) particle size. The objective of this research was to evaluate the influence of construction and demolition waste (CDW) particle size on the physical and mechanical properties of clay bricks. The methodology was applied, with a quantitative approach and a quasi-experimental design. The population comprised all manufactured bricks, and the sample consisted of 75 units, distributed into a control group without CDW and four experimental groups with particle sizes of 3/4″, 1/2″, 3/8″, and No. 4. Absorption, dimensional variation, and compressive strength were evaluated. The control bricks exhibited an absorption of 10.7%, dimensional stability within regulatory limits, and a compressive strength of 55 kg·cm^{-2}. Absorption increased to 13.0% with 3/8″ waste, while No. 4 showed lower absorption (11.7%). Dimensional variation remained within acceptable limits. The 3/8″ waste particles retained their dimensions better, while the No. 4 particles showed greater deviations in height. Regarding compressive strength, the coarse waste particles (3/4″ and No. 4) reached 65 and 64 kg·cm^{-2}, respectively, surpassing the control, while the 3/8″ particles registered only 26 kg·cm^{-2}, demonstrating that coarse particles favor compaction and structural development of the brick. In conclusion, the incorporation of CDW into clay bricks is a proven alternative, with particle size being a determining factor in optimizing its properties.

Instruction for Authors

The journal publishes in English languages, peer-reviewed original research, critical reviews and short communications, which have not been and will not be published elsewhere in substantially the same form. Author of an article is required to transfer the copyright to the journal publisher, however authors retain significant rights to use and share their own published papers. The published papers are available under the terms of the principles of Open Access Creative Commons CC BY-NC license. The submitting author must agree to pay the publication charge (see Charges).

The author of submitted materials (e.g. text, figures, tables etc.) is obligated to restricts the publishing rights. All contributors who do not meet the criteria for authorship should be listed in an Acknowledgements section of the manuscript. Authors should, therefore, add a statement on the type of assistance, if any, received from the sponsor or the sponsor's representative and include the names of any person who provided technical help, writing assistance, editorial support or any type of participation in writing the manuscript.

Uniform requirements for manuscripts

The manuscript should be submitted by the Open Journal System (OJS) at https://srees.sggw.edu.pl/about/submissions. All figures and tables should be placed near their reference in the main text and additionally sent in a form of data files (e.g. Excel, Visio, Adobe Illustrator, Adobe Photoshop, CorelDRAW). Figures are printed in black and white on paper version of the journal (color printing is combined with an additional fee calculated on a case-by-case basis), while on the website are published in color.

The size of the manuscript should be limited up to 10 pages including overview, summary, references and figures (the manuscript more than 13 pages is unacceptable); Please set the text format in single column with paragraphs (A4 paper format), all margins to 25 mm, use the font Times New Roman, typeface 12 points and line spacing one and half.

The submitted manuscript should include the following parts:

- name and SURNAME of the author(s) – up to 5 authors
- affiliation of the author(s), ORCID Id (optional)
- title of the work
- key words
- abstract (about 500 characters)
- text of the paper divided into: Introduction, Material and Methods, Results and Discussion, Conclusions, References and Summary
- references in APA style are listed fully in alphabetical order according to the last name of the first author and not numbered; please find the details below
- post and mailing address of the corresponding author:

  Author's address:
  Name, SURNAME
  Affiliation
  Street, number, postal code, City
  Country
  e-mail: adress@domain

- Plagiarism statement (https://srees.sggw.edu.pl/copyright)

Reference formatting

In the Scientific Review Engineering and Environmental Sciences the APA 7th edition style is used.

Detailed information

More information can be found: https://srees.sggw.edu.pl